

Carbonation Kinetics of Cementitious Materials Used in the Geological Disposal of Radioactive Waste

Jia Sun



A thesis submitted for the degree of Doctor of Philosophy of the
University of London

Department of Chemical Engineering
University College London
London WC1E 7JE

August 2010

ABSTRACTS

The use of cement based materials could be widespread in the long term management of radioactive materials in the United Kingdom. In the Geological Disposal Concepts proposed by the Radioactive Waste Management Directorate of the Nuclear Decommissioning Authority (NDA), several cement based materials are used in the long-term management of intermediate-level wastes. Much of the waste will be immobilised within stainless steel containers using cement grouts based on ordinary Portland cement (OPC) blended with blast furnace slag (BFS) or pulverised fuel ash (PFA). The resulting waste packages will be placed underground in a Geological Disposal Facility (or Repository) after a period of storage at the waste producers' sites. The repository will then be filled with cement based backfill. The encapsulation grouts and the backfill materials will perform as both a physical barrier and chemical barrier for confining the radioactive wastes.

During storage and disposal, some wastes may generate carbon dioxide from the degradation of organic materials and this will react with the cement based materials. Therefore, carbonation of the cementitious encapsulation grouts and backfill materials is of interest because of the resulting changes to their physical and chemical properties and also because of its ability to remove carbon-14 labelled

carbon dioxide from the gas phase. It is also important to understand the reaction kinetics under a range of conditions, due to the long-term nature of storage and disposal.

In this work, the carbonation progress of one backfill material and of two encapsulation grouts used in the UK has been studied in batch reactors. These materials are known as Nirex Reference Vault Backfill (NRVB), 3:1 PFA/OPC and 3:1 BFS/OPC. Based on the single dimensional carbonation experiments, fundamental parameters affecting the rate of carbonation were investigated and the carbon dioxide uptake capacity of each material was determined. For these three materials, an increase in relative humidity (75% to 100%) decreases the carbonation rate. A higher reaction pressure can facilitate the carbonation, but its effect was less obvious than the effect of relative humidity. The progression of the carbonation fronts have also been observed by various techniques and the shape of carbonation front was proved to be influenced by the relative humidity. Special attention was given to the modelling of the kinetics and mechanism of the carbonation reaction of these materials.

This work provides fundamental understanding of the carbonation reaction of NRVB, 3:1 PFA/OPC and 3:1 BFS/OPC of relevance to the future optimization of a geological disposal facility in the UK and to assessments of the performance of such a facility.

ACKNOWLEDGEMENTS

I would like to express my most sincere gratitude to my supervisor, Professor Stefaan J. R. Simons for the simulation, guidance and continual encouragement during the course of this work. I am considered a lucky person to have had the opportunity to work on this project.

I would like to thank Steve Williams of the Radioactive Waste Management Directorate of the UK's Nuclear Decommissioning Authority (NDA), for his comments, suggestions and insights.

I would like to extend my thanks to my colleagues, Marta Fernández Bertos, Sarah Gemernà and Nan Shao for their enormous help and constant support since my first day in UCL. Wish you all the best in your future careers.

I am thankful to Martin, Gran, John and Alan from the Mechanical Workshop for constructing the experimental apparatus; Mike Gorecki and Simon Barrass for their technical support; Pat Markey, Elaine Briggs and Mae for their administrative work.

The financial support of NDA and the Overseas Research Students Award Scheme is gratefully acknowledged.

Finally, I would like to thank my beloved family for their continual support and encouragement.

TABLE OF CONTENTS

Abstracts.....	2
Acknowledgements	4
Table of Contents	6
List of Figures	11
List of Tables	16
Notation.....	18
1 Introduction.....	20
1.1 General Introduction	20
1.1.1 Radioactive Wastes in the UK.....	20
1.1.2 The Phased Geological Repository Concept for Long-term Management of LLW/ILW	24
1.1.3 Cementitious Materials Used in the PGRC.....	26
1.2 Research Objectives & Structure of the Thesis.....	29
2 A Review of Cement and Carbonation.....	33
2.1 Definition of Cement.....	33
2.2 Portland Cements: History, Manufacture and Mineral Composition	34
2.3 Hydration of Portland Cements.....	37
2.4 Pozzolans and Pozzolanic Reaction.....	40

2.5	Blended Cements	41
2.5.1	Portland-Fly Ash Blend.....	41
2.5.2	Portland-Blast Furnace Slag Blend	43
2.6	Carbonation of Cementitious Materials	44
2.6.1	Introduction	44
2.6.2	Description of Reaction Process	45
2.6.3	Carbonation of Hydrated Cement	46
2.6.4	Factors Influencing Carbonation.....	50
2.6.5	Impacts of Carbonation on Cementitious Systems	56
2.6.6	Methods to Examine the Carbonation Products.....	58
2.6.7	Accelerated Carbonation.....	62
2.6.8	Carbonation of Blended Cements	65
2.7	Summary	66
3	Materials, Equipment and Methods	67
3.1	Materials.....	67
3.1.1	Specimen Preparation.....	67
3.1.2	Specimen Conditioning.....	71
3.1.3	Specimen Sealing	72
3.2	Experimental Apparatus	73
3.3	Experimental Method.....	78
3.3.1	Initial Bulk Density and Dry Porosity.....	78
3.3.2	Effect of Conditioning on Specimen Water Content.....	79

3.3.3	Carbonation Test	80
3.3.4	Analysis of the Property Changes Due to Carbonation	85
4	Experimental Results and Discussion	89
4.1	Introduction	89
4.2	Results of NRVB Carbonation Test.....	90
4.2.1	Effect of Conditioning.....	90
4.2.2	Carbonation Test Results.....	94
4.2.3	Observation of Carbonation Profile	98
4.2.4	Examination of Microstructure Using SEM	103
4.2.5	Examination of Mineralogy Changes.....	105
4.2.6	Examination of Carbonation Content.....	107
4.2.7	Availability of Reactive Calcium	109
4.3	Results of 3:1 PFA/OPC Grout	113
4.3.1	Effect of Conditioning.....	113
4.3.2	Results of Carbonation Test	116
4.3.3	Observation of Carbonation Profile	117
4.3.4	Examination of Microstructure Using SEM	120
4.3.5	Examination of Mineralogy Changes.....	121
4.3.6	Examination of Carbonation Content.....	123
4.4	Results of 3:1 BFS/OPC Grout	125
4.4.1	Effect of Conditioning.....	125
4.4.2	Results of Carbonation Test	128

4.4.3	Observation of Carbonation Profile	130
4.4.4	Examination of Microstructure Using SEM	131
4.4.5	Examination of Mineralogy Changes.....	132
4.4.6	Examination of Carbonation Content.....	133
4.5	Discussion	135
4.5.1	Carbonation of NRVB	136
4.5.2	Carbonation of 3:1 PFA/OPC.....	138
4.5.3	Carbonation of 3:1 BFS/OPC	140
4.5.4	Cracks due to Carbonation	140
5	Kinetic Analysis of Carbonation	141
5.1	Introduction.....	141
5.2	CO ₂ -Diffusion-Controlled Model	143
5.3	Adaption of the Model to the Carbonation Test Data	147
5.3.1	Interpretation of CO ₂ Pressure Variation.....	147
5.3.2	Analysis of Carbonation Rate Data of NRVB.....	147
5.3.3	Analysis of Carbonation Rate Data of 3:1 PFA/OPC Grout...	152
5.3.4	Analysis of Carbonation Rate Data of 3:1 BFS/OPC Grout...	158
5.4	Discussion	163
6	Conclusions and Future Work	164
6.1	Conclusions.....	164
6.2	Future Work.....	168
6.2.1	Effect of Temperature.....	168

6.2.2	Formation and Effect of Cracks	169
6.2.3	Competition of Carbonation Reactions.....	169
6.2.4	Kinetic Modelling	170
	Reference List	171
	Appendix A	187
	Appendix B	188

LIST OF FIGURES

Figure 1-1 Total radioactive waste volumes [NDA and Defra, 2008].....	23
Figure 1-2 Phased geological repository concept [Nirex, 2005].....	24
Figure 1-3 Standard ILW packages [Nirex, 2005]	28
Figure 2-1 An area from a 7-day old w/s 0.45 cement paste, cured at room temperature [Diamond, 2004]	38
Figure 3-1 NRVB specimen mounted in epoxy resin.....	72
Figure 3-2 Carbonation rig.....	74
Figure 3-3 Reactor I	75
Figure 3-4 Reactor II	75
Figure 3-5 Internal structural of carbonation chamber.....	76
Figure 4-1 Evolution of reaction with time for NRVB at pressure from 1bar to 5bar at relative humidity from 75% to 100% (Error in $X_{Ca} = \pm 0.039$)..	94
Figure 4-2 Plot of X_{Ca} vs. $\text{time}^{0.5}$ for NRVB at pressure from 1bar to 5bar at relative humidity from 75% to 100% (Error in $X_{Ca} = \pm 0.039$).....	95
Figure 4-3 Plot of X_{Ca} vs. $\text{time}^{0.5}$ at the first 400 minutes for NRVB at pressure from 1bar to 5bar at relative humidity from 75% to 100% (Error in $X_{Ca} =$ ± 0.039)	96
Figure 4-4 Cross-section of cut NRVB specimens with different carbonation	

durations, P=3bar, RH=75%	99
Figure 4-5 Plot of X_{Ca} vs. time ^{0.5} for NRVB carbonated at P=3bar, RH=75% with different reaction durations (Error in $X_{Ca} = \pm 0.039$)	101
Figure 4-6 Cross-section of a cut NRVB specimen after 6 hours carbonation, P=3bar, RH=85%	102
Figure 4-7 Cross-section of a cut NRVB specimen after 102 hours carbonation, P=3bar, RH=100%	103
Figure 4-8 SEM secondary electron microphotographs of non-carbonated NRVB, (a) low magnification, (b) high magnification	104
Figure 4-9 SEM secondary electron microphotographs of carbonated specimen of NRVB conditioned at 75% relative humidity, (a) Magnification X2,000 (b) Magnification X10,000	104
Figure 4-10 SEM secondary electron microphotographs of carbonated specimen of NRVB conditioned at 100% relative humidity, (a) Magnification X2,000 (b) Magnification X10,000	105
Figure 4-11 XRD diffractograms of fresh NRVB and carbonated NRVB (CC represents calcium carbonated, CH represents calcium hydroxide) ...	106
Figure 4-12 (a) TG/DTA/DTG curves of fresh NRVB	108
Figure 4-13 Comparison of carbonation depth between direct measurement and estimation from X_{Ca}	112
Figure 4-14 Evolution of Reaction with time for 3:1 PFA/OPC at pressure from 1bar to 5bar at relative humidity from 75% to 100% (Error in $X_{Ca} =$	

± 0.025)	117
Figure 4-15 Cross-section of cut 3:1 PFA/OPC specimens with different carbonation durations, P=3bar, RH=75%	118
Figure 4-16 Cross-section of cut 3:1 PFA/OPC specimen after 168 hours carbonation, P=3bar, RH=100%	120
Figure 4-17 SEM secondary electron microphotographs of non-carbonated specimen of 3:1 PFA/OPC grout, (a) Magnification X500 (b) Magnification X5,000	121
Figure 4-18 SEM secondary electron microphotographs of carbonated specimen of 3:1 PFA/OPC grout conditioned at 75% relative humidity, (a) Magnification X500 (b) Magnification X5,000	121
Figure 4-19 XRD diffractograms of Fresh 3:1 PFA/OPC and carbonated 3:1 PFA/OPC (CC represents calcium carbonate, S represents quartz)	122
Figure 4-20 (a) TG/DTA/DTG curves of fresh 3:1 PFA/OPC grout.....	123
Figure 4-21 Evolution of reaction with time for 3:1 BFS/OPC at pressure from 1bar to 5bar at relative humidity from 75% to 100% (Error in $X_{Ca} = \pm 0.013$)	129
Figure 4-22 Cross-section of fresh and partially carbonated 3:1 BFS/OPC specimens	130
Figure 4-23 SEM secondary electron microphotographs of non-carbonated specimen of 3:1 BFS/OPC grout, (a) Magnification X500 (b) Magnification X2,000	131

Figure 4-24 SEM secondary electron microphotographs of carbonated specimen of 3:1 BFS/OPC grout conditioned at 75% relative humidity, (a) Magnification X500 (b) Magnification X2,000	132
Figure 4-25 XRD diffractograms of Fresh 3:1 BFS/OPC and carbonated 3:1 BFS/OPC (CC represents calcium carbonated, CH represents calcium hydroxide, S represents quartz).....	133
Figure 4-26 (a) TG/DSC/DTG curves of fresh 3:1 BFS/OPC grout.....	134
Figure 4-27 Gas-filled porosity at different relative humidities.....	136
Figure 4-28 Schematic illustrating the carbonation profile of unsaturated NRVB	138
Figure 4-29 Schematic illustrating the carbonation profile of 3:1 PFA/OPC grout	139
Figure 5-1 Representation of a reacting cementitious matrix when diffusion through the carbonation layer is the controlling resistance.....	144
Figure 5-2 Analysis of diffusion-controlled model for 75% RH NRVB specimens	149
Figure 5-3 Analysis of diffusion-controlled model for 85% RH NRVB specimens	150
Figure 5-4 Analysis of diffusion-controlled model for 100% RH NRVB specimens	151
Figure 5-5 Analysis of diffusion-controlled model for 75% RH 3:1 PFA/OPC specimens	153

Figure 5-6 Analysis of diffusion-controlled model for 85% RH 3:1 PFA/OPC specimens	154
Figure 5-7 Analysis of diffusion-controlled model for 100% RH 3:1 PFA/OPC specimens	154
Figure 5-8 Relationship between $D_{e,Ave}$ and relative humidity for 3:1 PFA/OPC.....	155
Figure 5-9 Relationship between X_{Ca} calculated from experimental data and X_{Ca} determined by the kinetic model (3:1 PFA/OPC grout).....	156
Figure 5-10 Analysis of diffusion-controlled model for 75% RH 3:1 BFS/OPC specimens	158
Figure 5-11 Analysis of diffusion-controlled model for 85% RH 3:1 BFS/OPC specimens	159
Figure 5-12 Analysis of diffusion-controlled model for 100% RH 3:1 BFS/OPC specimen.....	160
Figure 5-13 Relationship between $D_{e,Ave}$ and relative humidity for 3:1 BFS/OPC.....	161
Figure 5-14 Relationship between X_{Ca} calculated from experimental data and X_{Ca} determined by the kinetic model (3:1 BFS/OPC grout)	162

LIST OF TABLES

Table 1-1 Categories of radioactive waste in the UK [Defra, 2008]	22
Table 2-1 Mineral composition of Portland cement	35
Table 2-2 Typical compound compositions of Portland cement [ACI, 2001]	36
Table 2-3 Effects of fly ash on fresh and hardened concrete.....	43
Table 2-4 Factors influencing the permeability of hydrated cementitious materials	55
Table 2-5 Variations in certain physical properties due to carbonation.....	58
Table 3-1 Mix proportions for NRVB, 3:1 BFS/OPC and 3:1 PFA/OPC	67
Table 3-2 The Physical and Chemical properties of OPC and Admixtures..	69
Table 3-3 CO ₂ uptake capacity	70
Table 4-1 Results of drying NRVB at 105 °C for 24 hours	90
Table 4-2 Results of conditioning NRVB at 75% RH for 5 months.....	91
Table 4-3 Results of conditioning NRVB at 85% RH for 5 months.....	91
Table 4-4 Results of conditioning NRVB at 100% RH for 5 months.....	91
Table 4-5 Average wet density of fresh NRVB of different ages	92
Table 4-6 NRVB gas-filled porosity and degree of water saturation.....	92
Table 4-7 Results of drying 3:1 PFA/OPC at 105 °C for 24 hours	113

Table 4-8 Results of conditioning 3:1 PFA/OPC at 75% RH for 5 months	114
Table 4-9 Results of conditioning 3:1 PFA/OPC at 85% RH for 5 months	114
Table 4-10 Results of conditioning 3:1 PFA/OPC at 100% RH for 5 months	115
Table 4-11 3:1 PFA/OPC gas-filled porosity and degree of water saturation	115
Table 4-12 Results of drying 3:1 BFS/OPC at 105 °C for 24 hours	125
Table 4-13 Results of conditioning 3:1 BFS /OPC at 75% RH for 1 month	126
Table 4-14 Results of conditioning 3:1 BFS /OPC at 85% RH for 1 month	126
Table 4-15 Results of conditioning 3:1 BFS /OPC at 100% RH for 1 month	127
Table 4-16 3:1 BFS/OPC gas-filled porosity and degree of water saturation	127
Table 5-1 Average effective diffusion coefficients of CO ₂ in 3:1 PFA/OPC specimens conditioned at 75%RH, 85% RH and 100% RH, respectively (Errors were determined by average deviation)	155
Table 5-2 Average effective diffusion coefficients of CO ₂ in 3:1 PFA/OPC specimens conditioned at 75%RH, 85% RH and 100% RH respectively (Errors were determined by average deviation)	160

NOTATION

Cement nomenclature: C CaO calcium oxide

S SiO₂ silicon oxide

H H₂O water

\bar{S} SO₄²⁻ sulphate

A Al₂O₃ aluminate

\bar{C} CO₂ carbon dioxide

C_A concentration of CO₂ at surface of any depth l

C_{Ac} concentration of CO₂ at the surface of carbonation front

C_{Ag} concentration of CO₂ in bulk gas phase

C_{As} concentration of CO₂ at the surface of the exposed solid surface

D_e effective diffusion coefficient of gaseous CO₂ in the product layer

d depth of carbonation

k reaction constant

L overall thickness of the solid matrix

l any depth in the carbonation layer

l_c depth of carbonation front

l_t depth of carbonation front according to direct measurement.

n_{Ca} mole concentration of reactive calcium in the specimen (mol m⁻³).

n'_{Ca} concentration of effective reactive calcium (mol m⁻³)

$n_{CO_2,t}$	mole amount of CO ₂ absorbed by NRVB at time t
n_t	mole of CO ₂ absorbed by time t per m ³ of the specimen (mol m ⁻³)
P_0	initial pressure when the reaction starts (bar)
P_t	pressure at time t (bar)
Q_A	flux of CO ₂ through surface of any depth l
Q_{Ac}	flux of CO ₂ to the carbonation front.
Q_{As}	flux of CO ₂ through exterior surface of solid matrix
R	gas constant, 0.083145 L bar K ⁻¹ mol ⁻¹
S	area of exterior surface.
T	temperature in the reactor at time (K)
V	volume of the solid matrix
$V_{reactor}$	gas volume in the reactor, which is 4.674 L
$V_{specimen}$	volume of the specimen
ΔW	weight loss due to drying
X_{Ca}	conversion of reactive calcium
ϕ	Porosity
ρ_{Ca}	molar density of reactive calcium in the solid matrix
ρ_{water}	water density at room temperature

1 INTRODUCTION

1.1 General Introduction

An important use of cement, Portland cement in particular, is its use in the encapsulation of many radioactive wastes for their long-term management [Glasser, 1992]. The immobilization potential of cement may be either physical or chemical [Atkins and Glasser, 1992]. Blended cements containing BFS and PFA are used in this manner.

1.1.1 Radioactive Wastes in the UK

Radioactivity was discovered at the end of the nineteenth century. Since then, radioactive materials have been used in the areas of military defence, nuclear power, medical treatment, as well as scientific research. Radioactive materials are hazardous because of the emissions associated with radioactive decay [Nirex, 2005]. Although the risk from radioactive materials reduces over time as the total activity decays, some radioactive materials will remain hazardous for hundreds of thousands of years and therefore require long-term isolation.

Radioactive waste is ‘any material that contains or is contaminated by

radionuclides at concentrations or radioactivity levels greater than the exempted quantities established by the competent authorities, and for which no use is foreseen' [McGinnes, 2007]. As a hazardous waste, radioactive waste can harm people and the environment and therefore is carefully controlled. According to the level of radioactivity and the heat produced by this radioactivity, radioactive waste is divided into three main categories, Low Level Waste (LLW), Intermediate Level Waste (ILW) and High Level Waste (HLW), which are described in Table 1-1.

In the UK, the major source of radioactive waste is the nuclear power industry, which includes manufacture of nuclear fuel, nuclear power stations, reprocessing of spent nuclear fuel and research & development programmes. Outside the nuclear power industry, defence activities, medical and industrial sources also contribute to the radioactive waste in the UK [Openshaw et al., 1989].

The 2007 UK Radioactive Waste Inventory reported that the total volume of radioactive waste that exists today and is forecast in the future is 3.4 million cubic metres [NDA and Defra, 2008]. As of April 2007, about 95% (3.2 million m³) of the waste already exists, mainly consisting of contaminated soils, building structures (e.g. concrete and metals), and reactor components (e.g. graphite and metals). The remaining 5% (0.2 million m³) of the radioactive waste has not been produced yet. It is a prediction from the future planned operations of the nuclear power industry, ongoing defence programmes and from the continued use of radioactivity for

medical and industrial purposes [NDA and Defra, 2008].

LLW	Wastes other than those suitable for disposal with ordinary domestic refuse but not exceeding specified levels of radioactivity. Overall, the major components of LLW are soil, building rubble and steel items such as ducting, piping and reinforcement from the dismantling and demolition of nuclear reactors and other nuclear facilities, and the clean up of nuclear sites. However, LLW currently being generated consists mainly of paper, plastics and scrap metal items that have been used in hospitals, research establishments and the nuclear industry.
ILW	Wastes exceeding the upper boundaries for LLW that do not generate sufficient heat for this to be taken into account in the design of waste storage or disposal facilities. The major components of ILW are metal items such as nuclear fuel casing and nuclear reactor components, graphite from reactor cores, and sludges from the treatment of radioactive liquid effluents.
HLW	Wastes in which the temperature may rise significantly as a result of their radioactivity, so this factor has to be taken into account in the design of waste storage or disposal facilities. HLW arises in the UK initially as a highly radioactive liquid, which is a by-product from the reprocessing of spent nuclear fuel.

Table 1-1 Categories of radioactive waste in the UK [Defra, 2008]

The volumes of LLW, ILW and HLW are shown in Figure 1-1. Although the volume of HLW is relatively small, it contains about 95% of the entire radioactivity in radioactive wastes. LLW contains less than 0.01% of the total radioactivity.

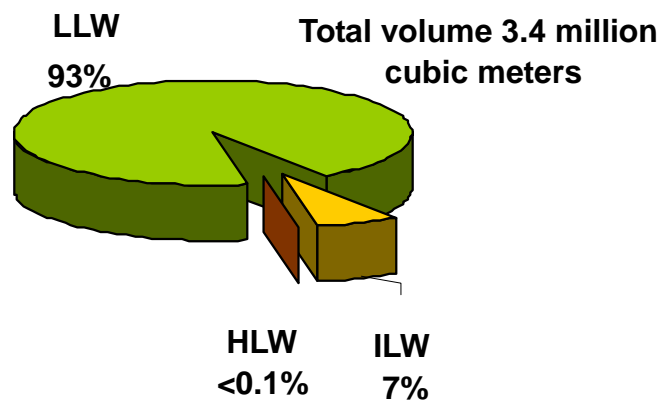


Figure 1-1 Total radioactive waste volumes [NDA and Defra, 2008]

How radioactive waste is dealt with depends on its radioactivity. Currently, most LLW is disposed of soon after it is produced to the national LLW disposal facility near Drigg in Cumbria. ILW is stored in tanks, vaults and drums, with most waste requiring concrete to shield operators from radiation. HLW is stored as liquid in water-cooled, stainless steel tanks or as glass blocks, and needs thick concrete walls to shield operators from the high radiation. [Nirex, 2005] Since much of the ILW and HLW remains a potential hazard for at least tens of thousands of years, it is a challenge to isolate its radioactivity from people and the environment for this length of time.

1.1.2 The Phased Geological Repository Concept for Long-term Management of LLW/ILW

As has been discussed previously, LLW and ILW account for more than 95% of the total volume of radioactive waste in the UK. Although their radioactivity level is too low to release significant heat, they contain enough radioactive materials to require special treatment to minimize any potential release into the biosphere [Gorce and Milestone, 2007]. To provide safe and long-term management for LLW and ILW, the UK Nuclear Decommissioning Authority (NDA) has developed a Phased Geological Repository Concept (PGRC) (Figure 1-2).

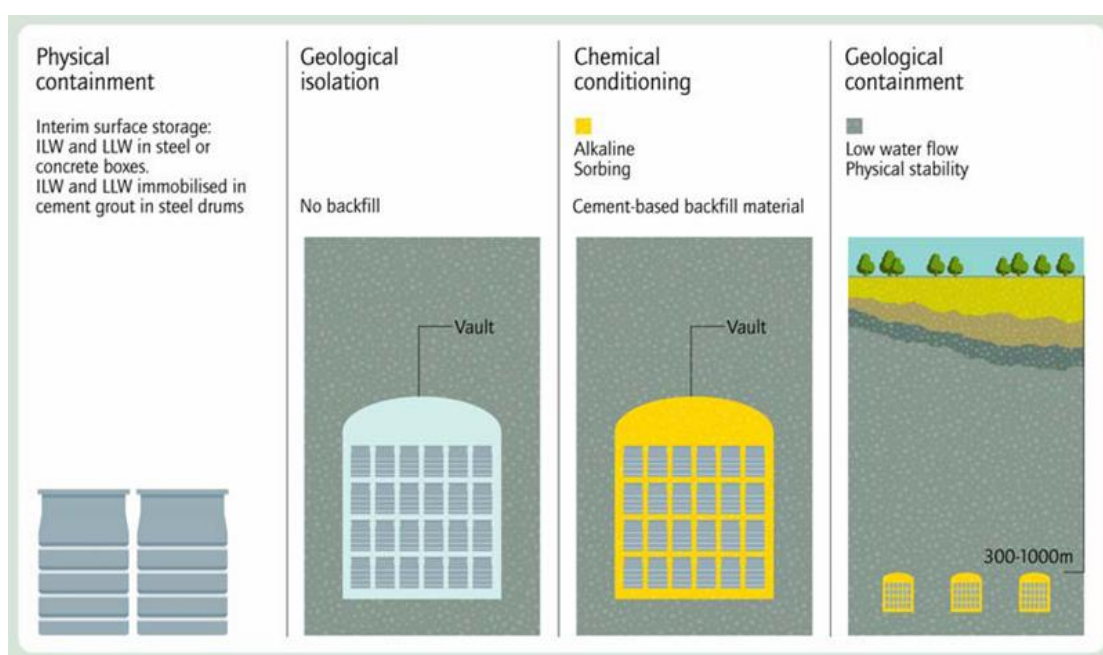


Figure 1-2 Phased geological repository concept [Nirex, 2005]

This concept is based on a deep geological repository situated in a hard rock and

includes a number of stages in the management and eventual disposal of radioactive waste:

Phase 1. Packaging the waste. The wastes would be encapsulated, within a cement-based grouting material within a standardised, highly engineered stainless steel or concrete container, by waste producers;

Phase 2. Surface storage. Packaged wastes would then be held at the site of origin in surface stores that have 50 years design life.

Phase 3. Transport. The waste packages would be transported to a repository.

Phase 4. Waste emplacement. To isolate them from the environment, waste packages would be emplaced in large purpose-built vaults that have been excavated in a stable geological environment deep under ground. This would provide a significant barrier of several hundred metres of rock.

Phase 5. Operational phase. The waste would be stored underground for an extended period (which could be hundreds of years), during which time the repository and its contents would be monitored and the waste would be retrievable.

Phase 6. Vault Backfilling. When and if there is sufficient confidence in the system, the repository vaults could be backfilled with a specially developed cement-based material which would provide one more barrier to the waste.

Phase 7. Post-closure phase. When backfilling has been completed, the repository can be closed and sealed. The multiple barriers would provide long-term containment of radioactivity in the repository without further human management.

1.1.3 Cementitious Materials Used in the PGRC

As described in Section 1.1.2, cementitious materials play very important roles in the PGRC, both as backfill materials and waste encapsulation grouts. The compositions of these materials have been carefully designed to meet the required performance.

Nirex Reference Vault Backfill (NRVB)

Backfill is a material that is used to fill drifts, shafts or other excavated spaces, either in areas more remote from the waste packages or in those areas surrounding waste packages [Francis et al., 1997]. As part of the PGRC, a high porosity cementitious material known as NRVB has been developed.

The NRVB would be a simple and robust engineered barrier to achieve the necessary degree of long-term waste isolation and containment in the PGRC as part of a multi-barrier containment system. The NRVB has been carefully specified to provide a number of benefits:

- 1) **Long-term maintenance of alkaline pore water chemistry.** The NRVB can chemically condition the in-flowing groundwater to high pH for long time scales (>pH 9 maintained for 1 million years [Harris, 1997]) to control the solubility of many important radionuclides and minimise corrosion of steel containers.
- 2) **Long-term maintenance of a high active-surface-area.** C-S-H formed during the hydration of cement has high porosity and can provide a very large surface area onto which many key radionuclides would attach.
- 3) **Relatively high porosity and permeability** to ensure homogeneous chemical conditions (so that localised concentrations of materials in wastes will not exhaust the desired chemical conditioning and thereby locally reduce the containment performance) and to permit the escape of gas generated by chemical reactions within the repository.
- 4) **Long-term reactivity with carbon dioxide.** Consisting of ordinary Portland cement (OPC), hydrated lime and limestone flour, the NRVB would remove carbonates from incoming groundwater and both non-active and ^{14}C -containing CO_2 produced from the degradation of particular radioactive wastes, such as graphite, cellulose and irradiated metals, by forming low solubility carbonates.

Waste Encapsulation Grouts: BFS/OPC Grout and PFA/OPC Grout

Current expectation is that most ILW would be immobilized and packaged in

containers (**Figure 1-3**), so that the waste packages are suitable for surface storage, transport to the repository and storage underground in a phased geological repository. The package full of immobilized waste provides a physical containment which is the first of the multiple barriers. At the backfill stage, the grouts would complement the NRVB in pH buffering and $^{14}\text{CO}_2$ absorption.



Figure 1-3 Standard ILW packages [Nirex, 2005]

Blended cement based on the partial replacement of Ordinary Portland Cement (OPC) by waste materials is currently used for encapsulation of nuclear waste in the UK. The preferred replacement materials are pulverised fuel ash (PFA) and blast furnace slag (BFS). Up to 75% PFA and 90% BFS, respectively, are employed in encapsulation grouts, which are much higher values than those used in the construction industry [Harris, 1997 and Borges et al., 2010]. These percentages are selected to help reduce the heat released during cement hydration and avoid thermal

cracking. Pastes of these percentages also have appropriate rheology in the liquid state, suitable for mixing with the waste and pouring into the encapsulation drums. 1:1 or 3:1 PFA/OPC and 3:1 or 9:1 BFS/OPC are commonly used mixtures [Harris, 1997].

1.2 Research Objectives & Structure of the Thesis

The reaction between CO_2 and cementitious materials can occur in every stage of the long-term management of radioactive wastes. The sources of CO_2 can be the gaseous CO_2 in the atmosphere, the gaseous CO_2 from the degradation of certain radioactive wastes and the $\text{CO}_2(\text{aq})$ in the groundwater. Radioactive ^{14}C -containing CO_2 will be generated by the degradation of particular components in the wastes, such as graphite, irradiated metals, and organic materials [Harris, 1997]. The benefit of carbonation is that the $^{14}\text{CO}_2(\text{g})$ generated will be absorbed by the calcium component of the cement, thereby preventing the release of $^{14}\text{CO}_2$ to the biosphere. The down side of the carbonation is that it may affect the maintenance of a high pH environment over long timescales. Therefore, in order to predict the long term performance of NRVB and encapsulation grouts, it is important to understand the rate of carbonation for these materials, as well as the property changes caused by carbonation.

Carbonation of cement and reinforced concrete has been studied exclusively since the 1950s in order to evaluate the performance and to predict the service life of concrete buildings and constructions [Parrott, 1987]. In recent decades, as the development of solidification/stabilisation technology of hazardous wastes has progressed, carbonation of blended cements has also been widely investigated [Borges et al., 2010, Fernández Bertos et al., 2004 and Lange et al., 1998]. According to these studies, the rate of carbonation largely depends on the environmental condition, to which the cementitious materials are exposed. Since the NRVB and encapsulation grouts would be buried in repositories deep underground, the pressure inside the repository could be as high as 7 MPa. Moreover, during backfilling, heat would be generated due to the hardening of the NRVB and the temperature in the repository could reach up to 80 °C. Although a great amount of research has been done on the carbonation of cementitious materials under moderate conditions, the data cannot be applied directly to all the conditions expected in a repository.

A number of studies have been conducted to investigate the properties of NRVB and grouts. Harris [1997] assessed the pH buffering provided by NRVB, PFA/OPC and BFS/OPC grouts. McCarter et al. [2004] investigated the hydration and drying of NRVB. Preliminary studies on the carbonation kinetics of NRVB and 3:1 BFS/OPC were also conducted [Harris et al, 2002 and Harris et al. 2003]. However, there are still uncertainties in quantifying the carbonation of NRVB and grouts:

- How fast will the reaction be? Is there enough time for the generated gases to react with the NRVB before being released from the repository?
- Do the products of the carbonation reaction restrict access to the amount of NRVB available for further carbonation?
- Are there enough alkaline components in the repository to maintain the high pH?

In this work, single dimensional carbonation experiments of NRVB, 3:1 PFA/OPC, and 3:1 BFS/OPC were carried out in batch reactors with the following objectives:

- To determine the effects of exposure conditions on the rate of carbonation for NRVB and both grouts.
- To understand the effect of carbonation on the pH, chemistry, and microstructure of the materials.
- To determine the carbon dioxide uptake capacities of the materials.
- To model the rate of carbonation based on the experimental results to provide an indication of the time required for the carbonation reaction to occur.

Apart from Chapter 1 Introduction and Chapter 6 Conclusions & Future Work, this thesis consists of four major chapters.

In Chapter 2, a fundamental literature review is presented. The compositions, properties and application of cementitious materials are introduced. The

carbonation reaction mechanism and the impact of carbonation on the properties of cementitious materials are reviewed.

Chapter 3 is the detailed description of materials and equipment, as well as the experimental procedures.

In Chapter 4 the experimental results of the carbonation test on NRVB, 3:1 PFA/OPC grout and 3:1 BFS/OPC grout are shown and discussed. The work reported for each material includes the effect of moisture conditioning, the effect of exposure conditions, the observation of carbonation profiles and the major physical and chemical changes due to carbonation reaction.

In Chapter 5, a diffusion-controlled model is developed based on Fick's first law of diffusion. The model is adapted to the carbonation test data of each material and a mathematical expression is developed to describe the reaction progress of each material.

2 A REVIEW OF CEMENT AND CARBONATION

2.1 Definition of Cement

Cement may be defined as an adhesive material that sets and hardens independently, and can bind stones, bricks, etc. when used in the construction of buildings and engineering works. Although cements with different compositions and properties have been developed for different applications, their principal constituents are compounds of lime, but they may also include certain allied compounds of magnesium [Blezard, 1998]. Cements used in construction are characterized as non-hydraulic or hydraulic, according to their strength gaining mechanism.

Non-hydraulic cements were the first form of cement invented in cement history, thousands of years ago [Blezard, 1998]. Non-hydraulic cements cannot harden while in contact with water. They set only by drying out, and gain strength very slowly by absorption of carbon dioxide (CO_2) from the atmosphere to form calcium carbonate. Non-hydraulic cements are rarely used in modern construction due to long periods of setting and drying.

Most construction cements today are hydraulic. Hydraulic cement is a hydraulic

binder, i.e. a finely ground inorganic material which, when mixed with water, forms a paste that sets and hardens by means of hydration reactions and processes and which, after hardening, retains its strength and stability, even in contact with water [Jackson, 1998]. The mechanisms of cement hydration and hardening will be reviewed later in this chapter. The ability to set and harden quickly, and gain greater relative strength, makes hydraulic cement the main cement utilised in modern day construction, the most common form of which is Portland cement.

2.2 Portland Cements: History, Manufacture and Mineral Composition

The main form of cement used in construction worldwide today is the hydraulic cement called Portland cement. Portland cement is made by heating a limestone and clay mixture in a kiln and pulverizing the resultant clinker.

The name ‘Portland’ originates from a trade name used by Joseph Aspdin in 1824 to describe the new cement he patented that year in England. He claimed the colour of the hardened product was similar to Portland stone, a high-quality limestone used in construction during that time period [Bensted, 1997; Lawrence, 1998].

Portland cement is a finely ground grey powder, with a very complex mineral composition, but made from very simple raw materials containing calcium oxide

(CaO), silica (SiO₂), aluminum oxide (Al₂O₃), and iron oxide (Fe₂O₃). The raw materials, usually limestone and clay, are heated in a kiln to 1400 – 1600° C, the temperature at which these materials chemically interact to form the compound collections called ‘clinker’. The clinker is then ground with a small amount of gypsum (CaSO₄ 2H₂O) (around 4-5%) to produce Portland cement [Afcin, 2000; Bensted, 1997; Jackson, 1998; Lawrence, 1998].

Portland cement is considered to consist of at least five principal chemical compounds (or phases), as listed in **Table 2-1**. These compounds are sometimes referred to by the chemical shorthand notation utilising the cement chemical nomenclature system.

Name	Formula	Nomenclature system*
Tricalcium silicate (alite)	3CaO SiO ₂	C ₃ S
Dicalcium silicate (belite)	2CaO SiO ₂	C ₂ S
Tricalcium aluminate	3CaO Al ₂ O ₃	C ₃ A
Tetracalcium aluminoferrite	4CaO Al ₂ O ₃ Fe ₂ O ₃	C ₄ AF
Calcium Sulfate Hydrate (gypsum)	CaSO ₄ 2H ₂ O or CaO SO ₃ 2H ₂ O	C $\overline{\text{S}}$ H ₂

*Shorthand notation routinely used by cement chemists using abbreviations for the oxides: CaO = C;

SiO₂ = S; Al₂O₃ = A; Fe₂O₃ = F; SO₃ = $\overline{\text{S}}$, CO₂ = $\overline{\text{C}}$ and H₂O = H.

Table 2-1 Mineral composition of Portland cement

The five main compounds may be present in different proportions and ground to

different fineness, resulting in slightly different chemical and physical properties for Portland cement. According to their properties and performance, five basic types of Portland cement have been standardised by the American Society for Testing and Materials (ASTM) [ASTM, 1995]. Table 2-2 lists these cements and their typical compositions.

Cement Type	Performance	C₃S	C₂S	C₃A	C₄AF	Fineness, m²/kg
I	General purpose	55	19	10	7	370
II	Moderate sulfate resistance	51	24	6	11	370
III	High early strength	56	19	10	7	540
IV	Low heat of hydration	28	49	4	12	380
V	Sulfate-resistant	38	43	4	9	380

Table 2-2 Typical compound compositions of Portland cement [ACI, 2001]

It is useful to point out here that Type I is also known as ordinary Portland Cement (OPC). OPC is suitable for all uses except where the special properties of the other types are required. OPC is used in most construction, such as buildings, culverts, reservoirs and masonry units. As stated in section 1.1 of this thesis, OPC has been selected in the UK as the binding component of the NRVB and encapsulation grouts.

2.3 Hydration of Portland Cements

In cement chemistry, hydration refers to the reaction of hydraulic cement with water.

Hydration, associated with both chemical and physico-mechanical changes of the system, causes Portland cement hardening and strength development [Odler, 1998].

The hydration of Portland cement is a rather complex process and has been studied for decades [Bensted, 1997; Matschei *et al.*, 2007; Odler, 1998; Papadakis *et al.*, 1992; Wang and Lee, 2009]. The main hydration reactions are summarised here:



C_3S is the main and most important constituent of Portland cement, as it controls setting and hardening. The hydration of C_3S is a complicated process and is still not fully understood. As products of hydration at ambient temperature, calcium hydroxide ($Ca(OH)_2$, abbreviated CH) and an amorphous calcium silicate hydrate (C-S-H) phase are formed. According to Groves *et al.* (1990), two distinct morphologies of C-S-H gel were present in C_3S paste: a homogeneous and particulate ‘inner product’ C-S-H, developed as hydration shells within the original

boundaries of the cement grains, and an fibrillar or needle-like ‘outer product’ C-S-H formed by through-solution deposition in the originally water-filled space. CH crystals are formed in pore solutions and well bonded to outer product C-S-H fibrils. The morphology of the hydration products are also shown in Figure 2-1. $x\text{CaO} \cdot y\text{SiO}_2 \cdot z\text{H}_2\text{O}$ is the general formula of C-S-H, where both x and y may vary over a wide range [Fuji and Kondo, 1974; Parrot *et al.*, 1984; Richardson and Groves, 1993]. It is believed that below 100 °C, C-S-H has a C/S ratio of less than 3.0, and the approximate typical stoichiometry is $\text{C}_3\text{S}_2\text{H}_3$ ($3\text{CaO} \cdot 2\text{SiO}_2 \cdot 3\text{H}_2\text{O}$).

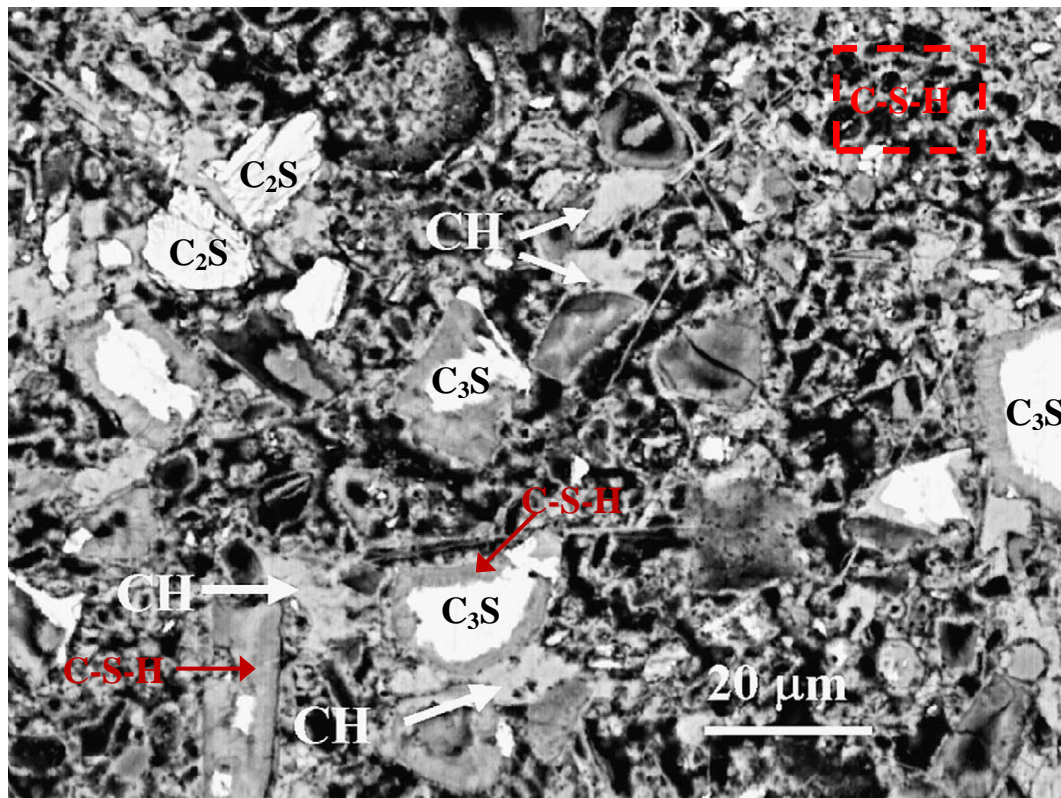


Figure 2-1 An area from a 7-day old w/s 0.45 cement paste, cured at room temperature [Diamond, 2004]

C_2S is another significant component of Portland cement. The cross-hatched appearance (as shown in Figure 2-1) is the characteristic of partially hydrated C_2S . Besides C-S-H, calcium hydroxide (CH) is also formed during the hydration of C_2S ; however, its amount is significantly lower than that existing in C_3S pastes with the same degree of hydration [Odler, 1998].

C_3A is much more reactive than C_3S and C_2S and could, on occasion, lead to premature stiffening (flash set) when first mixed with water [ACI, 2001]. However, in the presence of calcium sulphate, the hydration rate of C_3A can be slowed down distinctly. Therefore, gypsum ($\overline{C S H_2}$) is added to the Portland cement clinker, for the purpose of controlling the setting characteristics of C_3A . Equation (2.3) describes this reaction: in the presence of gypsum, entringite ($C_6A \overline{S}_3 H_{32}$ or $6CaO \cdot Al_2O_3 \cdot 3SO_2 \cdot 32H_2O$) is formed as the main hydration product of C_3A . After all the available amount of gypsum is used, Equation (2.4) takes place, yielding calcium aluminate monosulfate hydrate ($C_4A \overline{S} H_{12}$ or $4CaO \cdot Al_2O_3 \cdot SO_3 \cdot 12H_2O$).

The hydration products formed in the hydration of C_4AF are similar in many respects to those formed from C_3A . However, the rate of reaction is slower.

The hydration products described above give hydraulic cement its strength and stability. The C-S-H phase is the main product of Portland cement hydration and is also the main structure that produces strength. CH is the second most abundant

product. Although it has very little effect on the generation of strength, it is the main component that acts as a buffer to maintain the high pH of cement.

2.4 Pozzolans and Pozolanic Reaction

Pozzolans are inorganic materials that harden in water when mixed with calcium hydroxide or with materials that can release calcium hydroxide (e.g. Portland cement clinker) [Massazza, 1988]. Pozzolans are composed of the same main oxides as the clinker and OPC, but in different proportions and mineralogical compositions [Papadakis et. al., 1992]. Generally, pozzolans are rich in quartz (SiO_2) and poor in CaO, whereas clinker and OPC are rich in CaO and poor in SiO_2 .

Pozzolanic activity can be described by the following reaction:



When mixed with Portland cement and water, SiO_2 in Pozzolan reacts with the calcium hydroxide formed during hydration of the calcium silicates. The simultaneous presence of Portland cement and pozzolans modifies the respective reactions of hydration and improves the quality of concrete, both in terms of strength and durability.

The first known pozzolan was pozzolana, a volcanic ash, for which the category of

materials was named. The most commonly used pozzolan today is fly ash, though silica fume, ground granulated blast furnace slag, and other materials are also used as pozzolans.

Pozzolans are commonly used as an addition to Portland cement concrete mixtures to increase the long-term strength and other material properties of Portland cement concrete and in some cases reduce the material cost of concrete.

2.5 Blended Cements

Portland cement can be blended or interground with other materials to achieve certain properties. Blended cements are common in European countries because they require less energy to manufacture, they can be made of by-product materials that would normally be disposed of in landfill sites, thus reducing solid waste volumes, and offer performance benefits for certain applications. Fly ash and blast furnace slag blends are two of the most common blends of Portland cement [Lawrence, 1998].

2.5.1 Portland-Fly Ash Blend

Fly ash is a fine residue resulting from the burning of powdered coal at high temperature. The fly ash can be divided into two categories based on its calcium

content [Jackson, 1998; Wang and Lee, 2009]. The ash containing less than 10% of analytical CaO is known as low-calcium fly ash (Class F), which is a general product from the combustion of anthracite and bituminous coals. High-calcium fly ash (Class C), typically containing 15-40% of analytical CaO, is a product from the combustion of lignite and subbituminous coals. The low-calcium fly ash is a normal type of pozzolan that consists of silicate glass and is modified by aluminium and iron, and has become the predominant pozzolan in use throughout the world due to technical benefits and economic factors.

Fly ash of suitable fineness (similar or smaller than cement particles) and composition can be used to replace 20 to 50% volume of Portland cement. Applications using up to 70% have been successful [ACI, 2001]. However, various standards and codes have generally limited the use of fly ash to between 10% to 25% in structural concrete [Wang and Lee, 2009], as a higher portion of replacement may reduce the early strength of concrete.

Extensive literature is available on the effects of fly ash in both fresh and hardened concrete [Lawrence, 1998; Matschei *et al.*, 2007]. Table 2-3 is the summary of the benefits that can arise.

Fresh Concrete	Hardened Concrete
Increased paste volume	Increased strength (long-term)
Filled aggregate voids	Minimal effect on modulus of elasticity
Improved pumpability	Variable effects on creep and shrinkage
Extended set time	Decreased permeability
Decreased early rate of strength gain	Improved durability
Reduced heat evolution	

Table 2-3 Effects of fly ash on fresh and hardened concrete

2.5.2 Portland-Blast Furnace Slag Blend

Blast furnace slag (BFS) is made by rapid cooling of slag melt of suitable composition, as obtained by smelting iron ore in a blast furnace [Jackson, 1998]. The chemical composition of BFS is CaO (30%-50%), SiO₂ (28%-38%) and Al₂O₃ (8%-24%) [Moranville-Regourd, 1998]. In terms of its mineralogy, BFS is usually melilite (a solid solution series of gehlenite, 2CaO.Al₂O₃.SiO₂, and akermanite, 2CaO.MgO.2SiO₂), with a small amount (<1 per cent) of calcium sulphide (oldhamite). Sometimes merwinite (3CaO.MgO.2SiO₂) is also present and more rarely dicalcium silicate 2CaO.SiO₂ [UK Environment Agency, 2007].

Finely ground granulated blast furnace slag (GGBFS) possesses hydraulic cementitious properties and is commonly used in conjunction with Portland cement.

According to the cementitious activity of GGBFS, the characteristics of the Portland cement and the properties desired in the concrete, the common replacement dosages of GGBFS to cement is between 5 and 70% by mass.

It is difficult to compare the performance of concrete containing only Portland cement with concrete containing BFS. Chemical and physical characteristics of the BFS and of the Portland cement, BFS dosage, temperature, curing, and other factors can all affect the concrete properties. Generally, with high dosage of GGBFS added, concrete will have lower heat of hydration, longer time of setting, lower strength at early ages and lower permeability. Concrete containing GGBFS dosages greater than 35% by mass of cementitious materials also demonstrate an improvement in the resistance to sulphate attack.

2.6 Carbonation of Cementitious Materials

2.6.1 Introduction

Carbonation of cementitious materials normally involves a chemical reaction between atmospheric carbon dioxide and the products of cement hydration. The main cement hydrates, i.e. calcium silicate hydrate, calcium hydroxide and various calcium aluminate or ferro-aluminate hydrates, react to produce calcium carbonate, silica gel and hydrated aluminium and iron oxides, while the sulphate originally

present in the cement reverts to gypsum after complete carbonation [Parrott, 1987].

Although the carbonation of cement generally leads to an increase in its compressive strength [Groves *et al.*, 1990], it is one of the major physico-chemical processes that can limit the lifetime of reinforced concrete structures by reducing the protection of the interior steel bars from corrosion [Meier *et al.*, 2007]. Concrete prevents steel reinforcement from corrosion by forming a high alkalinity, protective oxide film. Chemical reactions due to the penetration of carbon dioxide into the cement matrix reduce the alkalinity of this passive oxide film and the steel becomes susceptible to corrosion caused by moisture and aggressive species (e.g. Cl^- , SO_4^{2-} etc.).

Carbonation has been one of the major areas in cement and concrete research since the 1950s. A review of the carbonation reactions in cementitious materials follows.

2.6.2 Description of Reaction Process

In general, carbonation of cement can be described as ionised CO_2 inducing solvation of calcium ions from the solid phase, which then re-precipitate in the pore space of the mixture as CaCO_3 , forming a solidified product [Fernández Bertos *et al.*, 2004].

The reaction between the solid and the CO_2 takes place on the surface of the solid

when water exists. This means that the reaction depends on the chemical adsorption of the CO_2 . The carbonation reaction is based on the following sequential mechanism:

1st) Diffusion of $\text{CO}_{2(g)}$ in the gaseous layer surrounding the solid

2nd) Diffusion of $\text{CO}_{2(g)}$ through the solid

3rd) Solvation of $\text{CO}_{2(g)}$ to $\text{CO}_{2(aq)}$ in the pore water

4th) Hydration of $\text{CO}_{2(aq)}$ to $\text{H}_2\text{CO}_{3(aq)}$

5th) Ionisation of H_2CO_3 to H^+ , HCO_3^- and CO_3^{2-}

6th) Dissolution of calcium containing phases to Ca^{2+}

7th) Nucleation of $\text{CaCO}_{3(s)}$

8th) Precipitation of solid phases

2.6.3 Carbonation of Hydrated Cement

The principal source of calcium ions in hydrated Portland cement is Ca(OH)_2 . Other hydration products are also capable of releasing calcium ions under certain conditions. The chemical reactions which characterise the carbonation reactions are described in this section.

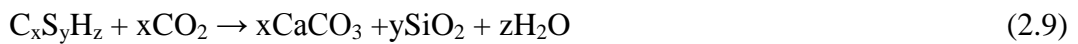
Equation (2.7) is the chemical process that characterises the carbonation reaction of Ca(OH)_2 . It is an irreversible exothermic reaction, which releases around 7.7 kJ/mol of heat [Richardson, 1988].



While Ca(OH)_2 plays a predominant role in the carbonation process, other constituents of the hydrated compound can be further converted. As shown in Equation (2.8), carbonation changes the composition of C-S-H gel by depleting its calcium content [Young *et al.* 1974].



As the reaction goes on, the C/S ratio keeps decreasing until the C-S-H is completely decalcified and finally transformed into calcium carbonate and highly polymerised silica gel (Equation (2.9)) [Richardson, 1988; Thiery *et al.*, 2007]. This gel is acid stable and maintains a similar morphology to the original hydrate (Yousuf *et al.* 1993).

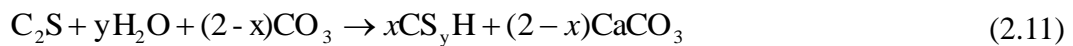
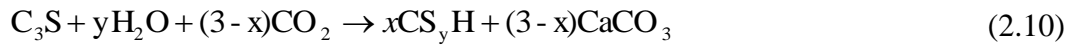


C-S-H appears to decompose into calcium carbonate by a pseudomorphous reaction that results in no change in morphology, whereas Ca(OH)_2 is believed to first dissolve into the water phase where it reacts with dissolved carbon dioxide and precipitates as calcium carbonate [Reardon, et al. 1989].

Apart from Ca(OH)_2 and C-S-H, small amounts of hydrated calcium aluminates (CAH), ferrites (CFH) and related complex hydrated salts that exist in the cementitious system can also be carbonated and decompose with the ultimate formation of CaCO_3 , hydrated silica and alumina, ferric oxide and hydrated calcium sulphate. CO_2 attacks Ca(OH)_2 first and will not attack the other compounds until the pH has dropped below 12.4 – the value for a saturated calcium hydroxide solution [Richardson, 1988].

Carbonation of Unhydrated Cement

It is also worth mentioning that carbonation can accelerate the hydration process of cement by converting C_3S and C_2S into CaCO_3 and C-S-H:



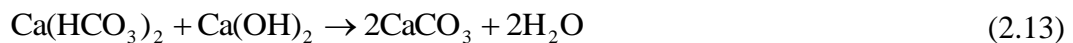
Therefore, the carbonation of unhydrated cement and fully hydrated cement are different reactions. We will be concerned only with the latter in the work reported here. Because comparing with the carbonation of NRVB and waste grouts, which would continue for hundreds of years, hydration reaction only happens in the early stage of radioactive waste storage.

Formation of Bicarbonate

Some authors believe that when water contains aggressive CO₂, the calcium carbonated in the outer layer dissolves to form the bicarbonate:



Some of the bicarbonate is washed out but some of the solution penetrates to combine with Ca(OH)₂ to form CaCO₃:



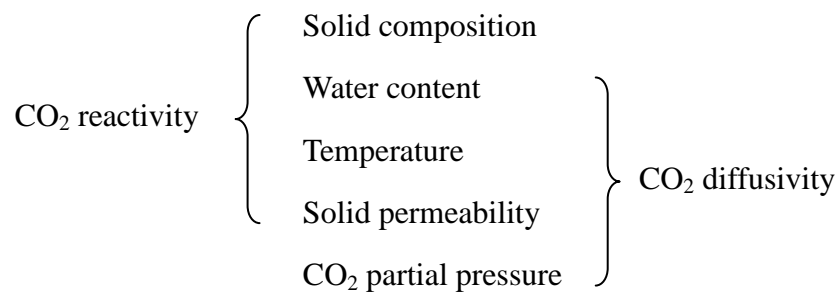
However, the minimum CO₂ level for the formation of bicarbonate is still unclear. It has been indicated that Ca(HCO₃)₂ might only occur in accelerated tests, where abundant amounts of CO₂ and water are available [Richardson, 1988].

In conclusion, the principal carbonation reaction is the conversion of Ca(OH)₂, and, to a lesser extent the C-S-H, to CaCO₃. The mechanism of reaction requires the dissolution of gaseous CO₂ into the pore water and involves the formation of a weak carbonic acid, which dissociates into hydrogen and carbonate ions. Carbonation of other hydroxides and hydrated compounds is possible, but plays a small part in the overall process. The amount of carbon dioxide needed to carbonate fully hydrated cement can be calculated from the oxide composition of the original

cement [Parrott, 1987].

2.6.4 Factors Influencing Carbonation

The main factors influencing the extent and quality of carbonation can be summarised to two aspects: reactivity and diffusivity of CO₂ [Fernández Bertos, 2005]. For a fully hydrated cementitious system, the following is a scheme of what these main factors are dependent on.



i) Solid Composition

The composition of the solid phase can give an idea of the extent of carbonation that can be achieved [Steinour, 1959]. The reactive calcium species in the cement (e.g. Ca(OH)₂, C-S-H, CAH) are the major phases participating in the carbonation reactions. However, for cements blended with PFA or BFS, other phases (e.g. Mg(OH)₂, K(OH) and Na(OH)) may also contribute to the carbonation through a variety of reaction pathways [Meier *et al.*, 2007].

The theoretical maximum CO₂ uptake capacity upon carbonation can be calculated as a function of the chemical composition of the original material using Huntzinger's formula [Huntzinger *et al.*, 2009], given in equation (2.14). This formulation assumes that all the magnesium oxide, sodium oxide, potassium oxide, and all the calcium oxide in the cement excluding that in calcium carbonate and calcium sulfate, are available to react with carbon dioxide to form carbonates. By comparison to the reaction achieved, it can give a measure of the effectiveness of carbonation for the particular solid and conditions used.

$$\begin{aligned} \%CO_2 \text{ (w/w)} = & 0.785(\%CaO - 0.56 \%Ca(CO_3) - 0.7 \%SO_3) + \\ & 1.091 \%MgO + 0.71 \%Na_2O + 0.468 \%K_2O \end{aligned} \quad (2.14)$$

ii) Water Content

Water content is the amount of free water existing in the pores of the solid matrix. It is an essential factor affecting the reactivity and diffusivity of carbon dioxide. The water takes part in the solvation and hydration of the CO₂. It also dissolves the Ca²⁺ ions from the solid that will react to form the CaCO₃ [Fernández Bertos, 2005]. With insufficient water, the CO₂ and calcium hydroxide will not be fully ionised, whereas too much water limits the reaction due to the blockage of the pores in the solid as the diffusivity of CO₂ is 10⁴ times smaller in water than in air [Denny, 1993]. Due to the differences of porosity and CO₂ uptake capacity, different cementitious systems require different water contents in order to achieve the same

degree of carbonation [Lange et. al., 1996].

The water content of a porous material depends on its pore structure as well as external relative humidity. When exposed to an environment with certain relative humidity, moisture exchanges occur between the atmosphere and the pores until a balance is formed. The free water left in the solid material tends to form a liquid film on the wall of large pores and fill the space of small pores. The relationship between the external relative humidity and the pore size that will remain saturated at that humidity is defined by the Kelvin equation [Comite, 1982]:

$$r = \frac{-2\gamma M \cos\theta}{\rho_w RT \ln H} \quad (2.15)$$

where r is the pore radius (m),

γ is the surface tension of water (0.076 N m^{-1}),

M is the molecular mass of water ($0.018 \text{ kg mol}^{-1}$),

θ is the contact angle of the interface with the capillary walls,

ρ_w is the density of water (1000 kg m^{-3}),

H is the external relative humidity.

For simplicity, the contact angle between water and solid is assumed to be 0° and

Equation (2.15) can be reduced to:

$$r = \frac{-2 \times 0.076 \times 0.018}{1000 \times 8.314 \times 273 \times \ln H} \approx -\frac{10^{-9}}{\ln H} \quad (2.16)$$

The Kelvin equation strictly applies to capillaries of uniform dimension and when applied to cementitious systems can only provide qualitative estimates, due to the rather complex pore geometries.

According to Equation (2.16), when the external relative humidity is zero, the water content in the cementitious material is also zero and carbonation reactions cannot proceed. When the external relative humidity is 100%, the material is fully saturated, as all the pores are filled with water which blocks the diffusion pathway of CO₂. Therefore the external relative humidity has a considerable and important influence on the rate and ultimate extent of carbonation [Verbeck, 1958]. A lot of experimental work has been done to determine the optimum external relative humidity. For most cementitious materials, carbonation is more rapid at an external relative humidity of 50%-60% [Fattuhi, 1998; Goñi and Guerrero, 2003; Verbeck, 1958]. At 50%-60% relative humidity, the equilibrium water content in the solid tends to reach optimum for the carbonation reaction.

Temperature

As temperature goes up, the diffusivity of CO₂ increases due to increased energy [Song *et al.*, 2006]. However, the solubility of carbon dioxide and calcium hydroxide decrease with increasing temperature and the decreasing solubilities

cause a decrease in the carbonation rate. The optimum reaction temperature for the highest carbonation rate is found to be at 20 °C for lime mortar [Van Balen and Van Gemert, 1994]. Liu *et al.* [2001] found that for lightweight concrete waste, the uptake of CO₂ increased with increasing temperature up to 60 °C (at atmospheric pressure).

Solid Permeability

The ingress of carbon dioxide into a cementitious system is a diffusion phenomenon. Different from diffusion in the atmosphere, the diffusion rate of CO₂ in the cementitious system will depend on the size of the pores and the tortuosity of the flow path. High porosity may lead to higher CO₂ diffusivity. CO₂ will not flow in pores whose diameter is smaller than 0.2 nm [Richardson, 1988]. Therefore, the relative permeability of the pore structure has more often been used to describe the fluid diffusivity in the pore structure.

Table 2-4 shows the effects of the solid properties on permeability of hydrated materials.

Partial Pressure of CO₂

The rate of material transfer depends on both the permeability and pressure gradient. As a result, the concentration of CO₂ is identified as a very important factor in the subsequent rate of carbonation achieved. A high concentration of CO₂ increases the

diffusion rate of CO₂ into the cementitious matrix, and hence increases the carbonation rate.

Property	Effect on permeability
Cement content	Higher cement content improves resistance to carbonation. Although the concentration of alkali is proportional to the cement content, the permeability may be decreased by increasing the cement content.
Aggregate Characteristics	Light weight coarse aggregate concrete is more vulnerable to carbon dioxide than dense fine aggregate concrete. As light weight aggregate creates high porosity which may lead to higher permeability.
Curing	In the context of carbonation the two fold benefit of curing has been recognised as decreased permeability and increased reserve basicity. A longer curing time produces a decrease in permeability.
Density	A trend towards decreased average depths and rates of carbonation is noticeable for higher density concrete.
Strength	A progressive decrease in the higher carbonation rate is noticeable for higher strength concretes [Khunthongkeaw et. al., 2006].
Surface quality	Carbonation is a phenomenon which affects the exposed surfaces. The permeability of a cast surface is much lower than that of a cut surface. On the other hand, due to the migration of cement towards the surface, at cast surface the cement content is higher.
Water/cement ratio	Water/cement ratio is a more critical factor in carbonation than the cement content. When water/cement ratio is low, the capillary pores are not capable of retaining contact with each other because their quantity and volume are reduced. As a result, the permeability of the concrete is also lower, which makes it more difficult for carbonation to proceed [Richardson, 1988].

Table 2-4 Factors influencing the permeability of hydrated cementitious materials

However, the use of a high concentration of CO_2 also increases the water content in the pores because of the high rate of reaction and evolution of water within the specimen. Therefore, with thin specimens at the optimum relative humidity, carbonation in low concentrations of CO_2 would be expected to proceed faster than in high concentrations.

Slight increases of CO_2 partial pressure in the atmosphere will accelerate the rate of reaction and influence the strength development. However, experimental work shows that increases in pressure from 1 to 2 atm have been found to increase the rate of the carbonation reaction for compacted cement mortars, whilst a further increase to 4 atm had little effect [Young et. al., 1974].

2.6.5 Impacts of Carbonation on Cementitious Systems

Apart from the effect of carbon dioxide on $\text{Ca}(\text{OH})_2$, C-S-H and other CO_2 reactive compounds, carbonation has been noted to influence other material properties and effects. Some of the major effects are introduced in this section.

Effect on pH Profile

One of the impacts of carbonation on cementitious materials is the change in the pH profile. The pore water has a solvent action on cementitious materials. The

dissolution of the Ca(OH)_2 and C-S-H buffer the pH of pore solution in equilibrium with the cementitious materials to values between 10.5 to 12.5 [Harris, 1997]. The corresponding total calcium (Ca^{2+} and $(\text{CaOH})^+$ ions) concentration in the saturated solution is approximately 0.02mol. The ingress and reaction of carbon dioxide leading to carbonation of calcium ions in the pore water and subsequently further dissolution of Ca(OH)_2 and C-S-H. The consumption of Ca(OH)_2 and C-S-H leads to a drop of pH values. A totally carbonated layer will have a pH of about 8.3 [Harris, 1997].

Effect on Physical Properties

Although carbonation may affect a wide range of structural properties, it would appear that the fundamental influence is to decrease the pore volume and permeability of cementitious system. Based on the calculation using specific gravities and molar volumes for Ca(OH)_2 and CaCO_3 , each mole of calcium hydroxide is converted to the carbonate with a consequent 11.8% increase in solid volume (Fernández Bertos, 2005). When CaCO_3 is precipitated in the pore structure, the increase in volume will lead to structural changes.

Table 2-5 shows the consequences of carbonation in a solid material.

Characteristic	Consequence
Density	CO ₂ is chemically bound as CaCO ₃ , which causes the increase in solid density. Livtvai stated that carbonation can increase the density of concrete by 1% to 4% [Richardson, 1988].
Porosity	The precipitation of the calcium carbonate produced by carbonation can lead step by step to a clogging of the pores. Rigo de silva et al. [2002] found a reduction of 5-12% of the open porosity of concrete provoked by carbonation. Another study showed a decrease of up to 26% in the pore volume of a cement-solidified waste system [Hills et. al., 1999].
Tortuosity and pore size distribution	The blockage of the pore space leads to an increase in the amount of small pores and the tortuosity of the carbonated solid.
Shrinkage	Carbonation will cause shrinkage of cementitious material (Verbeck, 1958). This may due to the evaporation of water generated from the carbonation reaction [Richardson, 1988].
Cracks	Because various kinds of restraint prevent the hardened cementitious material from contracting freely, cracking would be developed as a result of carbonation shrinkage.

Table 2-5 Variations in certain physical properties due to carbonation

2.6.6 Methods to Examine the Carbonation Products

To evaluate the carbonation in the concrete or other cementitious materials, various experimental methods are available. The most commonly used methods are described as follows:

pH Indicator

The most well known and easiest to use a pH indicator like phenolphthalein sprayed on the freshly broken surface of a given sample. In the non-carbonated part of the specimen where pore water is still highly alkaline, purple-red colouration is obtained, while in the carbonated part of the specimen, where due to the carbonation the alkalinity is reduced and no colouration occurs. In this way, it is possible to define a depth of carbonation related to the pH value of the interstitial solution. However, there is some concern over the accuracy of this method as carbonation is more complex than generally assumed.

Scanning Electron Microscopy (SEM)

SEM is one of the most versatile instruments available for the examination and analysis of the microstructural characteristics of solid objects [Tawabini, et al. 1995]. The SEM is a type of electron microscope that images a sample by scanning it with a high-energy beam of electrons in a raster scan pattern. The secondary electron imaging (SEI), uses the lower energy electrons emitted from the sample surface, and is the most commonly used detection mode. By SEI, the SEM can produce high-resolution images of a sample surface, revealing details of better than 100-200 Å for bulk specimens. Another detection mode is back scattered electron (BSE) detection which is used to obtain contrast between areas with different chemical compositions. BSE are often used in analytical SEM in conjunction with use of spectra obtained from characteristic X-rays.

Fresh fractures of hydrated cementitious materials can be observed by SEM. [Tam, et al., 2005 and Sauman, Z., 1971] Different forms of calcium carbonates and carbonated C-S-H can be revealed by such methods.

X-Ray Diffraction (XRD)

XRD is an indispensable technique for investigation of the crystal structure of solid matter. In principle, a beam of X-rays incident to a material is partly absorbed and partly scattered, and the rest is transmitted unmodified. Because a crystal is an ordered structure consisting of planes of atoms, incident X-rays undergo diffraction. The X-ray diffraction pattern of a pure substance is like a fingerprint of the substance; and in a mixture of substances each component produces its pattern independently of the others [Tawabini, et al., 1995]. Today about 50,000 inorganic and 25,000 organic single component crystalline phase diffraction patterns have been collected and stored on magnetic or optical media as standards. The main use of powder diffraction is to identify components in a sample by a search/match procedure. Furthermore, the areas under the peak are related to the quantity of each phase present in the sample. [Mohite, 2004]

In cement and concrete research, XRD is used to detect the presence of various (crystalline) chemical compounds which are typical of fresh or carbonated concrete (portlandite, calcite, vaterite, and aragonite) in a crushed sample of hydrated

cement paste [Hyvert, et al., 2010 and Borges, et al., 2010].

Thermal Analysis

Thermal gravimetric analysis (TGA) is a type of testing performed on samples that determines changes in weight in relation to change in temperature. It is commonly employed in research and analysis to determine the characteristics of materials. Simultaneous TGA/DTA measures both heat flow and weight changes (TGA) in a material as a function of temperature or time in a controlled atmosphere. Simultaneous measurement of these two properties not only improves productivity but also simplifies interpretation of the results. The complementary information obtained allows differentiation between endothermic and exothermic events with no associated weight loss (e.g., melting and crystallization) and those that involve a weight loss (e.g., degradation).

TGA/DTA can quantify the portlandite and the calcium carbonates resulting from carbonation, and is generally applied to hydrated cement pastes and concrete [Raham, et al., 1989 and Villain, et al., 2006].

Besides the characterisation techniques introduced above, there are other methods to evaluate the carbonation of cementitious materials. Polarization microscopy is used to identify the minerals in concrete. Non-destructive testing methods such as Gamma-densimetry [Villain, et al., 2006], Neutron Diffraction [El-Turki et al.,

2007 and Castellote et al., 2008] have been applied to cementitious systems in recent years.

2.6.7 Accelerated Carbonation

Carbonation of hydrated cement components of concrete, mortars and grouts has been widely studied since the invention of modern hydraulic cement [Parrot, 1987]. Most of the research at present is devoted to studying the factors influencing the process in the hope of establishing basic data to lead to an empirical method of predicting the rate of development of the carbonated zone and the service lifetime of reinforced concrete structures [Al-Kadhimi, et al., 1996]. However, carbonation may take many years under natural conditions due to the low CO₂ concentration in the air (about 0.035% by volume) [Houst, et al. 2002] and the reaction environment (e.g. temperature, humidity etc.) will change constantly during such long periods; this makes it very difficult to plan the investigations and compare the carbonation results.

In order to study the carbonation of concrete-based materials in a short time interval, accelerated test methods have been undertaken. In such work, concrete specimens are carbonated under relatively high CO₂-concentrations and fixed relative humidity and temperature. The results of these experiments can then be extrapolated to a natural setting. In most of the situations, two main assumptions

are taken into consideration: the relative humidity of the sample equals that of the carbonation chamber; the hydration reactions are complete or almost complete [Muntean, et al., 2005].

In accelerated carbonation tests, the concentration range of CO₂ must be carefully selected as the reaction behaviour may be different under accelerated reaction conditions compared to natural conditions. When the concentration of CO₂ is high, larger CaCO₃ crystals form, which are more likely to block the pore area, making further reaction more difficult [Bacocchi, et al. 2006 and Cizer, et al. 2006]. Besides calcium carbonate, water is produced by the carbonation reaction. Under natural conditions, the low reaction gives the released water enough time to diffuse and leave the specimen (if the RH level outside the sample is lower). However, in accelerated conditions, the released water may not have sufficient time to leave the sample. Therefore during the initial stage of accelerated carbonation, this may lead to large moisture gradients near the exposed surface where the pores are almost saturated [Bary, et al., 2004 and Papadakis, et al., 1989]. It was also reported that when the concentration of CO₂ was high (100%), the heat generated during reaction was so great that a temperature gradient can occur [Cultrone, et al., 2005].

In current practice, a partial pressure of carbon dioxide ranging from 1% to 10% P_{atm} is commonly used for the accelerated carbonation test [Borges, et al., 2010;

Hyvert, et al., 2010; Sulapha, et al., 2003 and Ho, et al., 1987]. The use of a moderate CO₂ level accelerates the carbonation rate without changing the reaction behaviour too much.

Although high CO₂ partial pressures (50% - 100% P_{atm}) are not recommended for the kinetic study, they can create artificially carbonated samples in short time. These samples can be used for characterizing the material's resistance to carbonation but are not fully relevant for predicting the carbonation kinetics under atmospheric CO₂ partial pressure [Houst, 1996; Rahman, et al., 1989 and Villain, et al. 2006].

A few studies on high pressure (P_{CO2} > P_{atm}) carbonation of cement-based backfill materials have been carried out to evaluate C¹⁴ attenuation in a radioactive waste repository. Harris, et al. [2002 and 2003] used pure CO₂ up to 2 bar to study the carbonation of NRVB and waste form grouts. Reardon, et al. [1989] investigated the carbonation of cementitious grout with pressure up to 800 psi (55 bar).

Another application of accelerated carbonation is to accelerate the curing of concrete. The hydration process of cementitious materials can be accelerated by carbonation, through Equation 2.10 and 2.11. The enhanced hydration degree usually increases the material strength and reduces its permeability, which are desirable properties for materials used to immobilize waste [García-González, et al.,

2008]. The possibility of enhanced concrete mechanical properties and durability, by treatment with compressed pure CO₂ or even up to supercritical CO₂ pressure/temperature conditions, have already been described for applications in cement-waste stabilization [Fernández Bertos, et al., 2004 and Purnell, et al., 2001].

2.6.8 Carbonation of Blended Cements

In published material, there is no general agreement between researchers as to whether using PFA or BFS in concrete tends to lessen the rate of carbonation or accelerated the rate [Atiş, 2003; Jiang, et al., 2000 and Sulapha, et al., 2003].

This disagreement in the literature can be attributed to two factors: first, the lower water requirement of PFA/BFS blended cement coupled with pore refinement through the formation of additional C-S-H may lead to a denser microstructure of the cement matrix, thus reducing the rate of diffusion of CO₂; second, the pozzolanic reaction consumes Ca(OH)₂ from the cement and thereby reduces the amount of Ca(OH)₂ available per unit area to react with the available CO₂ [Sulapha, P. et al, 2003]. With this reduction, carbonation quantities would intuitively increase, as there are less hydroxide components with which to react. If the reduction in permeability overcomes the reduction in hydroxide components, the overall carbonation is reduced [Sullivan-Green, L. et al., 2007].

2.7 Summary

According to this literature review, enormous research has been done to understand the carbonation of cementitious materials. However, as cementitious systems are very complicated, and there are so many factors which have an influence on the carbonation reaction, we have to be very careful when interpreting information from the literature, especially those involving carbonation reactions at high pressure.

3 MATERIALS, EQUIPMENT AND METHODS

3.1 Materials

3.1.1 Specimen Preparation

The NRVB, 3:1 PFA/OPC and 3:1 BFS/OPC specimens used in this research were prepared by Nexia Solutions Limited (now the National Nuclear Laboratory) by the request of the NDA. Mixture designs of NRVB, 3:1 PFA/OPC and 3:1 BFS/OPC are given in Table 3-1.

Samples	OPC (kg/m ³)	Hydrated Lime (kg/m ³)	Limestone Flour (kg/m ³)	PFA (kg/m ³)	BFS (kg/m ³)	Water (kg/m ³)	w/s ratio
NRVB	440	166	484	—	—	600	0.55
PFA/OPC	306	—	—	918	—	514	0.42
BFS/OPC	376	—	—	—	1128	496	0.33

Table 3-1 Mix proportions for NRVB, 3:1 BFS/OPC and 3:1 PFA/OPC

The three grouts were prepared using the same procedure. The solid-water mixtures

were prepared using a high shear mixer and poured into 100mm cube moulds. Immediately after casting, the moulds were placed inside a polythene cover and then transferred into a curing cell in which the temperature and relative humidity were constantly controlled at $20\text{ }^{\circ}\text{C} \pm 1\text{ }^{\circ}\text{C}$ and $95\% \pm 5\%$, respectively. To prevent the carbonation of the sample during curing, a Perspex lid and a tissue that had been soaked in a saturated solution of lime was then placed over each mould. After ~48 hours curing the prisms were then demoulded and individually wrapped in a tissue that had been soaked in a saturated lime solution. The prisms were then placed inside a sealed polythene bag and returned to the curing facility for storage. After 9 months curing, the upper surface formed during the original casting of the 100mm cube was removed and the rest was cut into 25mm cubes using a diamond tipped saw. Each individual cube was then immediately wrapped in a tissue that had been soaked in a saturated lime solution and then placed inside sealed polythene bags which then were delivered to UCL and stored in sealed plastic containers in ambient temperature for another 5 months prior to use.

The cement used was a standard OPC supplied by Castle Cement. The PFA and BFS were supplied by Frodingham Cement Company Ltd and Cemex UK Cement Limited, respectively. The physical and chemical properties of the OPC and admixtures are given in Table 3-2. Loss on ignition is the weight loss of sample due to heating (up to $900 - 1000\text{ }^{\circ}\text{C}$). As the weight loss of sample is due to the release of CO_2 from carbonates and the evaporation of moisture, a loss on ignition can

indicate the sum of H₂O% and CO₂% in the sample.

Binder	OPC	PFA	BFS
Supplier	Castle Cement	Appleby Group, Frodingham Cement Company Ltd.	Cemex UK Cement Limited
<i>Oxide (%W)</i>			
CaO%	64.7	3.3	41.25
SiO ₂	21.35	—	36.41
Al ₂ O ₃	5.91	—	12.82
Fe ₂ O ₃	2.6	—	0.61
MgO	2.61	—	7.56
MnO	—	—	0.23
Mn ₂ O ₃	—	—	0.26
SO ₃	2.53	—	—
K ₂ O	0.65	—	0.31
Na ₂ O	0.27	0.27	0.17
TiO ₂	—	—	0.47
Chloride	0.03	0.01	0.02
Loss on Ignition	0.9	5	—
<i>Phase (%)</i>			
Free lime	1.6	—	—
C ₃ S	50.5	—	—
C ₂ S	23.1	—	—
C ₃ A	10.3	—	—
Na ₂ O Equivalent	0.69	—	0.37
<i>Physical Propertie</i>			
Fineness (m ² /kg)	345	—	293
Density (kg/m ³)	3,160	2,250	2,930
Fineness retained on 45µm sieve (%)	—	9.4%	—
<i>Other Characteristic</i>			
Insoluble Residue%	0.64	—	—

Table 3-2 The Physical and Chemical properties of OPC and Admixtures

As shown in Equation (2.14) the CO₂ uptake capacity of a cementitious material depends on the concentrations of CaO, SO₃, MgO, Na₂O and K₂O in the solid. These concentrations can be calculated by the data provided in Table 3-1 and Table 3-2. For example, NRVB consists of 440kg/m³ OPC and 166kg/m³ hydrated lime. The CaO content of OPC and hydrated lime are 64.7% and 75.68% respectively. Therefore CaO in NRVB = 64.7% X 440 + 75.68% X 166 = 410.34 (kg/m³). The rest of the oxide species can be calculated by the same method and the CO₂ uptake capacity can be determined by Equation (2.14). The calculation results are shown in Table 3-3.

	NRVB	3:1 PFA/OPC	3:1 BFS/OPC
CaO (kg/m ³)	410.34	228.28	708.57
SO ₃ (kg/m ³)	11.13	7.74	9.51
MgO (kg/m ³)	11.48	7.99	96.11
Na ₂ O (kg/m ³)	1.19	3.30	2.93
K ₂ O (kg/m ³)	2.86	1.99	5.94
CO ₂ uptake capacity (kg/m ³)	330.71	186.93	660.72
CO₂ uptake capacity (mol/m³)	7516	4248	15016

Table 3-3 CO₂ uptake capacity

3.1.2 Specimen Conditioning

As the specimens received from Nexia Solutions were wrapped in wet tissue, their pore networks were filled with external water. The specimens were considered as fully saturated with water. When a wet specimen is carbonated under a relative humidity less than 100%, the moisture content of the specimen would decrease due to evaporation. The drying of pore water would then cause changes in the reaction kinetics. Three relative humidities (75%, 85% and 100%) were select for the carbonation tests to examine the effect of humidity on the carbonation kinetics. Therefore, to eliminate the effect of drying, specimens should be conditioned at selected relative humidity to constant weight, before being subjected to carbonation testing.

The NRVB, 3:1 PFA/OPC and 3:1 BFS/OPC specimens were conditioned at three different relative humidity conditions (75%, 85% and 100%) in desiccators over saturated solutions or water. All specimens were regularly weighed using a 0.01g precision balance. The equilibrium in moisture content was supposedly obtained when the loss in weight of every cube was smaller than 0.05% per week. To prevent carbonation by the CO₂ in the air, nitrogen was flashed into the desiccators each time they were opened.

A relative humidity of 100% was established by equilibration with pure water.

Lower relative humidities were obtained by using solutions of appropriate compositions, since the vapour pressure of a solution is reduced compared with that of pure water. In this work, saturated solutions of sodium chloride and potassium chloride were used to control the relative humidity to 75% and 85%, respectively [Harris et al., 2003]. To prevent dilution by water being evolved from the cement specimens, excess salts were mixed with deionised water.

3.1.3 Specimen Sealing

To simplify the interpretation of the experimental results, the specimens were sealed by casting into epoxy resin and left with only one surface exposed. An example of a sealed specimen is shown in Figure 3-1. As a result of doing this, the carbonation reaction proceeded in a single direction, which allowed an easier determination of the carbonation rate.



Figure 3-1 NRVB specimen mounted in epoxy resin

The 2-part epoxy resin used in this experiment was Logitech Epoxy Pack 301,

which has a very low viscosity and offers good adhesion to concrete. The performance of this material was investigated by Harries et al. (2003), who proved that CO₂ permeation through the resin was sufficiently slow as to effectively prevent the carbonation of the sealed surfaces.

All the cubes were cast in 50mm diameter polypropylene moulds. Due to the lack of an environmental controlled facility, the casting was performed in air. However, to prevent the specimens from being carbonated, the moulds were placed into the desiccators to allow the resin to cure. It took around 20 hours for the resin to set. The resin-sealed cubes were then removed from the moulds and placed back into the desiccators until the carbonation experiments were carried out.

3.2 Experimental Apparatus

Two identical 5 litre reaction chambers, both incorporating a heat exchanging plate, were used to ascertain the kinetic parameters of the carbonation reaction. Figure 3-2 shows the experimental rig designed and built at UCL.

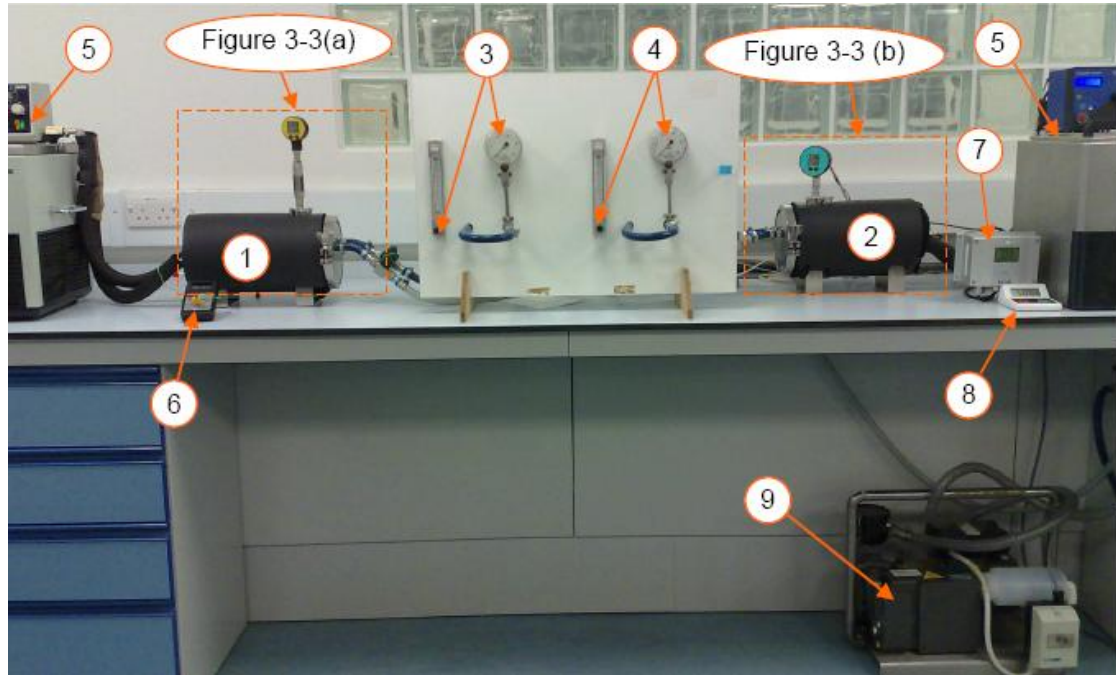


Figure 3-2 Carbonation rig

In Figure 3-2:

- (1) Reactor I was built in 2003 for accelerated carbonation studies.
- (2) Reactor II was built in 2007 for the purposes of the study reported here and the need for more experiments to be conducted over long time periods.
- (3) Rotameter controlling the inlet flow rate of carbon dioxide.
- (4) Rotameter controlling the inlet flow rate of nitrogen.
- (5) Thermostats connected to the heat exchanging plates in the reactors. By adjusting the temperature of the circulating water, the temperatures in the reactors can be controlled throughout the reaction.
- (6) Thermometer (1°C precision) from which the temperature in Reactor I can be read.

- (7) Vaisala HMT 334 temperature/humidity transmitter (0.1°C/0.1%RH precision) showing not only the temperature but also able to measure the relative humidity in Reactor II at high pressure and temperature.
- (8) Stopwatch used to measure the reaction time.
- (9) Vacuum pump connected to the outlets of the reactors. It is used to evacuate the residual air from the reactors prior to initial pressurisation.

The two reactors are shown in more detail in **Figure 3-3** and **Figure 3-4**.

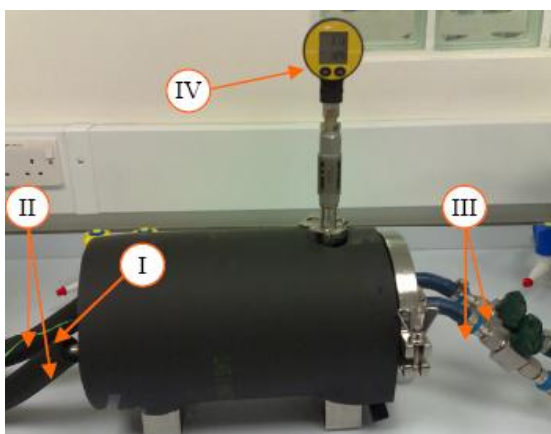


Figure 3-3 Reactor I

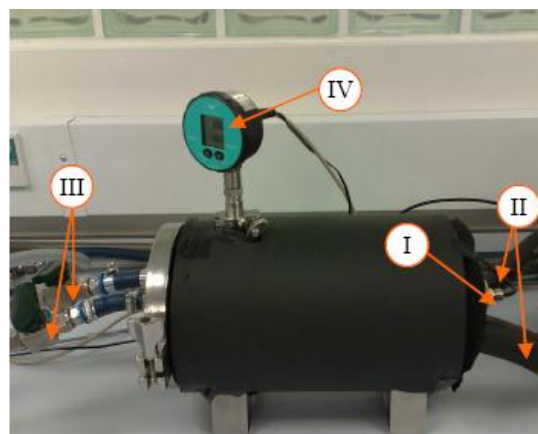


Figure 3-4 Reactor II

The carbonation reactors were made of stainless steel with a maximum design pressure of 6 bar. The lids were secured with clamps and were sealed by means of o-rings. Insulation jackets were placed around the reactors in order to minimise the temperature gradients of the atmosphere in the reactors.

From **Figure 3-3** and **Figure 3-4**, it can be seen that the two reactors are almost

identical, except the type and the size of the probes (I). The temperature probe in Reactor I was connected to the thermometer (see (6) in Figure 3-2). As an improvement for Reactor II, a temperature/humidity probe was installed which connected to (7) in Figure 3-2. The internal structure is described in Figure 3-5. More details and dimensions can be find from the technical drawings in Appendix A and B.

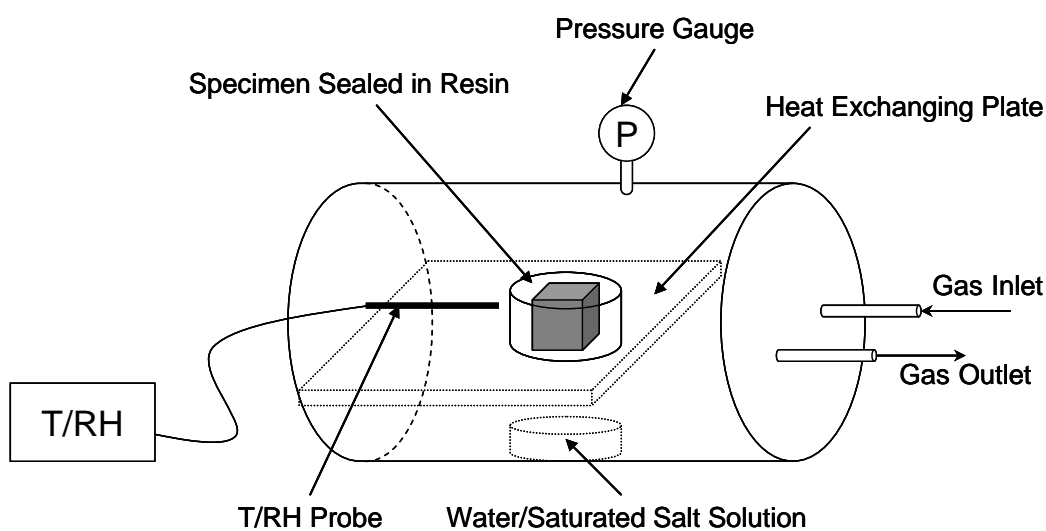


Figure 3-5 Internal structural of carbonation chamber

Inside each reactor is a heat exchanging plate used to maintain a constant temperature of the sample throughout the reaction. This is important as enthalpy changes during the reaction (the reaction is exothermic) can cause temporary deviations from isothermal conditions. Water is circulated through the plates, via the thermostats and the connections at the rear of the reactors (II in **Figure 3-3** and **Figure 3-4**).

Quarter turn valves were connected to the gas inlet and outlet (III in **Figure 3-3** and **Figure 3-4**) of each reactor. Prior to each experiment, a vacuum was developed in each reactor by a pump ((9) in Figure 3-2) connected to the outlet, and then the outlet valve was closed. At a chosen starting pressure (see next section), either nitrogen or carbon dioxide was fed into the reactor. The inlet valve was then closed and the reactor was completely sealed as a static batch reactor. Each reactor has a port for a digital pressure gauge (IV in **Figure 3-3** and **Figure 3-4**). The pressure gauge monitored the pressure change throughout the reaction process with an accuracy of 0.01bar. At the moment at which the reactor was sealed, the stopwatch was switched on. It took around 30 seconds for the system to settle. Then pressure, temperature and relative humidity were monitored and recorded with time. Hence, the starting point of each reaction was assumed to be 30 seconds after the inlet valve was closed.

As shown in Figure 3-5, the relative humidity in each reactor was controlled by placing a 100ml crystallising basin under the heat exchanging plate. 25 to 30 millilitres of water, saturated potassium chloride solution or saturated sodium chloride solution was filled in the crystallizing basin to maintain the relative humidity at 100%, 85% or 75%, respectively. The selected quantity of water or salt solution was small enough to reduce the impact of carbon dioxide dissolved in the water and large enough to provide moisture in the reactor. Moreover, sodium chloride and potassium chloride tend to crystallize at the edges of the container. The

crystals form a labyrinth that allows solution to rise by capillary action and crystallise further up the wall and spread everywhere. Therefore, relative small volumes of the salt solution would alleviate this effect.

3.3 Experimental Method

In this work, the experimental procedures were fundamentally the same for the NRVB and the two wasteform grouts (3:1 PFA/OPC grout and 3:1 BFS/OPC). For each material, the relation between relative humidity and pore water content was investigated. Carbonation tests were conducted within a range of relative humidity and pressure which were selected to simulate the environment in the repository. The rate of CO₂ uptake and its influencing factors were studied. In addition, property changes of the materials caused by carbonation were investigated using different analytical methods.

3.3.1 Initial Bulk Density and Dry Porosity

Prior to conditioning, wet specimens were weighed as soon as they were unwrapped from the wet tissues. The initial bulk density of each specimen was determined by dividing the wet mass of fresh specimens by their volume. Based on the assumption that the specimen was nominally cuboid (the error in specimen dimension was about ± 1 mm), the volume was calculated from the actual dimension

of the specimen, which was measured by slide calliper. For each material, an average density was calculated from all tested specimens.

As one of the most important factors that control the carbonation rate, the porosity of the NRVB, 3:1 PFA/OPC and 3:1 BFS/OPC samples was estimated. Five fresh specimens of each material were oven-dried at 105 °C for 24 hours. As the fresh grout specimens were wrapped in wet tissues, it was assumed that the pore networks were filled with external water and that the specimens were fully saturated. After drying water was removed from the pores, therefore the porosity (ϕ) of each material can be estimated by Equation (3.1):

$$\phi = \frac{\Delta W}{\rho_{water}} \times \frac{1}{V_{specimen}} \quad (3.1)$$

Where ΔW is the weight loss due to drying

ρ_{water} is the water density at room temperature (998.207 kg m⁻³ at 20 °C)

$V_{Specimen}$ is the volume of the specimen

3.3.2 Effect of Conditioning on Specimen Water Content

As discussed in Section 2.6.4, the water content of the specimen directly influences the rate of carbonation. The weight loss after conditioning was recorded for each specimen. Gas-filled porosity was calculated to evaluate the effect of relative

humidity on the water content in the specimen. The gas-filled porosity is the volume fraction of pores which are not blocked by water. It can also be estimated by Equation (3.1), in which ΔW is the equilibrium weight loss due to conditioning.

3.3.3 Carbonation Test

Three relative humidities (75%, 85% and 100%) were selected for the experiments. It was believed that humidities between 75% and 100% would be more likely to represent the water content of NRVB and wasteform grouts under repository conditions [Harris et al., 2003]. The humidities selected would also allow comparison of results between this and previous work [Harris et al. 2002 and 2003]. It has been stated in Section 3.2 that during the carbonation test, humidity in the reactor would be maintained using one of the saturated salt solutions or deionised water. Specimens which were conditioned at these relative humidities would be used to maintain the consistency of water content in the pores. During specimen conditioning, digital hydrometers were placed in the desiccators to monitor the conditioning humidity.

For each relative humidity, specimens were carbonated at initial pressure of 1bar, 3bar and 5 bar, respectively. Testing of the reactors showed that increasing the pressure in the reactor would cause gas leakage and that the leakage rate would be higher than the reaction rate when the pressure was higher than 5 bar. Therefore, 5

bar was selected as the upper limit of the initial pressure. The lower limit of 1 bar was selected for the convenience of comparison with previous work [Harris et al., 2002].

Pure CO₂ (Zero Grade) was used in all experiments to accelerate the natural carbonation, which is very slow. It is predicted that the CO₂ concentration in the repository will be much higher than the concentration in the atmosphere due to the depth of repository. The ¹⁴CO₂ generated by radioactive waste will also contribute to this. However, the actual concentration the CO₂ will reach in the repository is not yet known although bounding estimates can be made.

All the carbonation experiments were conducted at the temperature of 21 ±1 °C. It was observed that pore water evaporated from the specimen when the temperature in the reactor was higher than the ambient temperature. The higher the temperature, the faster the moisture loss from the specimen, which would cause a change in the CO₂ diffusion rate in the specimen and, hence, cause errors in the carbonation results. The reason is believed to be the temperature gradient in the reactor. As the gas in the reactor is in a static condition (no gas mixing facility is adopted), when the temperature of the heat exchanging plate increases, the gas around the heat exchanging plate would be hotter than the gas near the reactor wall. Although insulating material was wrapped around the outside of the reactor to prevent the loss of heat, a temperature gradient in the reactor was still inevitable. During the

reaction, the specimen was placed on the heat exchanging plate, which caused the evaporation of water from the specimen. Therefore, to prevent this, 21 ± 1 °C (close to ambient temperature) was the only temperature investigated at this stage.

During each test, the sealed specimen was placed on the heat exchanging plate (as shown in Figure 3-5,). After the lid was closed tight, the reactor was first evacuated and then pressurised with nitrogen to a selected pressure. The specimen was stored in nitrogen for approximately 68 hours and the pressure was monitored to determine the leakage rate of the gas. When the reactor was sealed properly, after 48 hours leak test, the pressure drop should be below 0.005bar for an initial pressure of 3bar. For a pressure of 5bar, the leakage rate should not exceed 0.04bar per 68 hours. The nitrogen in the reactor was then evacuated and replaced by carbon dioxide at the same pressure. After 30 seconds from the closure of gas inlet valve (to allow the pressure to settle down), temperature and drop in pressure were recorded throughout the reaction. The amount of CO₂ being consumed by the carbonation reaction can then be determined by the pressure drop:

$$n_t = \frac{(P_0 - P_t)V_{reactor}}{RT} \frac{1}{V_{specimen}} \quad (3.2)$$

Where n_t is the mole of CO₂ absorbed by time t per m³ of the specimen (mol m⁻³)

P_0 is the initial pressure when the reaction starts (bar)

P_t is the pressure at time t (bar)

$V_{reactor}$ is the gas volume in the reactor, which is 4.674 L

R is the gas constant, 0.083145 L bar K⁻¹ mol⁻¹

T is the temperature in the reactor at time (K)

In Equation (3.2), CO₂ is assumed to be an ideal gas. Although the assumption of ideal behaviour will result in the underestimation of the quantity of carbon dioxide in the reactor, it is insignificant for the interpretation of the experimental results [Harris et al., 2002].

For each set of experimental results, conversion of reactive calcium (X_{Ca}) vs. time was plotted to describe the progress of carbonation reaction.

$$X_{Ca} = \frac{n_t}{n_{Ca}} \quad (3.3)$$

n_{Ca} is the mole concentration of reactive calcium in the specimen (mol m⁻³). It equals to the CO₂ uptake capacity calculated in Section 3.1.1. As shown in Table 3-3, the concentration of reactive calcium in NRVB, 3:1 PFA/OPC and 3:1 BFS/OPC are 7516 mol/m³, 4248 mol/m³ and 15016 mol/m³ respectively.

It has be pointed out that the reaction time was not selected as a set value for all the experiments as the reaction rate could be very different for different materials and reaction conditions. For most of the experiments, when no obvious pressure drop

could be observed, reactions were terminated by discharge of the CO₂ from the reactor. However, if a reaction was slow ($X < 0.2$ within the first 5 days), it would be terminated after 1 month. The pressure drop caused by leakage would also be deducted from the observed pressure drop, before n_t was calculated.

The accuracy of the pressure gauges on both of the reactors was 0.01 bar. Any pressure observed oscillating between two pressures (e.g. 3.01 bar and 3.02 bar) was recorded as the lower pressure plus 0.005 (e.g. 3.015).

The reasons for using pressure change to monitor the progress of carbonation are:

- This method directly determines the amount and rate of CO₂ absorbed by the material, which is the primary concern in this study.
- According to previous studies the carbonation of NRVB under elevated CO₂ concentration is very fast [Harris et al., 2003] and the current method provides an instantaneous and continuous way to monitor the reaction progress.

Other authors have used specimen weight gain and Neutron Diffraction Tests for similar situations [El-Turki et al., 2007 and Castellote et al., 2008]. However, the first method is not accurate due to the generation and evaporation of moisture, and the second method is very complicated, both in operation and data analysis.

Acid/Base Indicators, X-Ray Diffraction (XRD), Thermogravimetry Analysis

(TGA) and scanning electron microscope (SEM) are more commonly applied methods to detect the carbonation progress of cement and concrete. However, they are more useful in physically distinguishing the carbonated from the non-carbonated layers and involve interruption to the reaction process. Therefore, these methods were only used to examine the effect of carbonation on material characteristics in this work.

3.3.4 Analysis of the Property Changes Due to Carbonation

The effect of carbonation on each material at selected reaction conditions was investigated. For each reaction condition, a set of specimens with different carbonation duration were prepared in the similar manner as stated in Section 3.3.3. With specimens at different carbonation stages, the carbonation profile can be observed.

3.3.4.1 Carbonation Profile Observation

As the carbonation test only showed the amount of CO₂ absorbed during the reaction, it could not show the travel pattern of gas in the specimen. Therefore, the carbonation profile through the reaction was observed. Specimens carbonated to different stages were dry cut by diamond saw to expose surfaces approximately perpendicular to the single unprotected face. The freshly cut surface was first examined visually, and then applied with phenolphthalein to distinguish the

carbonated and uncarbonated zones. Phenolphthalein is a colourless acid/base indicator which turns purple when the pH is above a value in the range of 8.3-10. The phenolphthalein indicator used in the work was purchased from Fisher Scientific with composition of 1% (w/w) phenolphthalein in 70% ethyl alcohol. The solution was sprayed onto the freshly cut surface which had been cleaned of dust and loose particles using a soft brush. If no colouration occurs, carbonation has taken place and thus the depth of the carbonated surface can be measured by slide calliper.

3.3.4.2 Morphology Characterisation

Apart from visual observation and phenolphthalein test, the morphology of the cut surfaces was observed by using a Hitachi S-3400N Scanning Electronic Microscope. A 5mm thick slice was cut from each partially carbonated specimen. The direction of cut was perpendicular to the unprotected face. Prior to analysis, the cut surface of the slice was dried in the oven at 105°C for 24 hours. To make the specimen electrically conducting, a thin layer of gold vapour was deposited onto the samples. When viewed in the SEM, signals emitted from the sample as a result of the specimen-primary electron beam interaction include secondary electrons (SE). In this study, an accelerating voltage of 15 kV was used for collecting the SE images. Images were taken from each side of the visual observed carbonation front.

3.3.4.3 Mineralogy Characterisation

The analysis of the mineral phases of fresh and carbonated specimens (carbonated at 75% RH and 5 bar initial pressure) were carried out through X-Ray Diffraction (XRD) using a Bruker-AXS D8 powder capillary diffractometer with a Cu anode generator in the range of 5-85° 2 θ . The settings fixed for the generator were 40 kV and 30 mA. Data collecting time was 600 seconds. Prior to the XRD analysis, specimens were dried in the oven at 105 °C for 24 hours, and were ground into powder using a pestle and mortar. The powder that passed through a 75 μ m sieve was sealed in a capillary tube of 0.4mm diameter which was suitable for the analysis. The data collected were analysed by EVA-XRD software.

3.3.4.4 Carbonate Content Characterisation

The thermograms produced by Differential Thermal Analysis and Thermogravimetry (DTA/TG) can distinguish between carbonated and non carbonated concrete by comparison of the different peaks. In this work, testing was conducted using a NET2SCH STA-449C DTA/TG analyser. The carbonate content of both fresh and carbonated specimens of each material were analysed. Around 2g of sample specimen were taken from the centre of each specimen cube and dried in the oven for 24 hours. The samples then were ground using a pestle and mortar, sieved and particles smaller than 75 μ m were used for DTA/TG. Approximately 10 mg of the prepared powder was heated in dry flowing Helium with a heat rate of 10° C per minute from 20° C to 1000° C. The weight loss measured by TGA and the heat release by DTA were used to estimate the amounts of calcium hydroxide and

calcium carbonate present in each specimen. It is believed that calcium hydroxide loses its chemically bound water between 350° C to 550° C, and calcium carbonate loses its chemically bound CO₂ between 600° C to 900° C [El-Turki et al., 2007].

It must be pointed out here that it was not possible in most cases to conduct the characterisation analyses immediately after the samples were prepared. Although the samples were sealed in air tight bags or glass bottles and stored in vacuum desiccators, their exposure to the CO₂ in the atmosphere was inevitable during the sample preparation process as glove box was not available in the laboratory. Moreover, hydration of cementitious materials is a very slow process. Continued changes in chemical and physical properties due to hydration can be observed across decades. Therefore, the characteristics of the specimens determined in this work only truly represent the properties during the period of measurement.

4 EXPERIMENTAL RESULTS AND DISCUSSION

4.1 Introduction

In this Chapter the experimental results of the carbonation tests on NRVB, 3:1 PFA/OPC grout and 3:1 BFS/OPC grout are shown and discussed. The work reported for each material included the following aspects:

- The effect of moisture conditioning on the microstructure of the materials was investigated. The gas-filled porosities were estimated to provide a provision of the carbonation behavior of the materials.
- The exposure conditions (initial CO₂ pressure and relative humidity) determining carbonation were evaluated.
- The carbonation profiles (movement of carbonation front) were observed and compared with the reaction progress curves based on CO₂ consumption rate.
- The major physical and chemical changes in each material after carbonation are also discussed

4.2 Results of NRVB Carbonation Test

4.2.1 Effect of Conditioning

The NRVB specimens and their weight changes during drying are summarised in Table 4-1. The specimens were numbered by the 'N0/N₀' system, in which 'N' represented NRVB, '0' represented for zero relative humidity in the oven and 'N₀' is the specimen number from 1 to 5. Specimens N0/4 and N0/5 were smaller than the normal sizes, but were still used in the test due to the lack of specimens.

<i>No.</i>	Volume (cm³)	Initial Mass (g)	Final Mass (g)	Change in Mass (g)
N0/1	15.84	26.73	18.14	-8.59
N0/2	16.74	28.09	19.04	-9.05
N0/3	15.56	26.19	17.66	-8.53
N0/4	11.52	19.39	13.20	-6.19
N0/5	11.58	19.45	13.23	-6.22

Table 4-1 Results of drying NRVB at 105 °C for 24 hours

The effect of specimen conditioning are recorded in **Table 4-2** to **Table 4-4** for conditioning at 75%, 85% and 100% relative humidity, respectively. All specimens were conditioned for a minimum period of 5 months and were numbered in the same pattern as the over dried specimens.

<i>No.</i>	Volume (cm³)	Initial Mass (g)	Final Mass (g)	Change in Mass (g)
N75/1	16.75	28.49	22.34	-6.15
N75/2	15.16	26.60	20.43	-6.17
N75/3	15.04	25.76	20.23	-5.53
N75/4	15.13	25.85	20.26	-5.59
N75/5	15.59	26.72	21.08	-5.64
N75/6	15/90	27.06	21.24	-5.82
N75/7	15.41	26.57	20.93	-5.62
N75/8	16.12	27.23	21.48	-5.75

Table 4-2 Results of conditioning NRVB at 75% RH for 5 months

<i>No.</i>	Volume (cm³)	Initial Mass (g)	Final Mass (g)	Change in Mass (g)
N85/1	15.04	25.57	20.88	-4.69
N85/2	15.28	26.09	21.39	-4.7
N85/3	15.41	26.29	21.56	-4.73
N85/4	15.40	26.40	21.81	-4.59
N85/5	15.25	26.08	21.37	-4.71
N85/6	15.50	26.01	21.21	-4.8

Table 4-3 Results of conditioning NRVB at 85% RH for 5 months

<i>No.</i>	Volume (cm³)	Initial Mass (g)	Final Mass (g)	Change in Mass (g)
N100/1	15.20	26.50	26.51	0.01
N100/2	15.61	26.76	26.75	-0.01
N100/3	15.13	25.82	25.77	-0.05
N100/4	15.13	25.83	25.85	0.02
N100/5	15.13	25.83	25.84	0.01

Table 4-4 Results of conditioning NRVB at 100% RH for 5 months

Based on the initial masses and volumes given in Table 4-1 to Table 4-4, the average initial bulk density (wet density) of NRVB used in this work was 1711 ± 16 kg m⁻³. This may be compared with the densities of NRVB used in previous work (as shown in **Table 4-5**). The NRVB material in this work was cured for 15 months, and its initial bulk density was very similar to the 18 months old NRVB materials. Although the 5 years old NRVB material used in previous work had slighter lower density, this may be due to the higher error.

	15 months NRVB	18 months NRVB	5 years NRVB
	(This work)	[Harris et al. 2003]	[Harris et al. 2002]
Wet Density (kg m ⁻³)	1711 ± 16	1706 ± 7	1650 ± 50

Table 4-5 Average wet density of fresh NRVB of different ages

The average weight loss and gas-filled porosity at each relative humidity are summarised in **Table 4-6**.

Relative Humidity	Weight Loss (%)	Gas-filled Porosity
0%	32.2 ± 0.2	0.54 ± 0.00
75%	21.6 ± 0.6	0.37 ± 0.01
85%	18.1 ± 0.3	0.31 ± 0.00
100%	0.0 ± 0.1	0.00 ± 0.00

Table 4-6 NRVB gas-filled porosity and degree of water saturation

The weight loss of oven dried NRVB is estimated as $32.2 \pm 0.2\%$. This value is similar to the previously measured value of 32.8% [Harris et al. 2002]. Meanwhile, the weight loss on drying gives an estimated porosity of 54%, which remains the same as has been observed previously [Harris et al. 2002].

The average fractional weight loss for conditioning at 75% relative humidity is $21.6 \pm 0.6\%$. This may be compared with the weight losses measured in previous work, $22.7 \pm 0.4\%$ [Harris et al. 2002] and $19.9 \pm 0.3\%$ [Harris et al. 2003]. The difference may be attributed to the age differences between the three batches of NRVB.

In this work the gas-filled porosity of NRVB at 75% relative humidity is estimated as 0.37 ± 0.01 . This may be compared with a value of 0.38 as reported by Harris et al. [2002].

The average weight loss for conditioning at 85% relative humidity has been reported to be $18.2 \pm 0.5\%$ [Harris et al. 2003]. This is very similar to the value ($18.1 \pm 0.3\%$) reported in **Table 4-6**. The gas-filled porosity in this work is 0.31, which is similar to that obtained for conditioning at 75% relative humidity. This similarity may suggest that the difference in these humidity conditions has a very small effect on the water content of NRVB.

Conditioning at 100% relative humidity shows no weight change, which confirmed that the specimens unwrapped from the wet tissues were fully saturated with water and all the pores were filled with water.

4.2.2 Carbonation Test Results

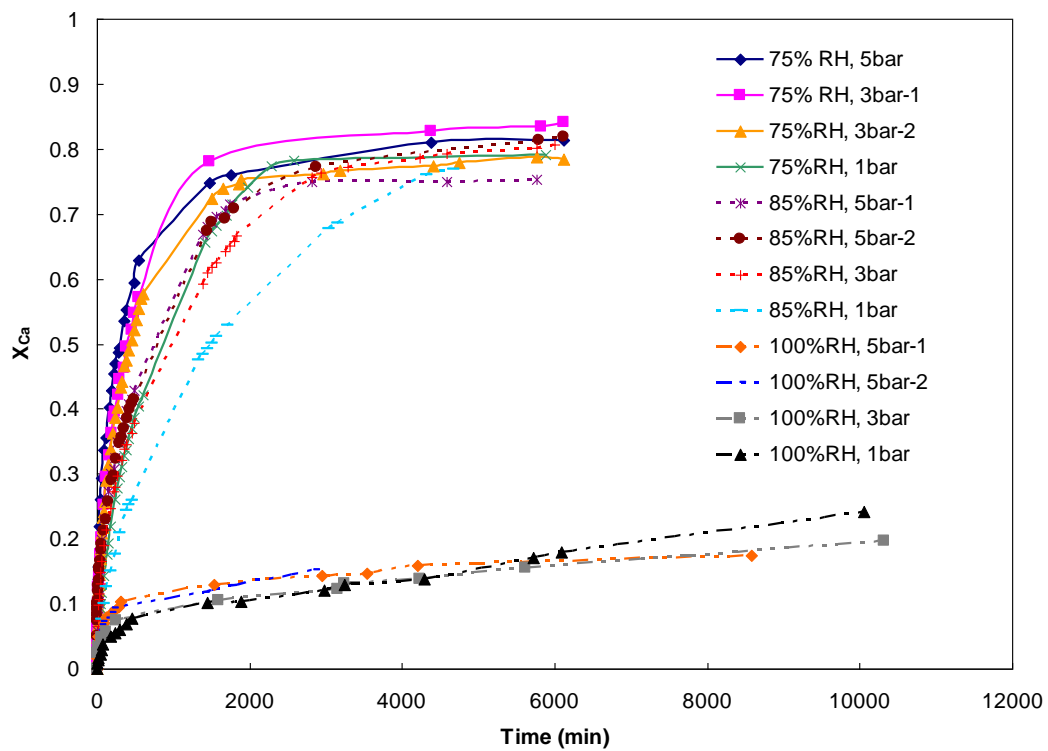


Figure 4-1 Evolution of reaction with time for NRVB at pressure from 1bar to 5bar at relative humidity from 75% to 100% (Error in $X_{Ca} = \pm 0.039$)

The effect of relative humidity and initial CO_2 pressure on the carbonation reaction of NRVB is shown in **Figure 4-1** in terms of conversion of reactive calcium (X_{Ca}) vs. time. As the reaction curves are very close to each other, X_{Ca} vs $time^{0.5}$ (as shown in **Figure 4-2**) were plotted for better observation. The evolutions of

reactions during the first 400 minutes are shown in **Figure 4-3**.

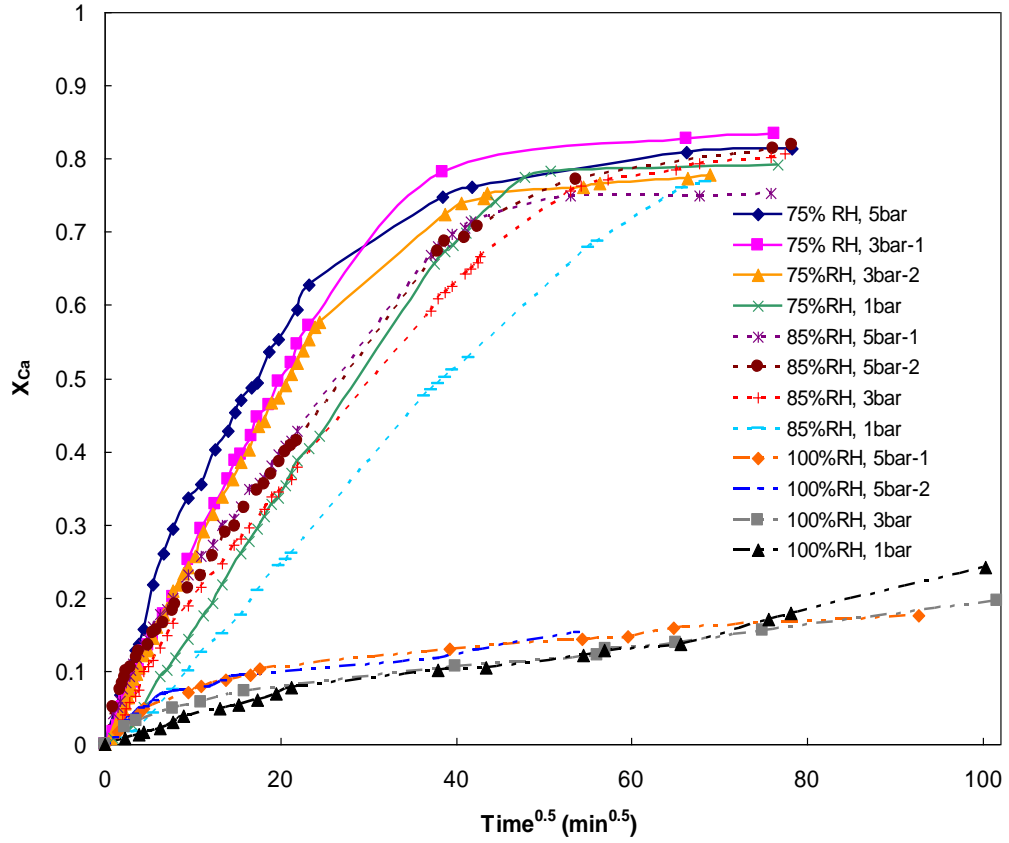


Figure 4-2 Plot of X_{Ca} vs. $\text{time}^{0.5}$ for NRVB at pressure from 1bar to 5bar at relative humidity from 75% to 100% (Error in $X_{Ca} = \pm 0.039$)

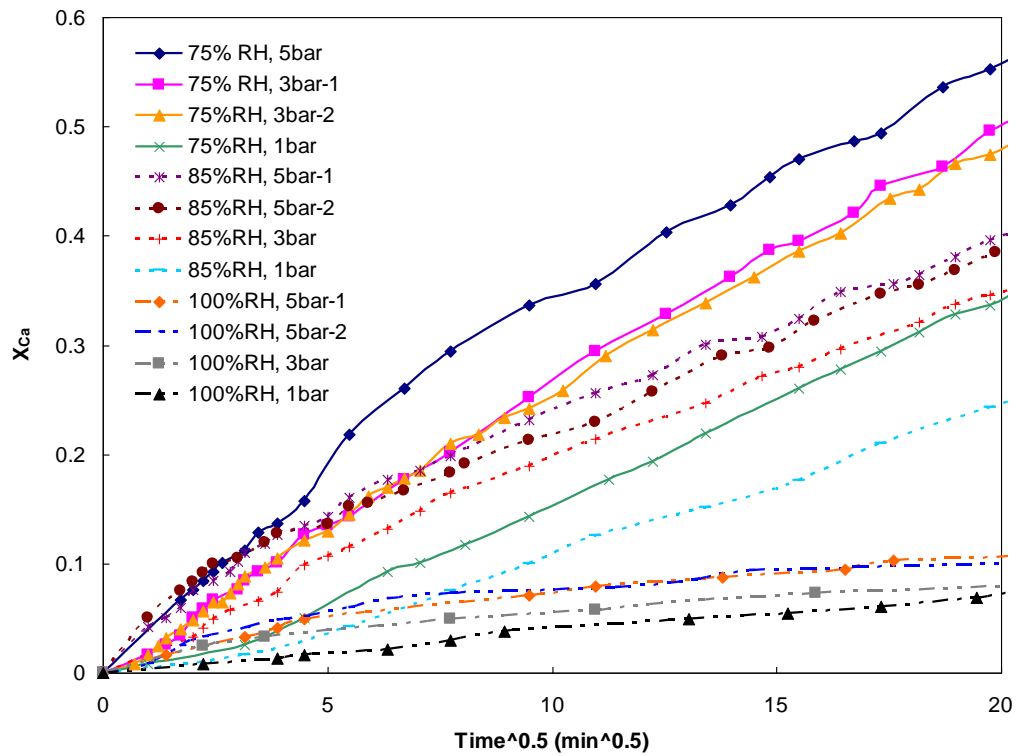


Figure 4-3 Plot of X_{Ca} vs. $time^{0.5}$ at the first 400 minutes for NRVB at pressure from 1bar to 5bar at relative humidity from 75% to 100% (Error in $X_{Ca} = \pm 0.039$)

4.2.2.1 Effect of relative humidity

The experiments showed that the lower the relative humidity the higher the rate of reaction. This was due to the easier diffusion of CO_2 into the pores of the solid, as water was not blocking the pores.

It can be observed that at relative humidities of 75% and 85% two reaction stages existed for each carbonation curve. During the first stage, the reaction was fast and around 75% conversion was achieved in most cases within 24 hours. After that, the reaction rate decreased dramatically. During the second stage, although it was still

possible to detect an uptake of CO₂, the reaction was so slow that the measurement was terminated after 102 hours. The maximum conversion that could be reached within 102 hours was around 84%.

The reactions at 100% relative humidity were very slow. The measurements terminated after 7 days due to the tight experiment schedule. The maximum conversion observed was around 24%.

4.2.2.2 Effect of initial CO₂ pressure

As shown in Error! Reference source not found. and **Figure 4-3**, the initial CO₂ pressure had a positive effect on the evolution of the carbonation reaction. However, this effect decreased as the relative humidity increased to 100%. This may be due to the low reaction rate with 100% relative humidity. At the relative humidity of 75% and 85%, it can be observed that as the CO₂ pressure was increased from 1bar to 5bar, its positive effect on the reaction rate decreased.

For each relative humidity, two set of experiments were conducted for a selected pressure to test the reproducibility of the data. It is shown that all the experiments repeated very well at the first stage of the reaction. However, during the second stage the data were slightly different, which showed that the uncertainty of the experiments increased as the reaction tended towards completion.

4.2.3 Observation of Carbonation Profile

i) RH = 75%

A set of specimens conditioned at 75% relative humidity and carbonated at 3 bar for 0.5 hour, 1 hour, 3 hours, 6 hours, 16.5 hours and 102 hours was examined by direct observation and the phenolphthalein test. The results are shown photographically in Figure 4-4.

For all partially carbonated specimens, a colour difference between the carbonated and non-carbonated zones was directly observed. As the reaction proceeded, a sharp carbonation interface, parallel to the exposed face, travelled towards the bottom of the specimen. The lighter colour in the carbonated zone may be attributed to the carbonation product, calcium carbonate, which has white crystals. The colour of the non-carbonated zone is darker due to the hydrates. The direct observation of reaction interface also shows that the darker non-carbonated zone had already disappeared at 16.5 hours. No obvious difference was observed between the 16.5 hours sample and 102 hours sample.

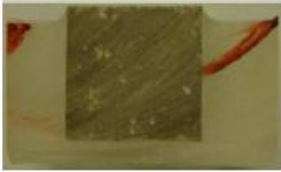

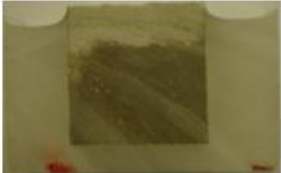



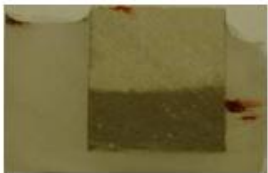







Reaction Time	Direct Observation	Phenolphthalein Test
Fresh NRVB		
0.5 hour		
1 hour		
3 hours		
6 hours		
16.5 hours		
102 hours		

Figure 4-4 Cross-section of cut NRVB specimens with different carbonation durations, P=3bar, RH=75%

As a supplement to the direct observations, the carbonated and non-carbonated

zones were distinguished by phenolphthalein indicator. Figure 4-4 shows that, as expected, after being sprayed with phenolphthalein, the fresh NRVB sample turned purple-red due to the high pH of the pore water. The partially carbonated sample showed the same purple-red colour below the carbonation interface as the fresh NRVB sample. However, above the carbonation interface, the sample appeared light pink instead of colourless. This means that the reactive calcium in the carbonated zone was not fully carbonated and there were still weak alkaline phases present. The closer to the exposure surface and the longer the reaction time was, the lighter the pink colour became. Therefore it is more precise to call the area above the carbonation interface a partially carbonated zone. After 16.5 hours, the purple-red non-carbonated zone disappeared, but the light pink colour still existed at the bottom of the specimen. At a reaction time of 102 hours, the sample was completely colourless.

During the preparation of the specimens for the carbonation profile observations, the reaction progress of each specimen was recorded. The reaction curves are presented in Figure 4-5. It can be seen that the transition point from stage 1 to stage 2 is around 16.5 hours. Figure 4-4 has demonstrated that after 16.5 hours of reaction, CO₂ reached the bottom of the specimen and only a small amount of weak alkaline compounds remained unreacted. Therefore the slow reaction rate in the second stage was due to the depletion of reactants.

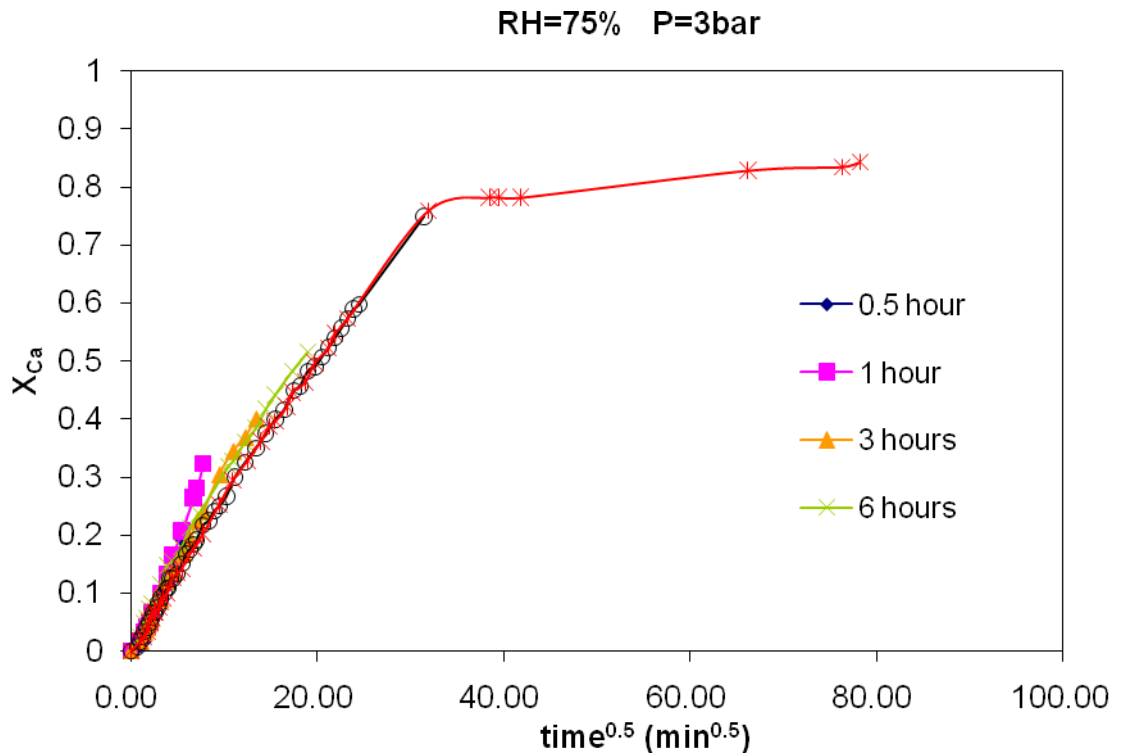


Figure 4-5 Plot of X_{Ca} vs. $\text{time}^{0.5}$ for NRVB carbonated at $P=3\text{bar}$, $RH=75\%$ with different reaction durations (Error in $X_{Ca} = \pm 0.039$)

It is also worth pointing out that the specimen carbonated for 102 hours showed no colour change after the phenolphthalein test, while the conversion of reactive calcium was only around 85%. This may be because the carbonation products (CaCO_3) block the pores and made the CO_2 difficult to reach the remaining reactants.

ii) $RH = 85\%$

A cut NRVB specimen, conditioned at 85% relative humidity, was carbonated for 6 hours with an initial CO_2 pressure of 3bar (Figure 4-6). Similar to the partially carbonated specimens conditioned at 75% relative humidity, a sharp carbonation

interface, parallel to the exposure surface, was clearly observable and the phenolphthalein indicator appeared purple-red in the non-carbonated zone and light pink in the carbonated zone. However, with a reaction time of 6 hours, the carbonation interface of the 85% relative humidity specimen was approximately 12 mm below the exposure surface, while the carbonation interface of the 75% relative humidity specimen was around 18 mm below the exposure surface. The difference in the interface positions confirms the observation depicted in **Error! Reference source not found.** and Figure 4-3 that relative humidity has an adverse effect on the reaction rate.



Reaction Time	Direct Observation	Phenolphthalein Test
6 hours		

Figure 4-6 Cross-section of a cut NRVB specimen after 6 hours carbonation,
P=3bar, RH=85%

ii) $RH = 100\%$

Figure 4-7 shows the carbonation profile of a cut NRVB specimen conditioned at 100% relative humidity. Although the interface between the carbonated and non-carbonated zone was distinct, it was not parallel to the exposure surface. In contrast to the 75% and 85% relative humidity specimens, phenolphthalein indicator above the carbonation interface was colourless, which means that all the

reactive calcium above the carbonation interface had reacted with CO_2 .



Reaction Time	Direct Observation	Phenolphthalein Test
102 hours		

Figure 4-7 Cross-section of a cut NRVB specimen after 102 hours carbonation,
P=3bar, RH=100%

4.2.4 Examination of Microstructure Using SEM

To compare the difference in the microstructure between the non-carbonated and carbonated zones, a partially carbonated NRVB specimen, which was carbonated at 75% relative humidity, was examined by SEM. Figure 4-8 shows the SEM images of non-carbonated material approximately 1 mm below the carbonation front. Figure 4-9 shows the SEM images of carbonated material approximately 1 mm *above* the carbonation front.

As shown in Figure 4-8, the non-carbonated zone consists of plates of portlandite (calcium hydroxide), which is the main constituent of hydrated lime, small numbers of fine crystals assigned to calcite, which is the main constituent of lime stone flour, and traces of needle shaped C-S-H, attributed to the hydration of OPC.

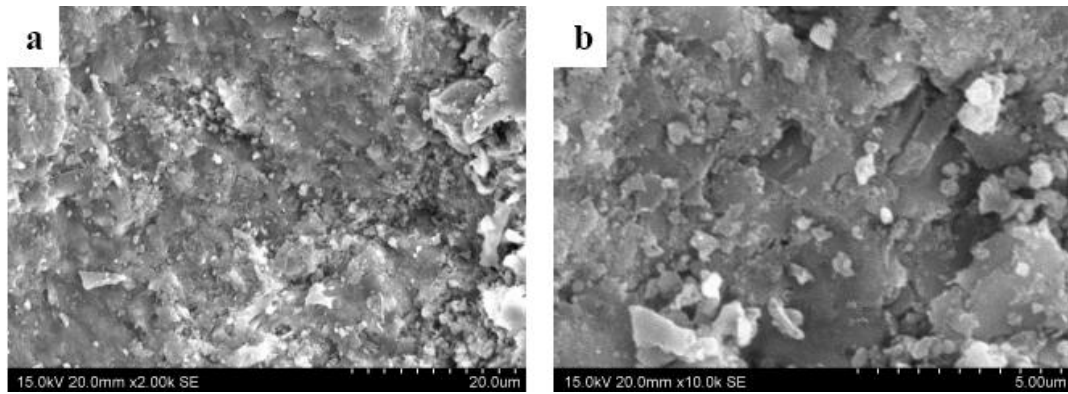


Figure 4-8 SEM secondary electron microphotographs of non-carbonated NRVB, (a) low magnification, (b) high magnification

Figure 4-9 shows a surface covered almost entirely with calcite crystals, indicating extensive carbonation. The abundance of portlandite plates has diminished and no evidence of C-S-H is visible.

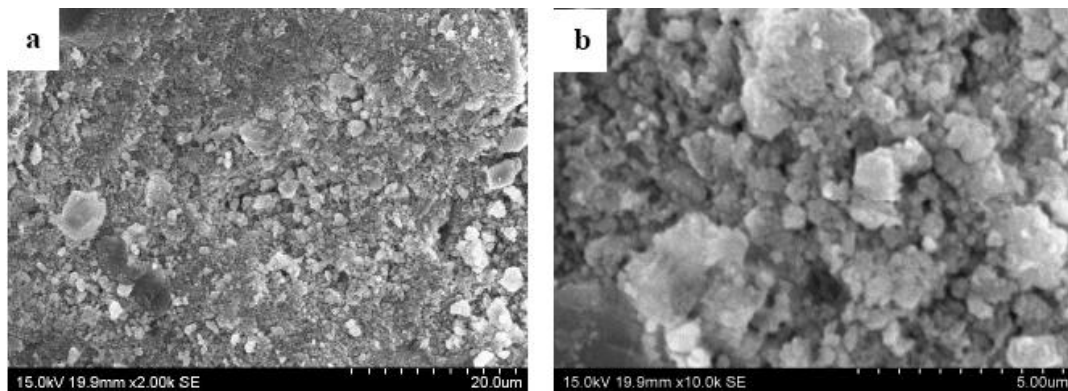


Figure 4-9 SEM secondary electron microphotographs of carbonated specimen of NRVB conditioned at 75% relative humidity, (a) Magnification X2,000 (b) Magnification X10,000

The different morphologies above and below the visually determined carbonation

interface confirmed the existence of a carbonated zone above the interface and a non-carbonated zone below the interface.

Figure 4-10 shows the SEM images of carbonated from a NRVB specimen conditioned at 100% relative humidity. Figure 4-9 and Figure 4-10 are very similar, except that the size of calcite grains is more uniform in the latter specimen. Harris et al. (2003) believed that the denser microstructure of saturated material might be due to the more even precipitation of calcite throughout the pore space.

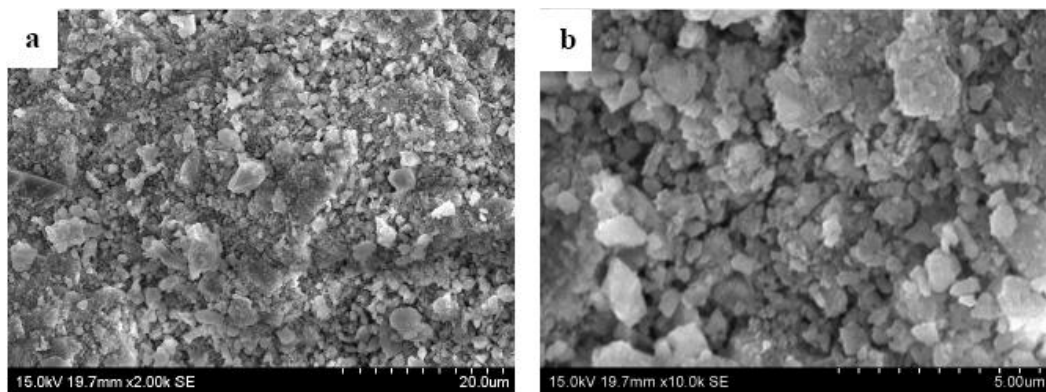


Figure 4-10 SEM secondary electron microphotographs of carbonated specimen of NRVB conditioned at 100% relative humidity, (a) Magnification X2,000 (b) Magnification X10,000

4.2.5 Examination of Mineralogy Changes

Figure 4-11 shows the XRD diffractograms of fresh NRVB and carbonated NRVB (conditioned at 75% relative humidity, P=3bar, reaction time is 102 hours). It can be

seen that the fresh NRVB specimen contained calcium hydroxide and calcium carbonate. Part of the calcium hydroxide was the hydrated lime added to the raw mixture and the rest was generated from the hydration of OPC. C-S-H and other hydrated products were not observed in the fresh NRVB, as they may exist in the form of amorphous rather than crystalline structures.

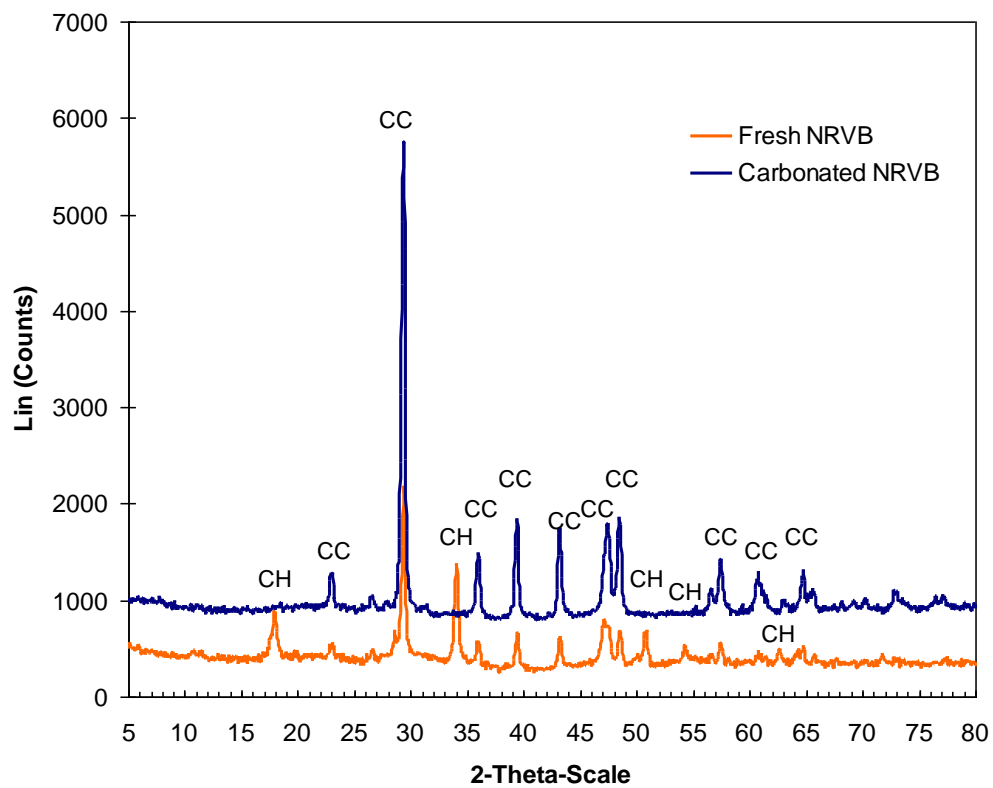


Figure 4-11 XRD diffractograms of fresh NRVB and carbonated NRVB (CC represents calcium carbonated, CH represents calcium hydroxide)

After 102 hours of carbonation, no peaks corresponding to calcium hydroxide can be found in the carbonated NRVB and the intensity of the peaks corresponding to calcium carbonate are higher.

4.2.6 Examination of Carbonation Content

When the fresh NRVB specimen was heated to 1000° C in the TGA instrument, the relationship between the temperature and weight loss of the specimen is shown in **Figure 4-12 (a)**. In this figure, the TG curve (thermogravimetric analysis curve) shows the percentage change in the weight (left vertical axis) as the temperature increases. The first derivative of the TG curve with respect to temperature yields the DTG curve, which is also shown in **Figure 4-12 (a)** using the right vertical axis. The positions of the three peaks in this DTG (differential thermogravimetric) curve indicate the percentage weight loss in the temperature range of the TG curve. The first peak appears at about 130 °C, which may be attributed to the loss of chemically bound water in C-S-H. The second peak appears between 400 to 460 °C and corresponds to the weight loss due to dehydration of calcium hydroxide. The corresponding negative peak of the DTA (differential thermal analysis) curve shows that the dehydration of calcium hydroxide is an endothermic reaction. The third peak, between 650 to 770 °C, is caused by the weight loss due to the decomposition of CaCO₃ (lime stone flour) and the consequent release of CO₂.

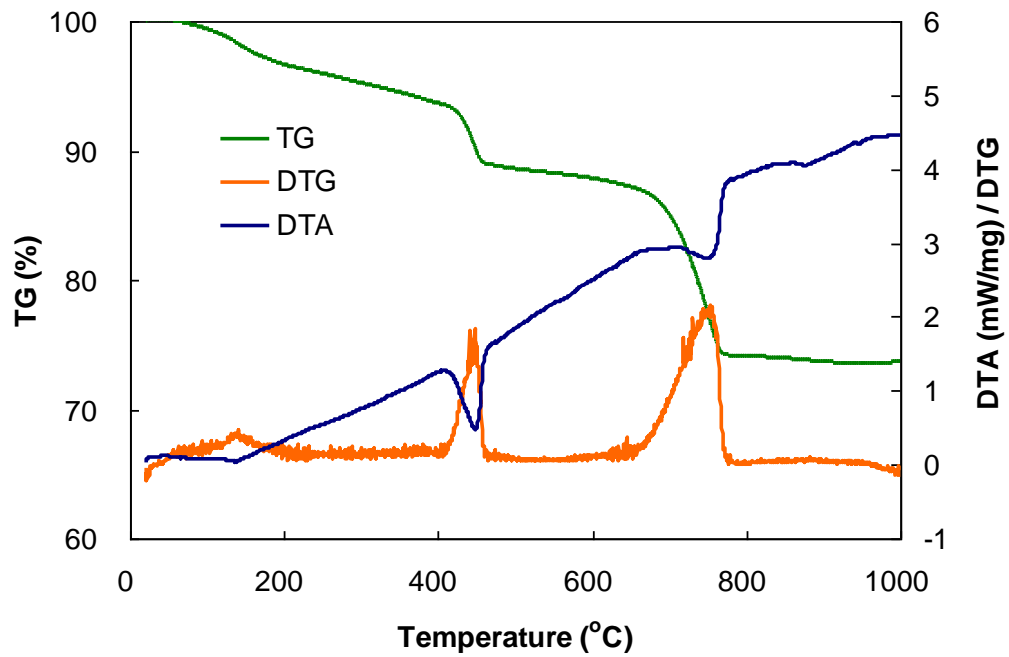


Figure 4-12 (a) TG/DTA/DTG curves of fresh NRVB

Figure 4-12 (b) shows the weight loss of a NRVB specimen carbonated for 102 hours. In this specimen, the weight loss due to the decomposition of CaCO_3 was increased. However, no calcium hydroxide exists anymore and only a minor trace of C-S-H can be observed.

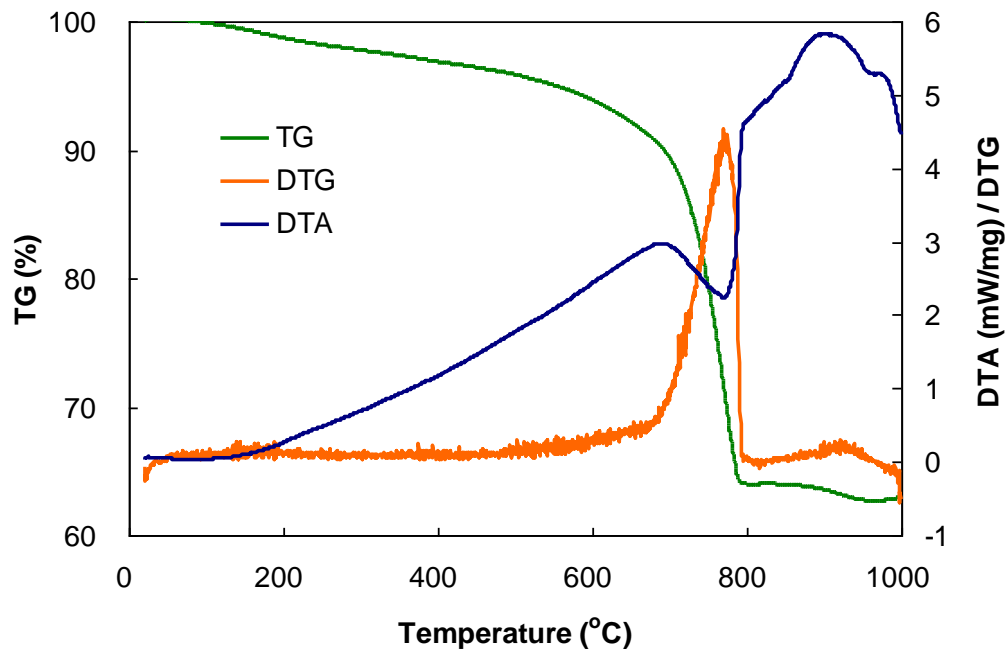


Figure 4-12 (b) TG/DTA/DTG curves of carbonated NRVB (RH=75%, P=3bar,
Reaction time=102 hours)

4.2.7 Availability of Reactive Calcium

The thermogravimetric analysis suggests that the reactive calcium in NRVB exists mainly in the form of calcium hydroxide and only small amounts of reactive calcium exist in the form of C-S-H. There is disagreement in the literature as to whether calcium hydroxide or C-S-H in hardened cement paste is more susceptible to carbonation. Some authors consider that calcium hydroxide reacts at an early stage and decalcification of C-S-H only occurs when the pH in the pore water drops to a certain level due to the consumption of calcium hydroxide [Borges et al., 2010 and Reardon et al., 1989]. Al-Kadhimi et al. [1996] suggest that C-S-H reacts in

parallel with the reaction of calcium hydroxide. Some recent work has even shown that C-S-H gel may be fully carbonated whilst calcium hydroxide is still present [Groves et al. 1996]. The experimental observation in this work suggests that in the unsaturated NRVB (NRVB conditioned at 75% and 85% relative humidities), it is the calcium hydroxide that is more susceptible to carbonation.

Atmospheric CO_2 enters porous concrete and diffuses relatively fast through the air-filled parts of the pores and very slowly through the water-filled parts. CO_2 is then consumed by the alkaline species (mainly calcium hydroxide) that are available in the pore water via a dissolution mechanism that removes them from the solid parts that are in contact with water. Carbonation may or may not consume all the available reactive calcium depending on the diffusion rate of CO_2 in the solid matrix. A carbonation front is formed and moves when the chemical reaction is faster compared to the diffusion of CO_2 .

The diffusion of CO_2 in unsaturated NRVB is relatively fast due to the high gas-filled porosity. It is believed that the diffusion rate of CO_2 is slower than its reaction rate with calcium hydroxide, which is the reason a distinct carbonation front can be observed. In contrast, the decalcification rate of C-S-H is slower than the CO_2 diffusion rate, which explains the slight colour change of phenolphthalein indicator in the zone above the carbonation front. Below the carbonation front, no carbonation occurs, since no CO_2 has yet diffused into that region.

One of the reasons of using NRVB in a radioactive waste repository is to consume all the ^{14}C -containing CO_2 before it leaves the repository. To guarantee this, the effective CO_2 uptake capacity of NRVB should be determined. The reactive calcium in NRVB that can react with CO_2 was determined by Equation 1.25 and is 7516 mol m^{-3} . However, the concentration of effective calcium that can retain the $^{14}\text{CO}_2$ in the repository could be much lower.

Figure 4-13 shows the depth to which CO_2 penetrated the NRVB samples at different points in time. The blue columns represent the depth of carbonation front by direct measurement. The pink columns are the depths calculated from the reactive calcium conversion (X_{Ca}) at the same time point. It is proved that for NRVB the concentration of reactive calcium cannot be used as the effective CO_2 up-take capacity. Doing so may cause an over-estimation of the ability of the NRVB to consume CO_2 .

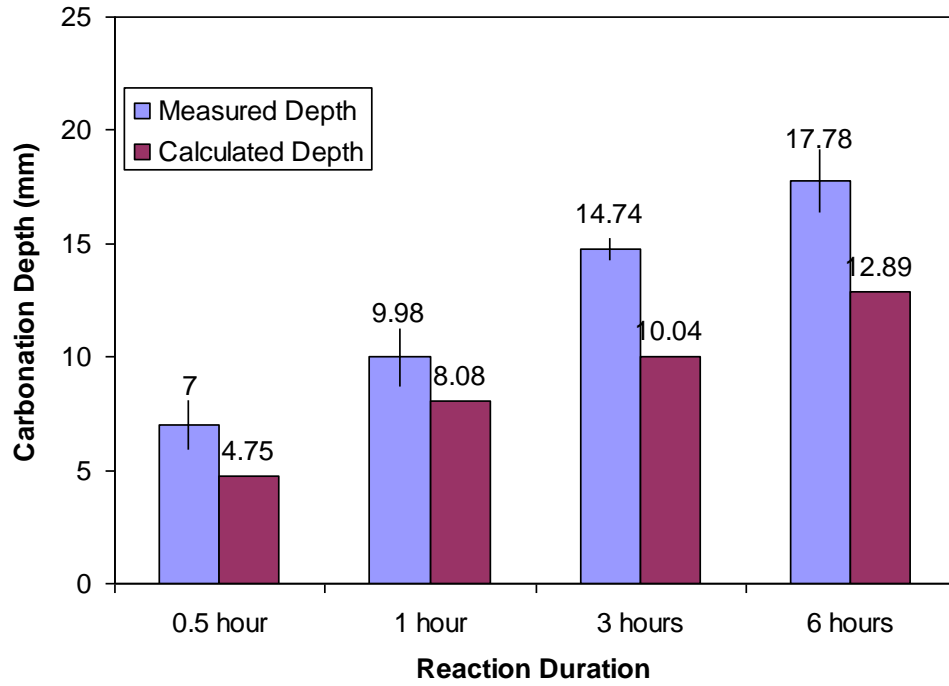


Figure 4-13 Comparison of carbonation depth between direct measurement and estimation from X_{Ca}

The concentration of effective reactive calcium (effective CO_2 uptake capacity) of NRVB can be calculated by Equation (4.1):

$$n'_{Ca} = n_{co_2,t} \times \frac{L}{l_t} \quad (4.1)$$

Where n'_{Ca} is the concentration of effective reactive calcium ($mol\ m^{-3}$)

$n_{co_2,t}$ is the mole amount of CO_2 absorbed by NRVB at time t

L is the dimension of NRVB specimen which is 25mm

l_t is the depth of carbonation front according to direct measurement.

According to the experimental data of partially carbonated specimens, the Effective

Reactive Calcium of NRVB is approximately 5437 mol m^{-3} , 30% lower than that determined theoretically on the timescale of the experiments. It is suggested, therefore, that this figure could be applicable when calculating the volume of NRVB required to act as an effective chemical barrier.

4.3 Results of 3:1 PFA/OPC Grout

4.3.1 Effect of Conditioning

The 3:1 PFA/OPC specimens and their weight changes during drying are summarised in **Table 4-7**. The specimens were numbered by the ‘P0/№’ system, in which ‘P’ represented 3:1 PFA/OPC, ‘0’ represented for zero relative humidity in the oven and ‘№’ is the specimen number from 1 to 5.

<i>No.</i>	Volume (cm³)	Initial Mass (g)	Final Mass (g)	Change in Mass (g)
P0/1	15.47	26.45	21.05	-5.4
P0/2	15.90	27.45	20	-7.45
P0/3	16.05	27.86	21.34	-6.52
P0/4	16.25	27.83	21.52	-6.31
P0/5	15.47	26.46	19.91	-6.55

Table 4-7 Results of drying 3:1 PFA/OPC at 105 °C for 24 hours

The effects of specimen conditioning are recorded in **Table 4-8** to **Table 4-10** for conditioning at 75%, 85% and 100% relative humidity, respectively. All specimens

were conditioned for a minimum period of 5 months.

<i>No.</i>	Volume (cm³)	Initial Mass (g)	Final Mass (g)	Change in Mass (g)
P75/1	15.66	26.53	23.72	-2.81
P75/2	15.59	26.6	23.78	-2.82
P75/3	15.56	26.92	24.74	-2.18
P75/4	15.22	26.51	24.45	-2.06
P75/5	15.71	26.63	23.8	-2.83
P75/6	15.41	26.41	23.8	-2.61
P75/7	15.97	27.54	25.32	-2.22

Table 4-8 Results of conditioning 3:1 PFA/OPC at 75% RH for 5 months

<i>No.</i>	Volume (cm³)	Initial Mass (g)	Final Mass (g)	Change in Mass (g)
P85/1	15.10	25.91	24.63	-1.28
P85/2	15.53	25.93	24.55	-1.38
P85/3	15.64	25.8	24.73	-1.07
P85/4	15.13	26.24	25.22	-1.02
P85/5	15.28	26.26	25.17	-1.09
P85/6	15.22	25.87	24.5	-1.37

Table 4-9 Results of conditioning 3:1 PFA/OPC at 85% RH for 5 months

<i>No.</i>	Volume (cm³)	Initial Mass (g)	Final Mass (g)	Change in Mass (g)
P100/1	15.65	26.5	26.51	0.01
P100/2	15.53	26.38	26.37	-0.01
P100/3	15.41	25.83	25.85	0.02
P100/4	15.75	26.76	26.77	0.01
P100/5	15.01	25.88	25.88	0

Table 4-10 Results of conditioning 3:1 PFA/OPC at 100% RH for 5 months

Based on the initial masses and volumes given in Table 4-7 to Table 4-10, the average initial bulk density (wet density) of 3:1 PFA/OPC grout used in this work is $1708 \pm 22 \text{ kg/m}^3$, which is very similar to the bulk density of NRVB ($1711 \pm 16 \text{ kg/m}^3$).

The average weight loss and gas-filled porosity at each relative humidity are summarised in **Table 4-11**. The percentage weight loss of oven dried 3:1 PFA/OPC is estimated as $23.7 \pm 2.2\%$. Its estimated porosity is 0.41 ± 0.04 , which is lower than the porosity of NRVB.

Relative Humidity	Weight Loss (%) ^(a)	Gas-filled Porosity ^(a)
0%	23.7 ± 2.2	0.41 ± 0.04
75%	9.4 ± 1.2	0.16 ± 0.02
85%	4.6 ± 0.6	0.08 ± 0.01
100%	0.0 ± 0.0	0.00 ± 0.00

Table 4-11 3:1 PFA/OPC gas-filled porosity and degree of water saturation

The percentage weight loss on conditioning has been measured as $9.4 \pm 1.2\%$ for conditioning at 75% relative humidity and $4.6 \pm 0.6\%$ for conditioning at 85% relative humidity. The gas-filled porosity at 75% and 85% relative humidity are estimated as 0.16 ± 0.02 and 0.08 ± 0.01 , respectively.

Conditioning at 100% relative humidity shows no weight change, which confirms that the 3:1 PFA/OPC specimens unwrapped from the wet tissues were fully saturated with water, i.e. all the pores were filled with water.

4.3.2 Results of Carbonation Test

The effect of relative humidity and initial CO₂ pressure on the carbonation reaction of 3:1 PFA/OPC is shown in **Figure 4-14** in terms of conversion of reactive calcium (X_{Ca}) vs. time.

The gas-filled porosity of 3:1 PFA/OPC was 16%, 8% and 0% at the relative humidities of 75%, 85% and 100%, respectively. As expected, increasing the relative humidity decreases the rate of carbonation. Although the elevated initial CO₂ pressure enhanced the reaction rate, its effect is not as significant as that of relative humidity.

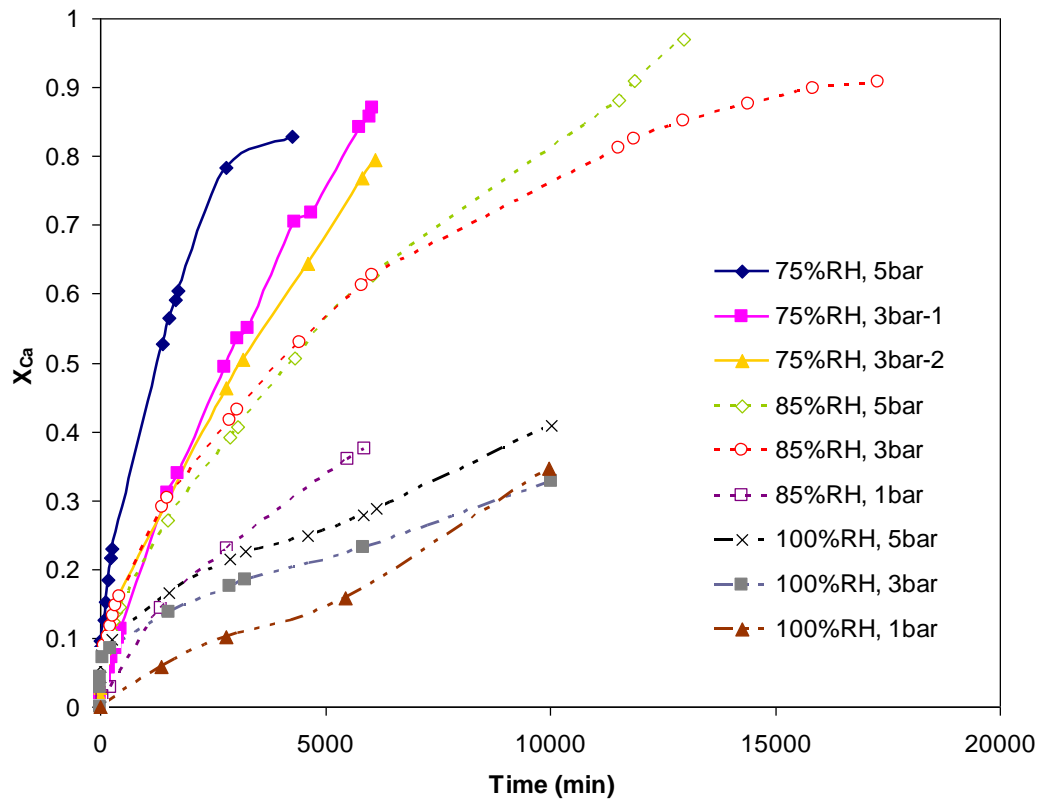


Figure 4-14 Evolution of Reaction with time for 3:1 PFA/OPC at pressure from 1bar to 5bar at relative humidity from 75% to 100% (Error in $X_{Ca} = \pm 0.025$)

4.3.3 Observation of Carbonation Profile

A set of specimens conditioned at 75% relative humidity and carbonated at 3 bar for 1 hour, 17 hours and 106 hours was examined by direct observation and the phenolphthalein test. The results are shown in photographs in **Figure 4-15**.

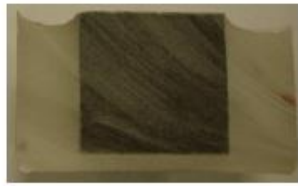

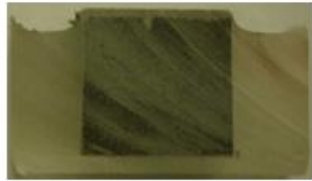



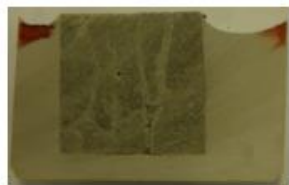
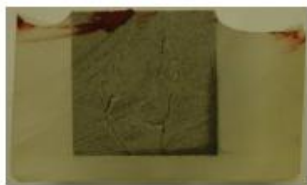
Reaction Time	Direct Observation	Phenolphthalein Test
Fresh 3:1 PFA/OPC		
1 hour		
17 hours		
106 hours		

Figure 4-15 Cross-section of cut 3:1 PFA/OPC specimens with different carbonation durations, P=3bar, RH=75%

Similar to the partially carbonated NRVB specimens, obvious colour differences between the carbonated and non-carbonated zones can be observed. However, the phenolphthalein test showed no colour change above the carbonation interface and the pink colour of the non-carbonated zone appeared lighter than that of the non-carbonated NRVB. After conditioning at 75% relative humidity, the gas-filled porosity of 3:1 PFA/OPC was 16%, while the gas-filled porosity of NRVB was 37%, more than twice that of the 3:1 PFA/OPC. Therefore, unlike the NRVB, the diffusion rate of CO₂ in 3:1 PFA/OPC could be slower than the chemical reaction

rate and the reactive calcium could be fully carbonated above the carbonation front.

The pH value of pore water in 3:1 PFA/OPC was also much lower than that in the NRVB, because most of the calcium hydroxide in PFA/OPC grout was turned into C-S-H with less alkalinity due to the pozzolanic reaction.

Quite often tiny cracks due to drying shrinkage could be observed on the surface of the unsaturated 3:1 PFA/OPC specimens. As the effective diffusion coefficient of CO₂ in a crack is higher than in cement pores, carbonation would tend to occur along the cracks, leading to inconsistencies in the carbonation front. When only small amounts of calcium hydroxide are present, C-S-H is rapidly decalcified and the decalcification causes shrinkage with a significant rise in permeability [Borges et al. 2010]. The carbonation shrinkage would create micro-cracks and amplify the existing cracks. Therefore, as demonstrated in **Figure 4-15**, the cracks become wider and deeper as the reaction proceeds. In the specimen carbonated for 106 hours, the colour along the cracks is even lighter, which means the carbonation along the cracks is more intense. Fully decalcified areas could exist along the length and in the region of the cracks and, hence, the C-S-H with low C/S ratio may still exist where there are no cracks.

In contract, as shown in **Figure 4-16**, no cracks appeared in the specimen conditioned at 100% relative humidity. As the specimen was fully saturated with water, the diffusion rate of CO₂ was so slow that neither drying shrinkage nor

carbonation shrinkage could be observed.

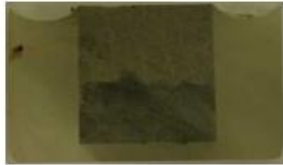
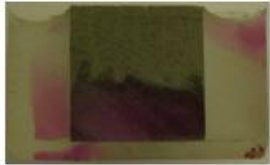
Reaction Time	Direct Observation	Phenolphthalein Test
168 hours 100% RH		

Figure 4-16 Cross-section of cut 3:1 PFA/OPC specimen after 168 hours
carbonation, P=3bar, RH=100%

4.3.4 Examination of Microstructure Using SEM

To compare the differences in microstructure between the non-carbonated and carbonated zones, a partially carbonated 3:1 PFA/OPC specimen, carbonated at 75% relative humidity, was examined by SEM.

Comparing **Figure 4-17(a)** with **Figure 4-18(a)**, the non-carbonated surface is smoother. In **Figure 4-17(b)** which is a higher magnitude SEM image, glassy spheres of PFA can be observed. However, after carbonation, they were covered by calcium carbonate, the carbonation product (**Figure 4-18(b)**).

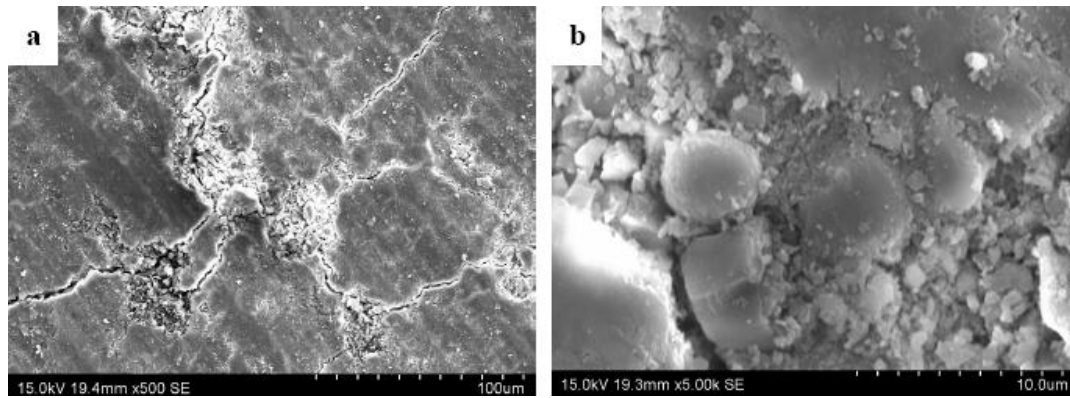


Figure 4-17 SEM secondary electron microphotographs of non-carbonated specimen of 3:1 PFA/OPC grout, (a) Magnification X500 (b) Magnification X5,000

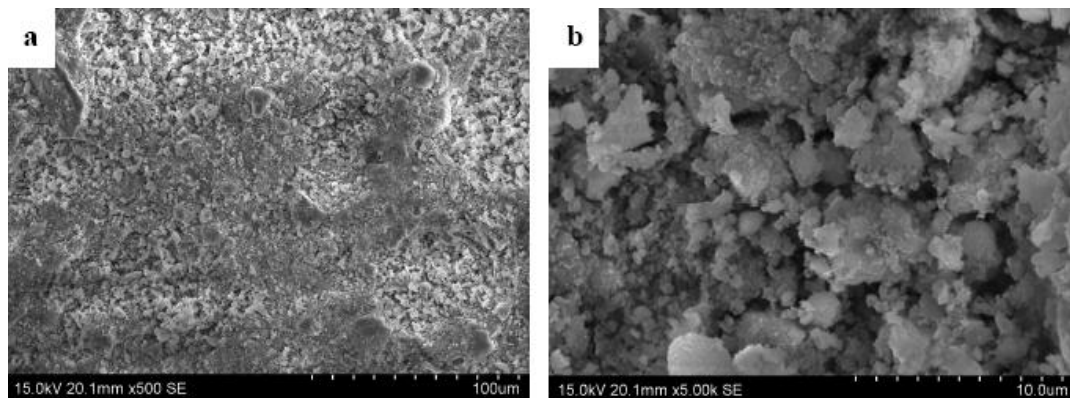


Figure 4-18 SEM secondary electron microphotographs of carbonated specimen of 3:1 PFA/OPC grout conditioned at 75% relative humidity, (a) Magnification X500 (b) Magnification X5,000

4.3.5 Examination of Mineralogy Changes

Figure 4-19 shows the XRD diffractograms of fresh 3:1 PFA/OPC and carbonated 3:1 PFA/OPC (conditioned at 75% relative humidity, P=3bar, reaction time is 106

hours). It can be seen that the only phase showing in fresh 3:1 PFA/OPC specimen is quartz. This may suggest that all the calcium hydroxide crystals generated from the hydration of OPC were consumed by the pozzolanic reaction and the reaction product, amorphous C-S-H, could not be detected by XRD.

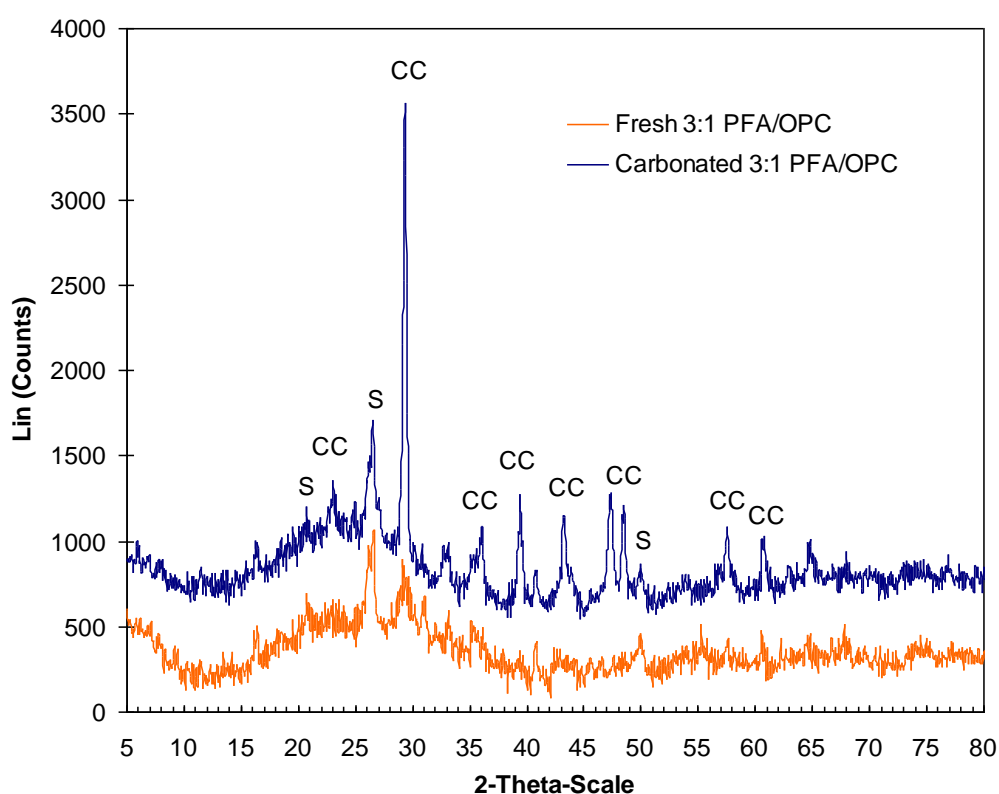


Figure 4-19 XRD diffractograms of Fresh 3:1 PFA/OPC and carbonated 3:1 PFA/OPC (CC represents calcium carbonate, S represents quartz)

After 106 hours carbonation, peaks corresponding to calcium carbonate can be found in the carbonated 3:1 PFA/OPC and the intensity of peaks corresponding to quartz has not changed at all.

4.3.6 Examination of Carbonation Content

According to the thermogravimetric analysis of fresh 3:1 PFA/OPC (**Figure 4-20(a)**), the only weight change occurred between 100 to 200 °C, which was due to the loss of water from C-S-H. The absence of calcium hydroxide confirmed the finding from XRD analysis that all the calcium hydroxide was consumed by the PFA after 15 months curing.

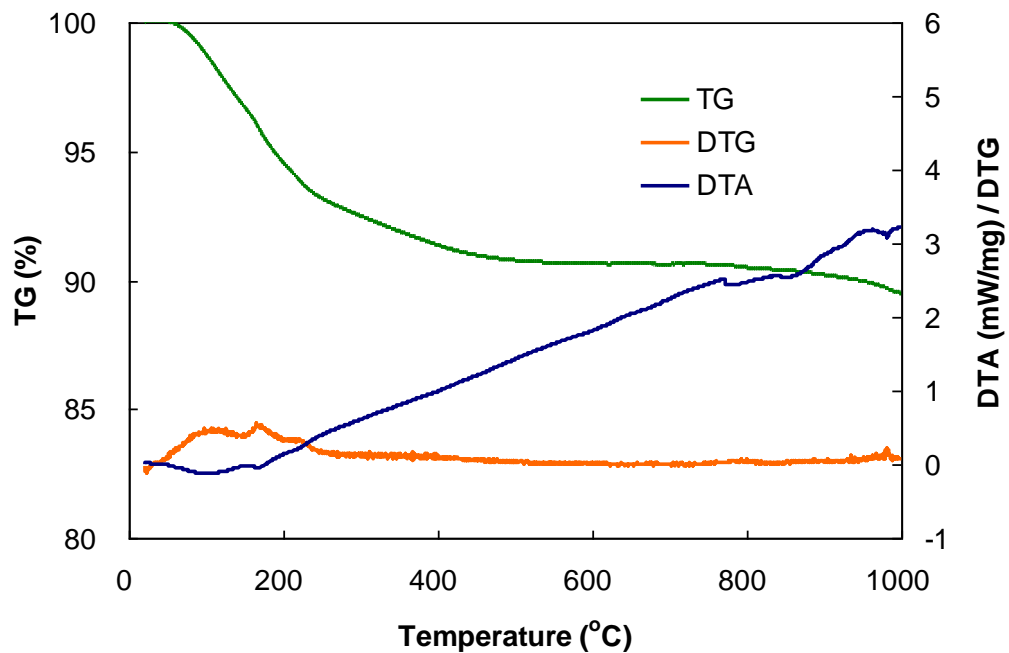


Figure 4-20 (a) TG/DTA/DTG curves of fresh 3:1 PFA/OPC grout

The TG, DTA and DTG curves of 3:1 PFA/OPC specimen carbonated for 106 hours are shown in **Figure 4-20(b)**. Minor traces of C-S-H can be observed and the main weight loss is between 650 to 750 °C due to the decomposition of calcium carbonate.

According to this weight change, the amount of CO_2 absorbed by the 3:1 PFA/OPC specimen was calculated. The calculated value was around 2100 mol m^{-3} , which is only half the amount of reactive calcium in PFA/OPC (4248 mol m^{-3}). This difference may be due to the complex chemical nature of cement and PFA, which precluded exact quantitation by TGA (Carl Knopf et al., 1999). Therefore, the TGA results were confined to relative comparisons only.

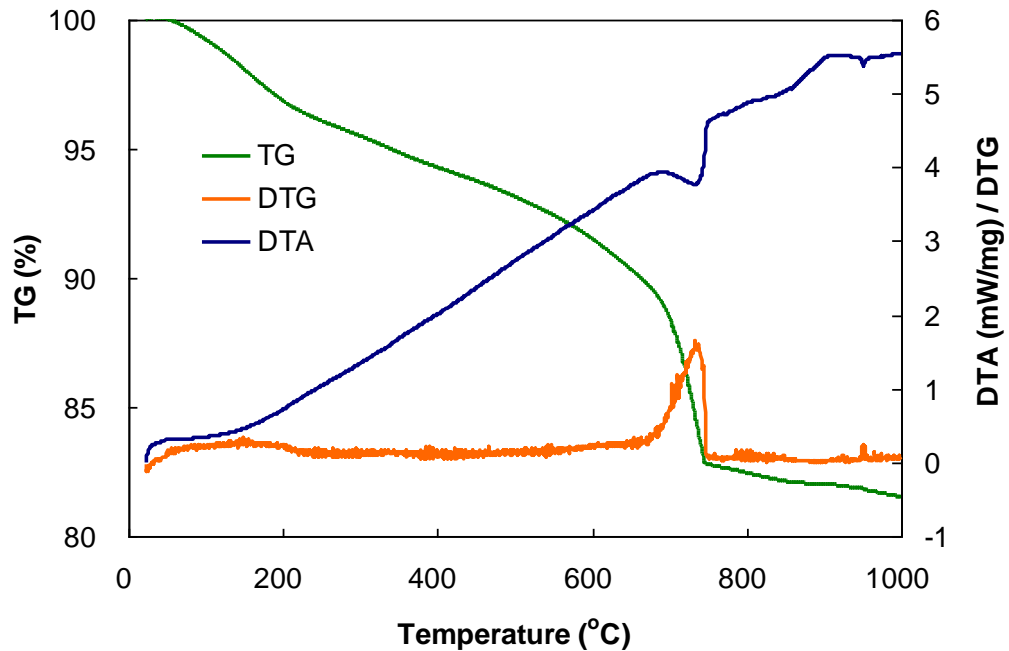


Figure 4-20 (b) TG/DTA/DTG curves of carbonated 3:1 PFA/OPC grout

4.4 Results of 3:1 BFS/OPC Grout

4.4.1 Effect of Conditioning

The 3:1 BFS/OPC specimens and their weight changes during drying are summarised in **Table 4-12**. The specimens were numbered by the 'B0/№' system, in which 'B' represented 3:1 BFS/OPC, '0' represented for zero relative humidity in the oven and '№' is the specimen number from 1 to 5.

<i>No.</i>	Volume (cm³)	Initial Mass (g)	Final Mass (g)	Change in Mass (g)
B0/1	16.18	31.37	25.31	-6.06
B0/2	16.27	32.18	25.8	-6.38
B0/3	16.45	33.42	27.42	-6
B0/4	16.15	31.66	24.94	-6.72
B0/5	16.09	31.65	25.08	-6.57

Table 4-12 Results of drying 3:1 BFS/OPC at 105 °C for 24 hours

The effects of specimen conditioning are recorded in Table 4-13 to Table 4-15 for conditioning at 75%, 85% and 100% relative humidity, respectively. All specimens were conditioned for a minimum period of 1 month.

Based on the initial masses and volumes given in **Table 4-12** to Table 4-15, the average initial bulk density (wet density) of 3:1 BFS/OPC grout used in this work is $1992 \pm 30 \text{ kg/m}^3$. This may be compared with the previous estimated density of

1930±50 kg/m³ (Harris et al. 2002). The slight difference between the batches of 3:1 BFS/OPC grouts may be due to the specimen ages. The current measurements are based upon a batch of 3:1 BFS/OPC cured for 15 months. The previous measurements used a different batch of 6 month-old 3:1 BFS/OPC. Therefore, the higher material density in this work may be due to the longer period of hydration.

<i>No.</i>	Volume (cm³)	Initial Mass (g)	Final Mass (g)	Change in Mass (g)
B75/1	16.37	0.19	0.19	-0.19
B75/2	16.54	0.23	0.23	-0.23
B75/3	17.11	0.24	0.24	-0.24
B75/4	16.96	0.21	0.21	-0.21
B75/5	16.37	0.19	0.19	-0.19
B75/6	15.90	0.23	0.23	-0.23

Table 4-13 Results of conditioning 3:1 BFS /OPC at 75% RH for 1 month

<i>No.</i>	Volume (cm³)	Initial Mass (g)	Final Mass (g)	Change in Mass (g)
B85/1	15.38	31.49	31.36	-0.13
B85/2	15.65	30.8	30.66	-0.14
B85/3	15.44	30.54	30.38	-0.16
B85/4	15.75	31.7	31.58	-0.12
B85/5	15.70	31.07	30.92	-0.15
B85/6	16.00	31.99	31.82	-0.17

Table 4-14 Results of conditioning 3:1 BFS /OPC at 85% RH for 1 month

<i>No.</i>	Volume (cm³)	Initial Mass (g)	Final Mass (g)	Change in Mass (g)
B100/1	16.43	33.22	33.29	0.07
B100/2	17.16	34.57	34.65	0.08
B100/3	15.59	31	31.07	0.07
B100/4	15.97	30.75	30.75	0
B100/5	16.56	33.76	33.81	0.05

Table 4-15 Results of conditioning 3:1 BFS /OPC at 100% RH for 1 month

The average weight loss and gas-filled porosity at each relative humidity are summarised in Table 4-16.

Relative Humidity	Weight Loss (%)^(a)	Gas-filled Porosity^(a)
0%	19.82 \pm 1.15	0.392 \pm 0.019
75%	0.65 \pm 0.06	0.013 \pm 0.001
85%	0.45 \pm 0.06	0.009 \pm 0.001
100%	-0.16 \pm 0.09	-0.003 \pm 0.002

Table 4-16 3:1 BFS/OPC gas-filled porosity and degree of water saturation

The percentage weight loss of oven dried 3:1 BFS/OPC is estimated as 19.82 \pm 1.15%. This value is similar to the previously measured value of 20.0% (Harris et al. 2002). Meanwhile, the weight loss on drying gives an estimated porosity of 0.39 \pm 0.02, which remains the same as has been observed previously (Harris et al. 2002).

The percentage weight loss on conditioning has been measured as 0.65 \pm 0.06% for

conditioning at 75% relative humidity and $0.45 \pm 0.6\%$ for conditioning at 85% relative humidity. The gas-filled porosity at 75% and 85% relative humidity are estimated as 0.013 ± 0.001 and 0.009 ± 0.001 , respectively. In previous work, the gas-filled porosity was estimated as 0.021 for conditioning at 75% relative humidity. The difference between the gas-filled porosities of two batches of 3:1 BFS/OPC may be due to the different duration of hydration. It has been shown that hydration could make cement based materials denser. [Beaudoin et al. 1994]

Conditioning at 100% relative humidity shows a slight increase in weight ($0.16 \pm 0.09\%$), which may due to slight self-desiccation during curing in sealed conditions [Harris et al. 2002].

4.4.2 Results of Carbonation Test

The effect of relative humidity and initial CO_2 pressure on the carbonation reaction of 3:1 BFS/OPC is shown in Figure 4-21 in terms of conversion of reactive calcium (X_{Ca}) vs. time.

Comparing with NRVB and 3:1 PFA/OPC, the carbonation of 3:1 BFS/OPC was very slow. This may be due to the low porosity and fine pore size of 3:1 BFS/OPC. As shown in Table 4-16, the gas-filled porosity at 75% and 85% relative humidity was only 1.3% and 0.9%, respectively, which are ten times smaller than the

gas-filled porosity of 3:1 PFA/OPC at the same relative humidity.

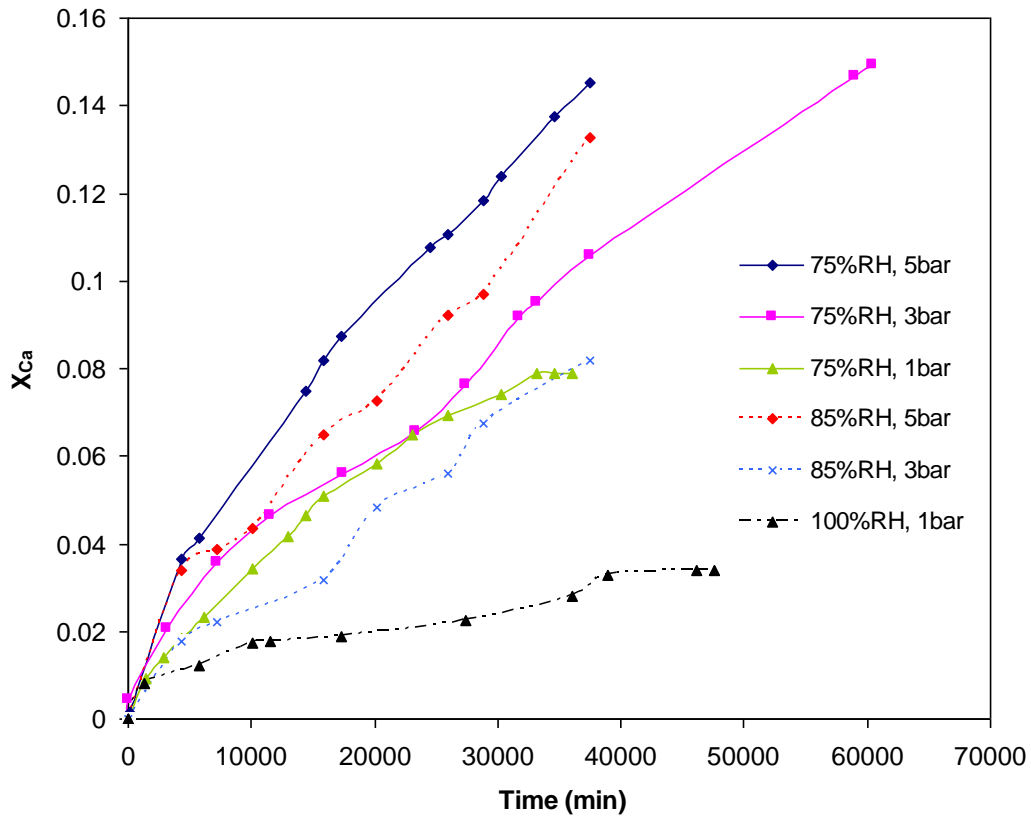


Figure 4-21 Evolution of reaction with time for 3:1 BFS/OPC at pressure from 1bar to 5bar at relative humidity from 75% to 100% (Error in $X_{Ca} = \pm 0.013$)

Figure 4-21 shows that increasing relative humidity caused a decrease in the rate of reaction. For the specimens conditioned at both 75% relative humidity and 85% relative humidity, the reaction rate with an initial CO_2 pressure of 5 bar is faster than the rate at 3 bar and 1 bar. Due to the slow reaction rate, the uncertainty in the results is also larger. Therefore, several sets of experimental results were discarded due to obvious compounded errors.

4.4.3 Observation of Carbonation Profile

From Figure 4-22 we can see a clear colour difference between the carbonated and non-carbonated zones by direct observation. The carbonation interface was irregular in shape due to the cracks. The microcracking can be explained when carbonation of C-S-H is considered (Borges et al. 2010). Although the reaction proceeded for 26 days, the average depth of the carbonated layer was lower than 6 mm.





Reaction Time	Direct Observation	Phenolphthalein Test
Fresh 3:1 BFS/OPC		
26 days (P=3bar, RH=75%)		

Figure 4-22 Cross-section of fresh and partially carbonated 3:1 BFS/OPC specimens

The phenolphthalein test showed the same carbonation interface as by direct observation. No colour appeared above the carbonation interface, which means the pH in the carbonated layer was lower than 8.3.

4.4.4 Examination of Microstructure Using SEM

To compare the difference in microstructure between the non-carbonated and carbonated zones, the partially carbonated 3:1 BFS/OPC specimen shown in Figure 4-22 was examined by SEM. The cut surface of the non-carbonated zone (Figure 4-23) is smoother and micro-cracks due to drying shrinkage can be observed. The carbonated surface (Figure 4-24) is rougher and covered by calcium carbonate. Wider cracks can also be observed in Figure 4-23, which may due to the carbonation shrinkage.

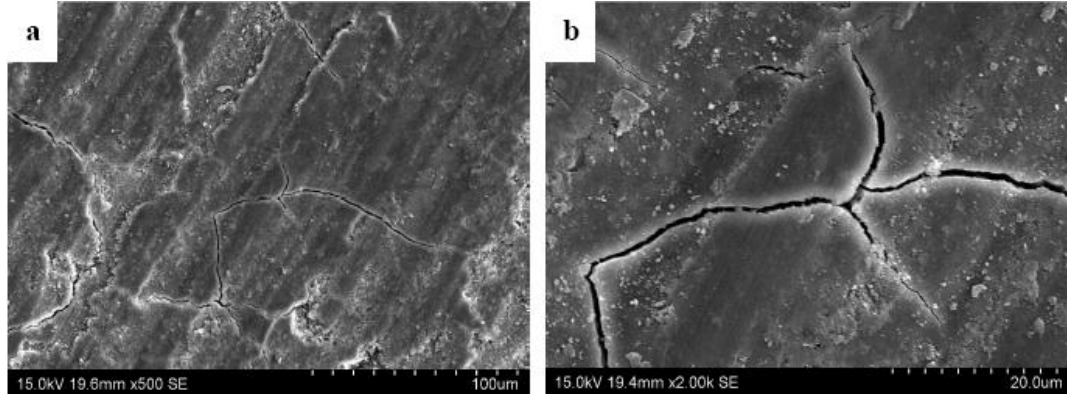


Figure 4-23 SEM secondary electron microphotographs of non-carbonated specimen of 3:1 BFS/OPC grout, (a) Magnification X500 (b) Magnification X2,000

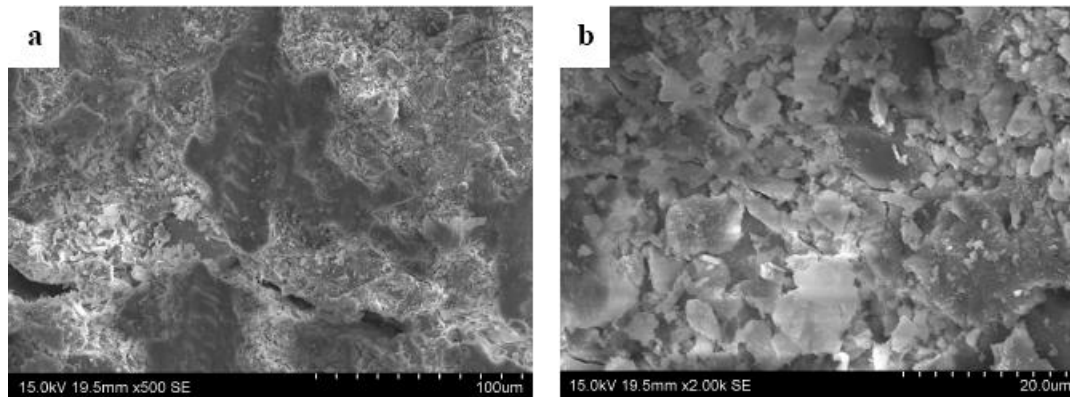


Figure 4-24 SEM secondary electron microphotographs of carbonated specimen of 3:1 BFS/OPC grout conditioned at 75% relative humidity, (a) Magnification X500 (b) Magnification X2,000

4.4.5 Examination of Mineralogy Changes

The XRD signals (Figure 4-25) of 3:1 BFS/OPC are very noisy due to the complex composition of BFS. However, the difference between fresh and carbonated specimens can still be distinguished. Some of the peaks corresponding to calcium hydroxide disappear after carbonation. Peaks representing calcium carbonate and quartz can only be identified in the carbonated 3:1 BFS/OPC.

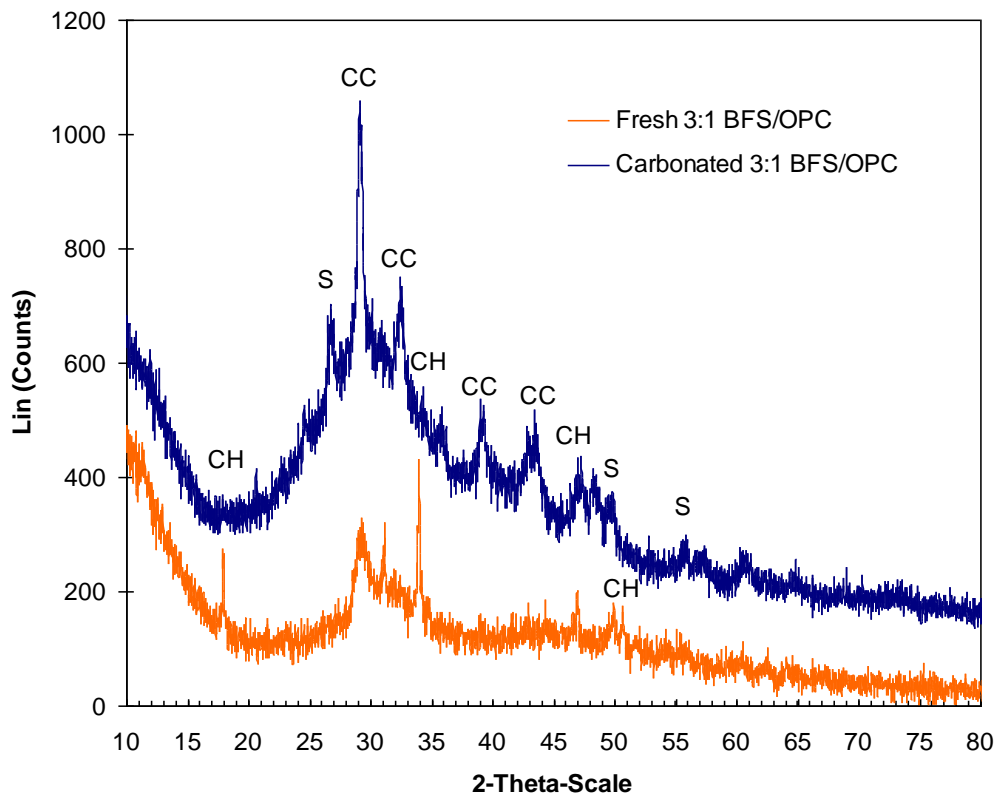


Figure 4-25 XRD diffractograms of Fresh 3:1 BFS/OPC and carbonated 3:1 BFS/OPC (CC represents calcium carbonated, CH represents calcium hydroxide, S represents quartz)

4.4.6 Examination of Carbonation Content

Thermal analysis of fresh 3:1 BFS/OPC (Figure 4-26 (a)) suggests that the reactive calcium existed in the form of C-S-H as well as calcium hydroxide. According to the DTG curve in Figure 4-26 (b), the peak corresponding to the dehydration of C-S-H (100 to 200 °C) still exists in the carbonated zone, while the peak corresponding to the decomposition of calcium hydroxide disappeared. This suggests that the carbonation rate of calcium hydroxide was faster than that of C-S-H.

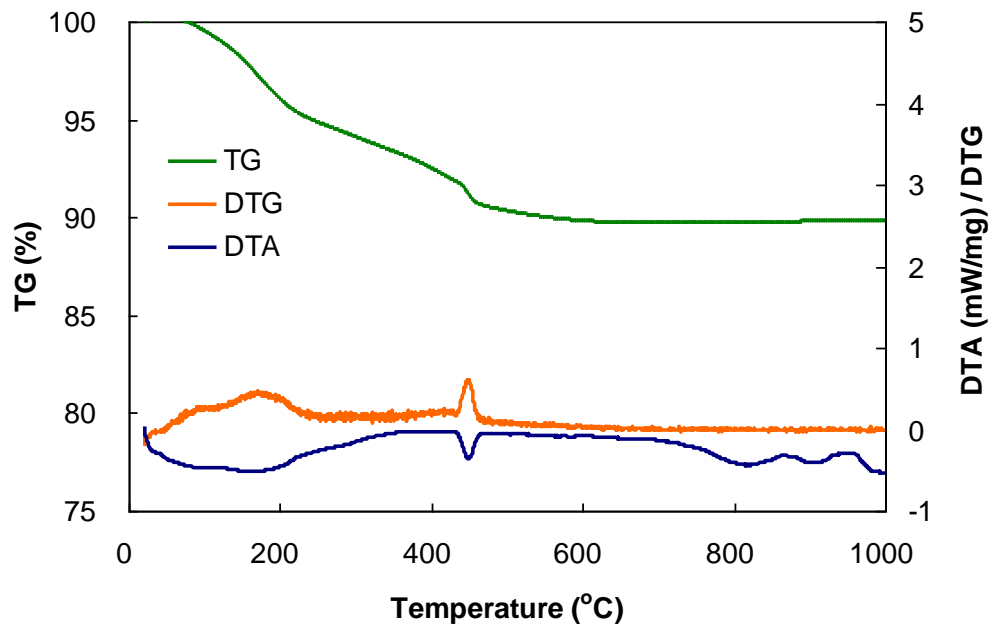


Figure 4-26 (a) TG/DSC/DTG curves of fresh 3:1 BFS/OPC grout

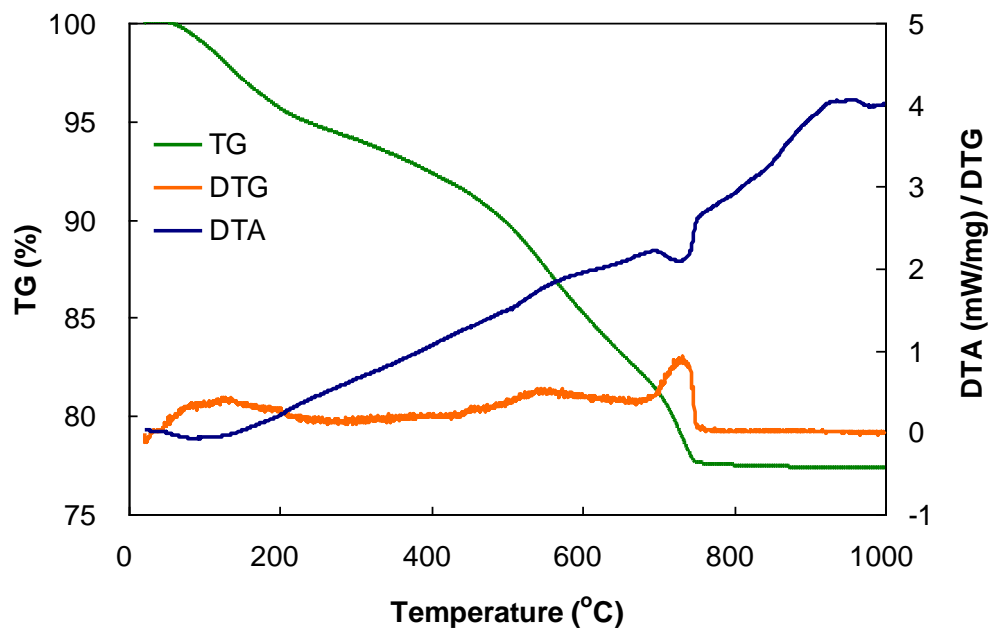


Figure 4-26 (b) TG/DSC/DTG curves of carbonated 3:1 BFS/OPC grout

4.5 Discussion

Carbonation studies conducted on NRVB, 3:1 PFA/OPC grout and 3:1 BFS/OPC grout suggest that: increasing the degree of water saturation (controlled by conditioning) in the solid matrix decelerates the carbonation progress; a higher pressure of CO₂ enhances carbonation; the effect of CO₂ pressure is less significant than the effect of degree of saturation.

Due to the difference in pore size, NRVB and waste-form grouts presented different degrees of saturation although they were conditioned at the same humidity. In Figure 4-27 gas-filled porosities of NRVB, 3:1 PFA/OPC and 3:1 BFS/OPC at different relative humidities are compared. In NRVB, more than 55% of the pore space remained unsaturated after being conditioned at 85% RH. However, in 3:1 BFS/OPC, the saturation degree reached almost 97% even at 75% RH. This suggests that not only the overall porosity but also the average pore size of 3:1 BFS/OPC is much smaller than that of NRVB. The large dry porosity and pore diameter of NRVB is due to the addition of lime stone flour and the high water/solid ratio (0.55).

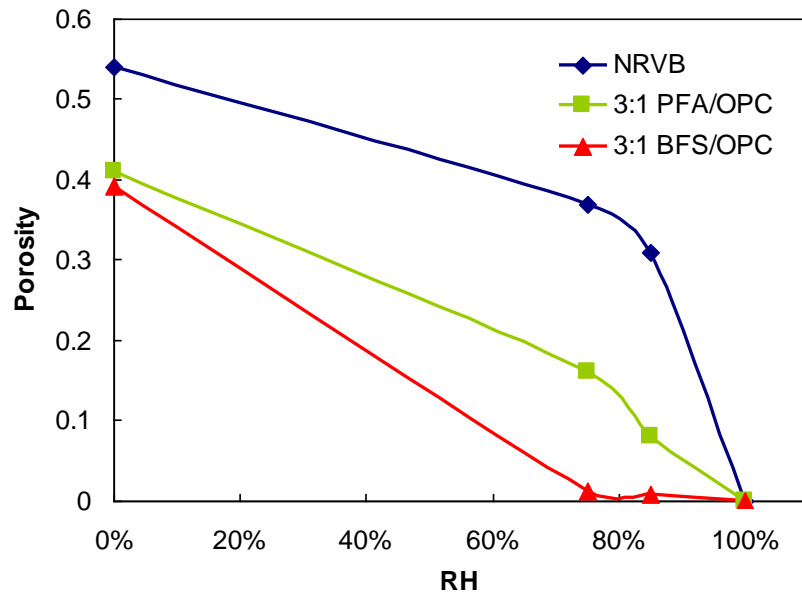


Figure 4-27 Gas-filled porosity at different relative humidities

4.5.1 Carbonation of NRVB

According to the TG/DTA analysis, Ca(OH)_2 is the main alkaline phase in the NRVB that can react with CO_2 . C-S-H also contributes to the carbonation reaction but less so than Ca(OH)_2 . Experiments suggest that CO_2 firstly reacts with Ca(OH)_2 . As the available Ca(OH)_2 starts depleting, the pH in the pore water drops and C-S-H starts to release Ca^{2+} for further carbonation until the Ca in C-S-H is depleted.

The experimental results reveal that four zones can be identified with reference to carbonation progression in unsaturated NRVB (Refer to Figure 4-28):

- A zone of total carbonation of both Ca(OH)_2 and C-S-H. This state is reached

after the reaction has proceeded for several hours. This fully carbonated zone appears light grey in colour and is undetectable by phenolphthalein spray.

- A zone of partial carbonation, where only Ca(OH)_2 is completely carbonated. C-S-H is partially carbonated in this zone and its pH of pore solution is relatively lower than Ca(OH)_2 . However the alkalinity is high enough to cause a slight colour change (light pink) with phenolphthalein spray. This zone has the same light grey colour as that of the fully carbonated zone. The two zones can be distinguished by the phenolphthalein test.

- A zone with partially carbonated Ca(OH)_2 . However, the carbonation state of C-S-H is not very clear. This zone is very narrow (less than 0.5 mm thick) and can be treated as a sharp carbonation front. It signifies the position where CO_2 can reach in the solid matrix.

- A noncarbonated zone. The colour of this zone is dark grey and can be distinguished from the partially carbonated zone by direct observation. The phenolphthalein test indicates purple red.

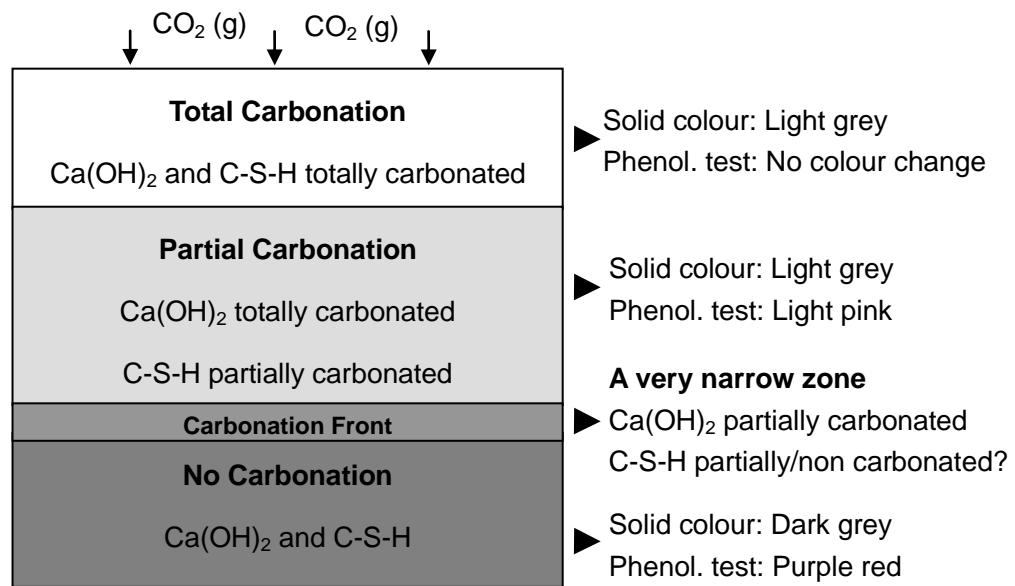


Figure 4-28 Schematic illustrating the carbonation profile of unsaturated NRVB

The carbonation profile in fully saturated NRVB is very different. The partially carbonated zone cannot be detected by phenolphthalein spray. The carbonation front is also in an irregular shape instead of parallel to the reaction surface. The same phenomenon with saturated NRVB was also observed by Harris et al. [2003]. The absence of a partially carbonated zone can be attributed to the slow diffusion of CO₂ in the pores saturated with water. However, the reason for a non-parallel carbonation front is still not clear.

4.5.2 Carbonation of 3:1 PFA/OPC

Analytical results suggest that most of the calcium hydroxide crystals generated from the hydration of OPC were turned into C-S-H by the Pozzolanic reaction.

Somewhat differently from the carbonation profile of unsaturated NRVB, three zones are observed for both unsaturated and saturated 3:1 PFA/OPC grouts (as shown in Figure 4-29):

- A zone of total carbonation of C-S-H. This fully carbonated zone appears light grey in colour and is undetectable on a phenolphthalein spray.
- A very narrow transition zone, where C-S-H is partially carbonated. This zone is narrow enough to be treated as a sharp carbonation front.
- A non-carbonated zone. The colour of this zone is dark grey and can be distinguished from the fully carbonated zone by direct observation. The phenolphthalein test indicates light pink due to the lower alkalinity of C-S-H gel.

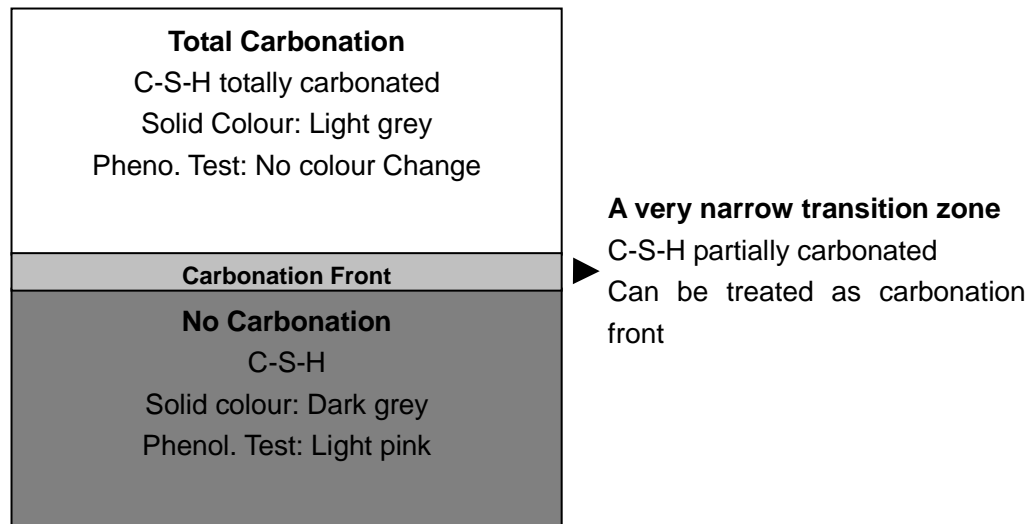


Figure 4-29 Schematic illustrating the carbonation profile of 3:1 PFA/OPC grout

4.5.3 Carbonation of 3:1 BFS/OPC

Thermal analysis of fresh 3:1 BFS/OPC suggests that the reactive calcium exists in the form of C-S-H as well as $\text{Ca}(\text{OH})_2$. However, C-S-H is more predominant in quantity. The reaction between CO_2 and 3:1 BFS/OPC was very slow due to the low gas-filled porosity of the grout. The carbonation profile of 3:1 BFS/OPC is similar to that of 3:1 PFA/OPC, except the pH value of the non-carbonated zone is higher and a phenolphthalein spray turns it into purple red.

4.5.4 Cracks due to Carbonation

When CO_2 attacks C-S-H, the removal of interlayer Ca^{2+} ions from C-S-H creates an excess of negative charge, which is balanced through subsequent formation of Si-OH groups. Condensation of neighbouring Si-OH groups to Si-O-Si linkages then forms silica gel [Chen, et al. 2006]. This condensation increases the mean silicate chain length and forms bridges between neighbouring regions, thus pulling them closer together leading to shrinkage. As a result, CO_2 attack causes polymerisation of the silicate chain in C-S-H, which may cause a volumetric decrease (shrinkage) and cracking [Bourges, et al., 2010]. This explains the formation of cracks in 3:1 PFA/OPC and 3:1 BFS/OPC during carbonation. C-S-H is the main component that can react with CO_2 in the waste-form grouts therefore the shrinkage caused by carbonation is more intensive than that in NRVB.

5 KINETIC ANALYSIS OF CARBONATION

5.1 Introduction

One of the objectives of the carbonation test is to understand the reaction kinetics. Based on the reaction kinetics, a mathematic model can be developed, which would allow prediction of the extent of carbonation. There are various models in the literature that can be used as a basis for such a model. These can roughly be split into two categories: the Explicit Prediction Laws and Complex Models.

The Explicit Laws can be based on either empirical or theoretical considerations, or a mixture of both, and have a long history in carbonation modelling [Khunthongkeaw, et al., 2006, Loo, et al., 1994, Sisomphon and Franke, 2007, De Ceukelaire and Van Nieuwenburg, 1993]. Usually they consist of one explicit formula predicting the carbonation depth at a given time, sometimes called Carbonation Laws. The most often used carbonation law is the Square Root Law (also known as the Parabolic Law), a formula relating the depth of carbonation to the square root of exposure time, which was first presented in 1928, and has been proved by a number of authors ever since [Richardson, 1988].

In practice, the explicit prediction models are preferred because they are easy to

handle. However, they can only be used under several strong assumptions and are not precise to describe the effect of certain parameters, such as cement type or water-to-cement ratio.

In contrast, Complex Models usually are based on mass and/or heat balances, which consist of systems of partial differential equations modelling the full carbonation process [Burkan Isgor and Ghani Razaqpur, 2004, Peter, et al., 2005, Saetta, et al. 1993, Steffens, et al., 2002]. Explicit analytical solutions for these models exist only in very special cases, therefore in general they have to be solved numerically.

Most Complex Models are based on microphysical/chemical approaches [Ishida and maekawa, 2000] and are more capable of capturing effects for a range of spatial scales, such as the different pore sizes in cement-based materials or fractures. However, to establish these models geometrical, material and exposure data have to be available.

In the current work, an explicit prediction formula based on Fick's first law of diffusion is applied to the carbonation data of NRVB, 3:1 PFA/OPC grout and 3:1 BFS/OPC grout, respectively. The model was selected because: 1) mixture composition and water-to-cement ratio of each tested material are not variables but constant values; 2) the microstructural data necessary for the development of a complex model were not sufficient.

5.2 CO₂-Diffusion-Controlled Model

The reaction process of CO₂ and cement has been described in Section 2.6.2. It is well accepted that the diffusion of CO₂ through the cementitious matrix is the slowest, rate-controlling step. A CO₂-Diffusion-Controlled Model can be developed based on Fick's first law of diffusion and the following assumptions:

- The reaction proceeds in a simple one-dimensional geometry
- The fully carbonated layer and fresh uncarbonated zone is separated by a sharp carbonation front
- The permeability and diffusion coefficient for CO₂ migration through the depth of the growing carbonated layer remain constant
- The reaction progresses under steady state.

Figure 5-1 illustrates the situation in which the resistance to diffusion through the carbonated layer controls the rate of reaction. Since the resistance of the gas film to the diffusion of CO₂ is neglected, the concentration of CO₂ at the surface of the exposed solid surface (C_{As}) is equal to that in the bulk gas phase (C_{Ag}). Other symbols in Figure 5.1 represent:

L overall thickness of the solid matrix

l any depth in the carbonation layer

l_c depth of carbonation front

C_A concentration of CO_2 at surface of any depth l

C_{Ac} concentration of CO_2 at the surface of carbonation front

Q_{As} flux of CO_2 through exterior surface of solid matrix

Q_A flux of CO_2 through surface of any depth l

Q_{Ac} flux of CO_2 to the carbonation front.

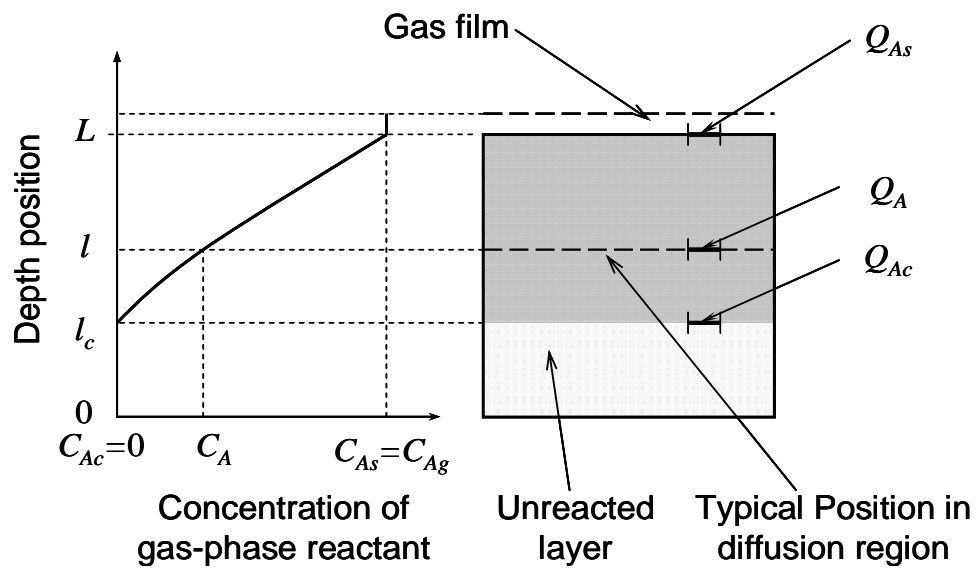


Figure 5-1 Representation of a reacting cementitious matrix when diffusion through the carbonation layer is the controlling resistance

Because the reaction is assumed to be at steady state, the rate of reaction of CO_2 at any instant is given by its rate of diffusion to the reaction surface, which is constant.

$$-\frac{dN_A}{dt} = SQ_A = SQ_{As} = SQ_{Ac} = \text{constant} \quad (5.1)$$

Q_A can be expressed by Fick's diffusion Law

$$Q_A = D_e \frac{dC_A}{dl} \quad (5.2)$$

where D_e is the effective diffusion coefficient of gaseous CO_2 in the product layer.

Combining Equation (5.1) and (5.2), we obtain for any l

$$-\frac{dN_A}{dt} = SD_e \frac{dC_A}{dl} = \text{constant} \quad (5.3)$$

where S is the area of exterior surface.

Integrating across the carbonated layer from L to l_c , we obtain

$$-\frac{dN_A}{dt} \int_L^{l_c} dl = SD_e \frac{dC_A}{dl} = SD_e \int_{C_{As}=C_{Ag}}^{C_{Ac}=0} dC_A \quad (5.4)$$

or

$$-\frac{dN_A}{dt} (L - l_c) = SD_e C_{Ag} \quad (5.5)$$

This expression represents the conditions of a reacting matrix at any time.

If we let ρ_{Ca} be the molar density of reactive calcium in the solid matrix and V be the volume of the solid matrix, the disappearance of dN_{Ca} moles is then given by

$$-dN_{Ca} = -dN_A = -\rho_{Ca} dV = -\rho_{Ca} S dl_c \quad (5.6)$$

Combine Equation (5.5) and (5.6), we obtain

$$-\rho_{Ca} \int_L^{l_c} (L - l_c) dl_c = D_e C_{Ag} \int_0^t dt \quad (5.7)$$

or

$$t = \frac{\rho_{Ca}}{2D_e C_{Ag}} (L - l_c)^2 \quad (5.8)$$

For the complete conversion of the solid matrix, $l_c = 0$ and the time required is

$$\tau = \frac{\rho_{Ca} L^2}{2D_e C_{Ag}} \quad (5.9)$$

The progression of reaction in terms of the time required for complete conversion is found by dividing Equation 5.8 by Equation 5.9

$$\frac{t}{\tau} = X_{Ca}^2 \quad (5.10)$$

In the end, D_e can be determined by combining Equation (5.9) and Equation (5.10)

$$D_e = \frac{\rho_{Ca} L^2 X_{Ca}^2}{2C_{Ag} t} \quad (5.11)$$

Equation (5.11) confirms the validity of the Square Root Law.

5.3 Adaption of the Model to the Carbonation Test Data

5.3.1 Interpretation of CO₂ Pressure Variation

In the current carbonation test, X_{Ca} at different reaction times t was recorded for determining D_e . However, since the concentration of CO₂ in the reactor (C_{CO_2}) decreased throughout the reaction, a differential form of Equation (5.11) is required to determine D_e :

$$D_e = \frac{\rho_{Ca} L^2 X_{Ca}}{C_{CO_2}} \frac{dX_{Ca}}{dt} \quad (5.12)$$

D_e can then be calculated for mid-points between each pair of pressure measurements, based upon the average reaction rate between the two measurements and the cumulative extent of carbonation at the mid point.

5.3.2 Analysis of Carbonation Rate Data of NRVB

As discussed in Section 4.2, in NRVB, calcium hydroxide is the main alkaline phase that can react with CO₂ and C-S-H also contributes to the carbonation reaction; when the NRVB is unsaturated, reaction rate of calcium hydroxide > diffusion rate of CO₂ in the solid matrix > decalcification rate of C-S-H. Although a shape carbonation front can be observed in 75% and 85% RH specimens

respectively, unreacted calcium still existed. As the purpose of modelling the carbonation of NRVB is to predict the extent that CO₂ could travel with time, only the amount of fully reacted calcium above the carbonation front would be taken into consideration. Therefore, the molar density of effective calcium is applied as ρ_{Ca} , which is 5437 mol m⁻³.

The results of the carbonation tests of 75% and 85% RH conditioned specimens are shown in Figure 5-2 and Figure 5-3, respectively. These figures show that at both relative humidities, the estimated values of D_e were quite constant throughout the reaction, except fluctuations at the start of the reaction. There are several factors which may cause the fluctuation at the initial stage (first 10 to 20 minutes) of carbonation:

- Prior to the experiment, the carbonation chamber was vacuumed to move the residue air. This action may also remove the moisture from the specimen surface, which would cause higher gas-filled porosity near the specimen surface.
- To initiate the reaction, CO₂ was flashed into the carbonation chamber, which caused a temporary elevation of the temperature and pressure gradients.
- When the reaction first started, significant amounts of heat and water were generated near the specimen surface, which may have affected the reaction rate.

The average effective diffusion coefficient ($D_{e,Ave}$) of CO₂ at each relative humidity was derived and is indicated as a solid line in Figure 5-2 and Figure 5-3, respectively. The effective diffusion coefficient of NRVB conditioned at 75% and 85% relative humidity are $(2.07 \pm 0.87) \times 10^{-5} \text{ m}^2 \text{ s}^{-1}$ and $(1.04 \pm 0.87) \times 10^{-5} \text{ m}^2 \text{ s}^{-1}$, respectively.

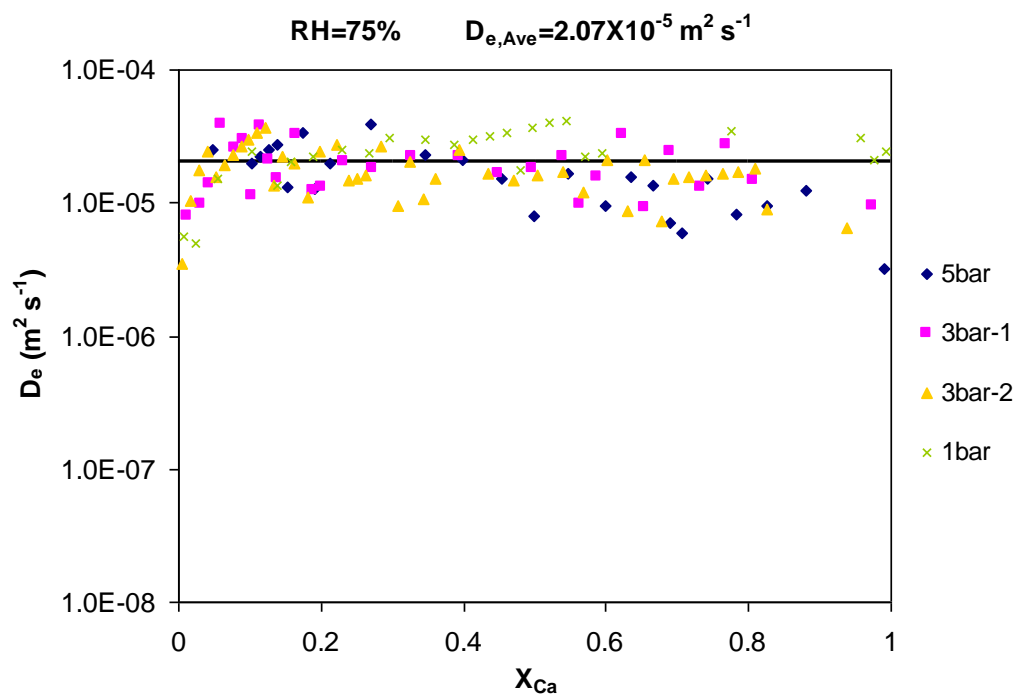


Figure 5-2 Analysis of diffusion-controlled model for 75% RH NRVB specimens

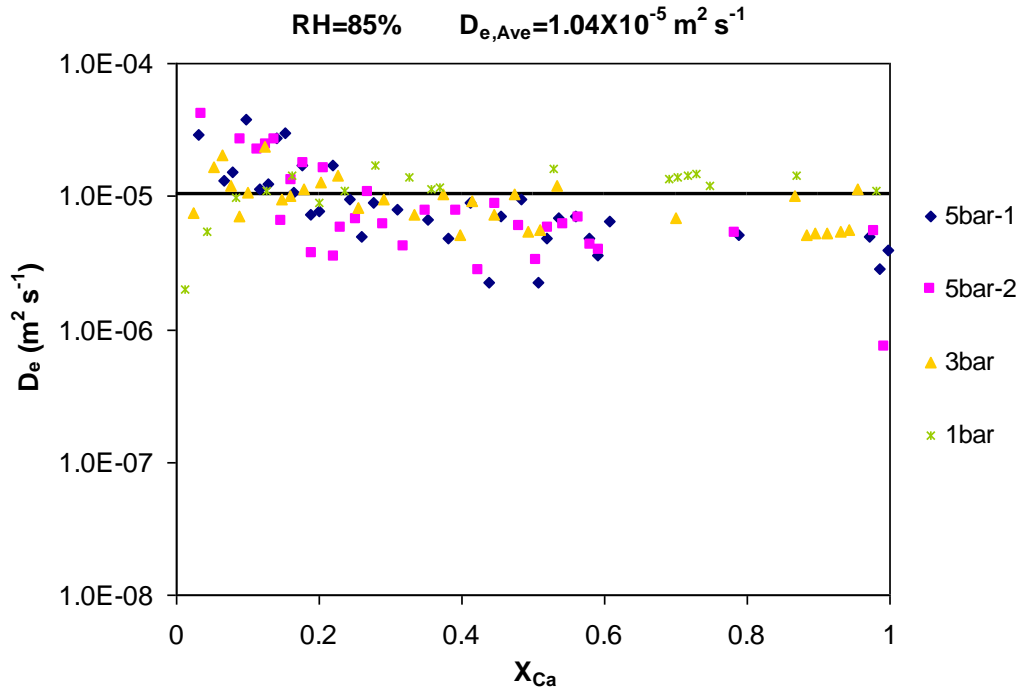


Figure 5-3 Analysis of diffusion-controlled model for 85% RH NRVB specimens

The results of specimens conditioned at 100% are shown in Figure 5-4 with the interpretation based on the proposed diffusion-controlled model. As discussed in Section 4.2, all the reactive calcium was carbonated above the sharp carbonation front, therefore, the theoretical concentration of reactive calcium (7516 mol m^{-3}) was applied as ρ_{Ca} .

The effective diffusion coefficients predicted from the experimental results were clearly not consistent with the application of the diffusion-controlled model. D_e decreases significantly as carbonation proceeds.

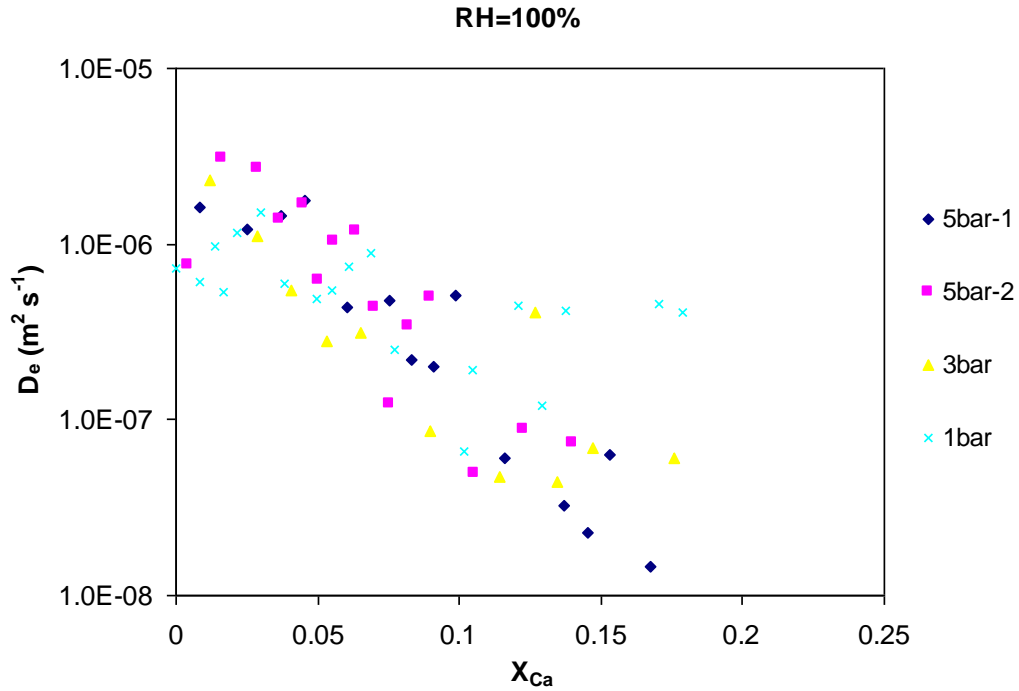


Figure 5-4 Analysis of diffusion-controlled model for 100% RH NRVB specimens

Harris et al. (2003) proposed two distinctly different carbonation regimes:

- a) ‘unsaturated’ regime – carbonation is governed by parabolic kinetics (Square Root Law) and the rate constant is apparently insensitive to the pertaining conditions;
- b) ‘saturated’ regime – carbonation is affected by the changing properties of the carbonated material and parabolic kinetics do not apply. The carbonation rate is sensitive to the conditions and decreases rapidly as carbonation proceeds.

These two regimes were also observed in this work. The proposed

CO₂-diffusion-controlled model only applied to the ‘unsaturated’ regime (NRVB conditioned at 75% and 85% RH).

The reason that the carbonation of saturated NRVB presented a very different kinetic property to the unsaturated conditions may be the high water content in the solid matrix. NRVB has a high porosity of 54%, which means that when NRVB is fully saturated, 54% percent of the total volume is occupied by water. The current diffusion-controlled model is based on the gas/solid reaction. However, when water becomes a major part of the cementitious matrix, its effect has to be taken into consideration. Therefore, the current model is not sufficient to simulate the carbonation of saturated NRVB.

5.3.3 Analysis of Carbonation Rate Data of 3:1 PFA/OPC Grout

As discussed in Section 4.3, the molar density of reactive calcium (ρ_{Ca}) in 3:1 PFA/OPC grout was estimated to be 4248 mol m⁻³, and the C-S-H is the only calcium containing compound that has been observed. A sharp carbonation front was observed and the carbonation of C-S-H was proved to be faster than the diffusion rate of CO₂, which satisfied the assumption of the CO₂-diffusion-control model.

The results of the carbonation tests of 75%, 85% and 100% RH conditioned

specimens are shown in Figure 5-5 to Figure 5-7, respectively. These figures show that at each relative humidity, the estimated values of D_e were quite constant throughout the reaction, except for fluctuations at the start of each test. As discussed in Section 5.3.2, this may be because the reaction was not stabilised in the first 10-20 minutes of the test.

The average effective diffusion coefficient ($D_{e,Ave}$) of CO_2 at each relative humidity was derived and is indicated as a solid line in Figure 5-5 to Figure 5-7, respectively.

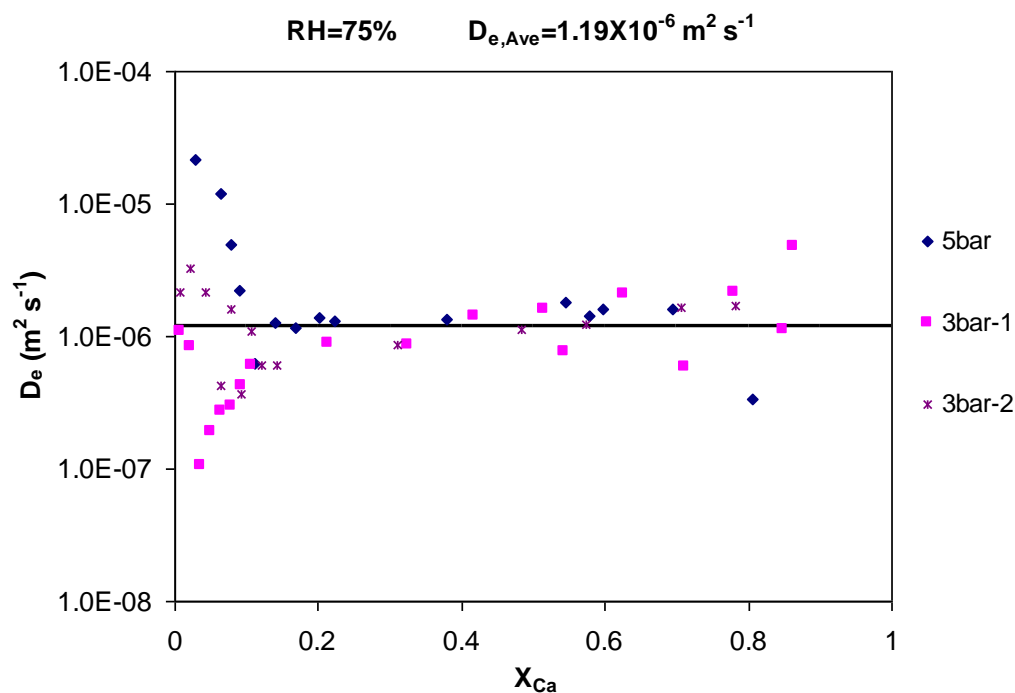


Figure 5-5 Analysis of diffusion-controlled model for 75% RH 3:1 PFA/OPC specimens

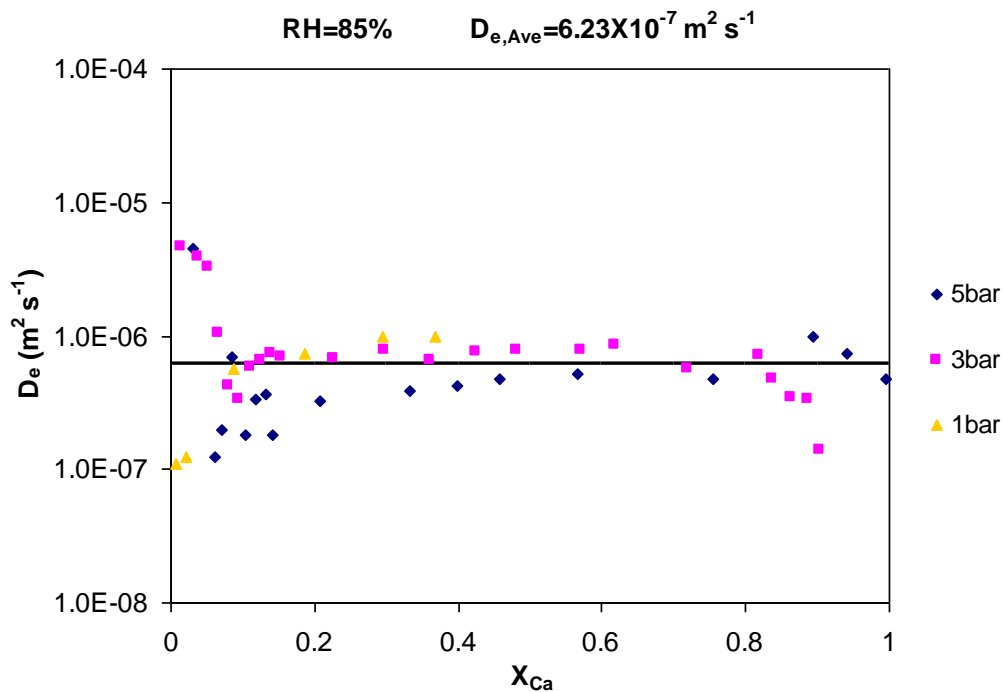


Figure 5-6 Analysis of diffusion-controlled model for 85% RH 3:1 PFA/OPC

specimens

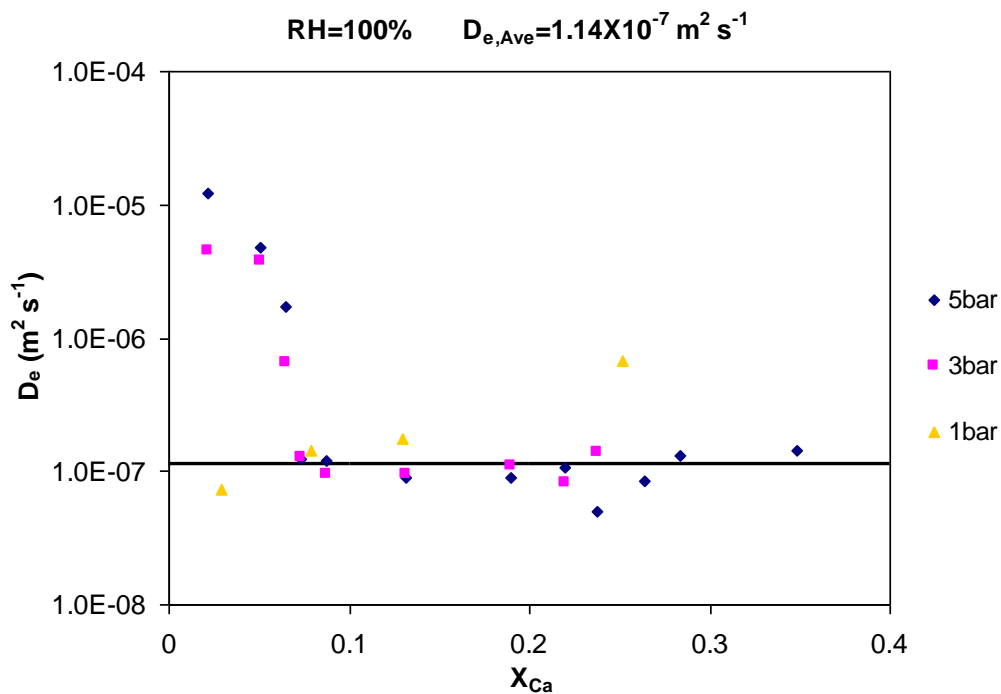


Figure 5-7 Analysis of diffusion-controlled model for 100% RH 3:1 PFA/OPC

specimens

Table 5-1 lists the average effective diffusion coefficients of CO₂ in 3:1 PFA/OPC specimens conditioned at 75%RH, 85% RH and 100% RH, respectively. The higher the relative humidity, the lower the $D_{e,Ave}$.

RH	$D_{e,Ave}$ (m ² s ⁻¹)	Error (m ² s ⁻¹)
75%	1.19×10^{-6}	$\pm 0.52 \times 10^{-6}$
85%	6.23×10^{-7}	$\pm 2.25 \times 10^{-7}$
100%	1.14×10^{-7}	$\pm 0.30 \times 10^{-7}$

Table 5-1 Average effective diffusion coefficients of CO₂ in 3:1 PFA/OPC

specimens conditioned at 75%RH, 85% RH and 100% RH, respectively (Errors were determined by average deviation)

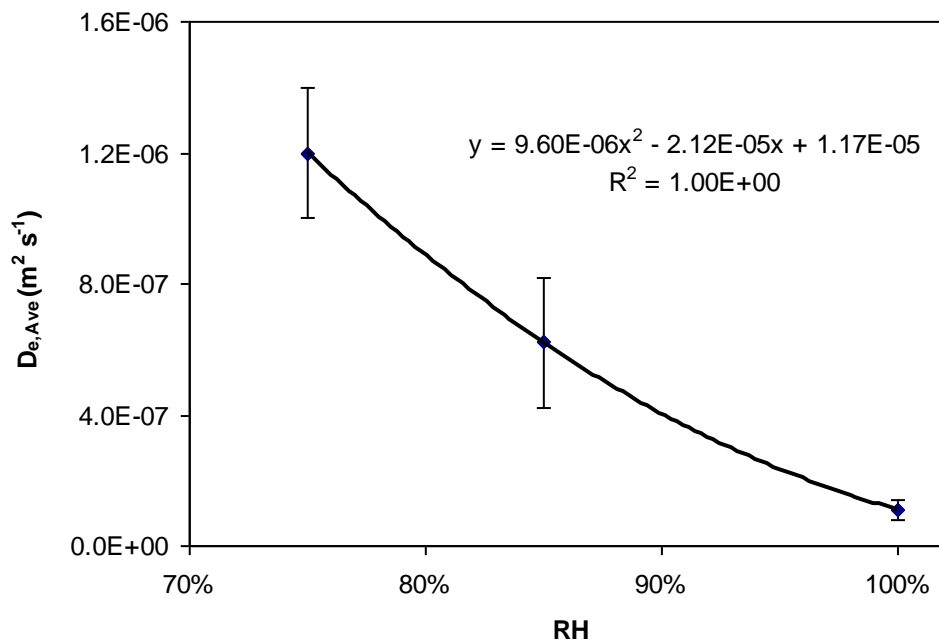


Figure 5-8 Relationship between $D_{e,Ave}$ and relative humidity for 3:1 PFA/OPC

The relationship between $D_{e,Ave}$ and relative humidity is plotted in Figure 5-8 and

Equation 5.13 is the empirical equation of the fitted trend curve.

$$D_e = 9.6 \times 10^{-6} RH^2 - 2.12 \times 10^{-5} RH + 1.17 \times 10^{-5} \quad (5.13)$$

By Combining Equation (5.13) with Equation (5.11), X_{Ca} at any t in a batch reactor can be predicated if RH and the concentration of CO_2 are known.

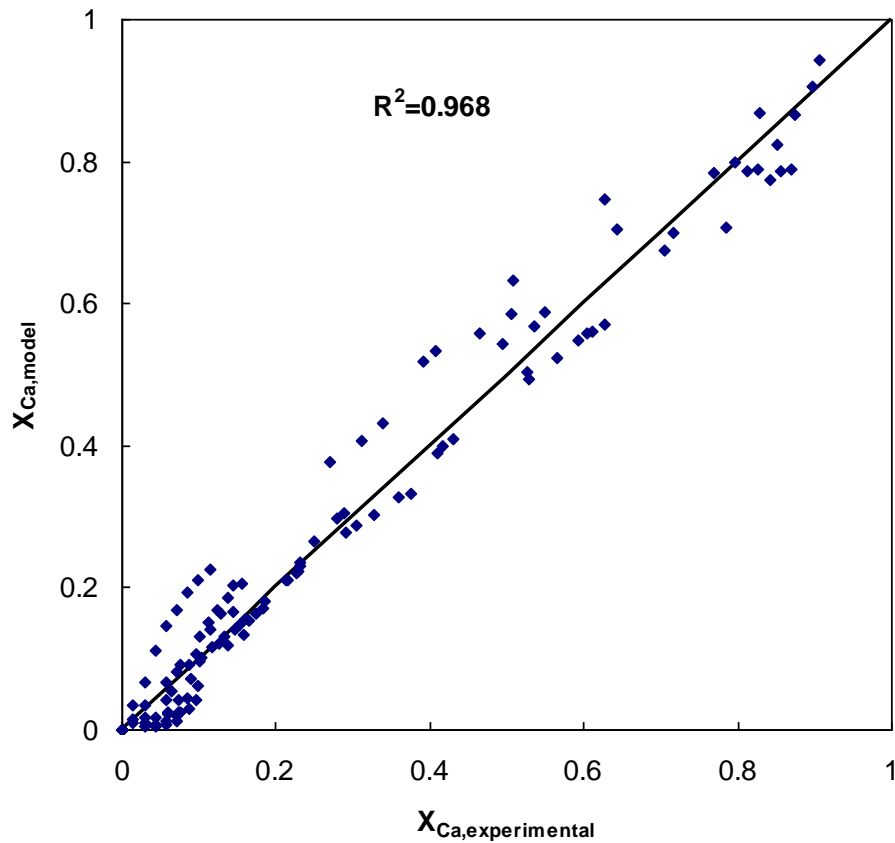


Figure 5-9 Relationship between X_{Ca} calculated from experimental data and

X_{Ca} determined by the kinetic model (3:1 PFA/OPC grout)

As shown in Figure 5-9, X_{Ca} calculated from experimental data were compared with X_{Ca} determined by the kinetic model and showed an R^2 of 0.968, which means the model can simulate the carbonation process of 3:1 PFA/OPC very well.

Because $(L - l_c)$ is the depth of carbonation (d), Equation 5.8 can be converted into the form of Square Root Law (Equation (5.14)) which can be applied to more general situations such as unlimited reaction and constant CO_2 concentration that would represent the conditions in the repository.

$$d = k\sqrt{t} \quad (5.14)$$

The reaction constant k can be calculated by Equation (5.15):

$$k = \sqrt{\frac{2D_e C_{CO2}}{\rho_{Ca}}} = \sqrt{\frac{2C_{CO2} (9.6 \times 10^{-6} RH^2 - 2.12 \times 10^{-5} RH + 1.17 \times 10^{-5})}{4248}} \quad (5.15)$$

The reaction conditions that Equation (5.14) is valid for are: $T=20^\circ C$, RH range from 75% to 100%, 100% CO_2 with pressure range from 1bar to 5bar.

Due to the effect of cracks in the carbonated 3:1 PFA/OPC Specimens, carbonation depths were not able to be measured precisely. Therefore, Equation(5.14) and (5.15) are not verified by the experimental result.

5.3.4 Analysis of Carbonation Rate Data of 3:1 BFS/OPC Grout

As discussed in Section 4.4, the molar density of reactive calcium (ρ_{Ca}) in 3:1 BFS/OPC grout was estimated to be 15016 mol m^{-3} . The main reactive compound in 3:1 BFS/OPC grout is C-S-H, along with small amounts of calcium hydroxide. A sharp carbonation front was observed, which satisfied the assumption of the CO_2 -diffusion-control model.

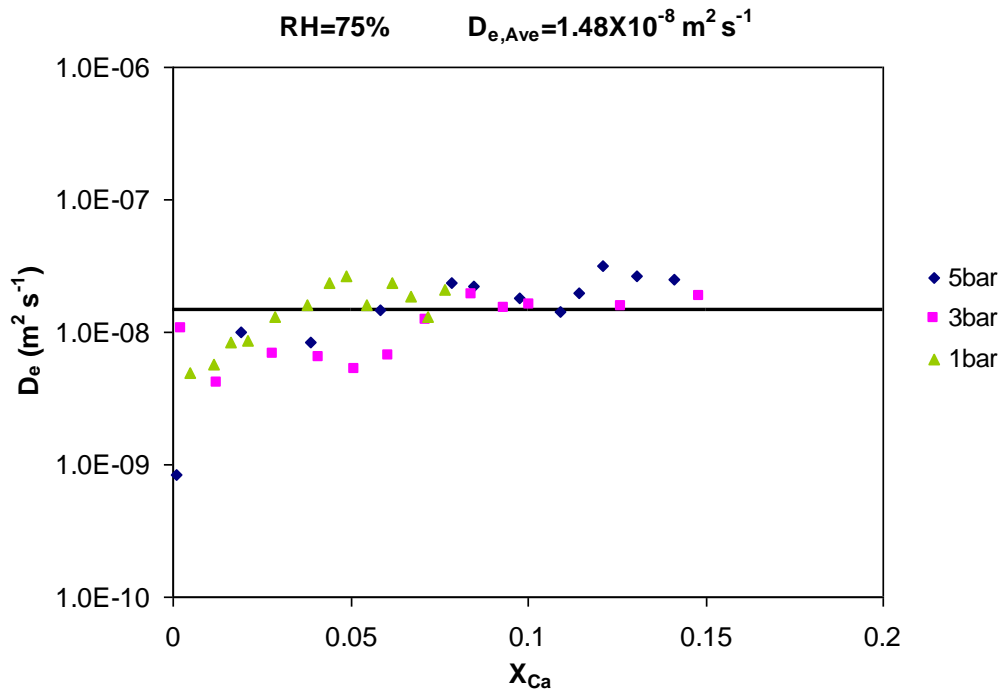


Figure 5-10 Analysis of diffusion-controlled model for 75% RH 3:1 BFS/OPC specimens

The results of carbonation tests of 75%, 85% and 100% RH conditioned specimens are shown in Figure 5-10 to Figure 5-12, respectively. These figures show that at

each relative humidity, the estimated values of D_e were quite constant throughout the reaction. The average effective diffusion coefficient ($D_{e,Ave}$) of CO₂ at each relative humidity was derived and indicated as a solid line in Figure 5-10 to Figure 5-12, respectively.

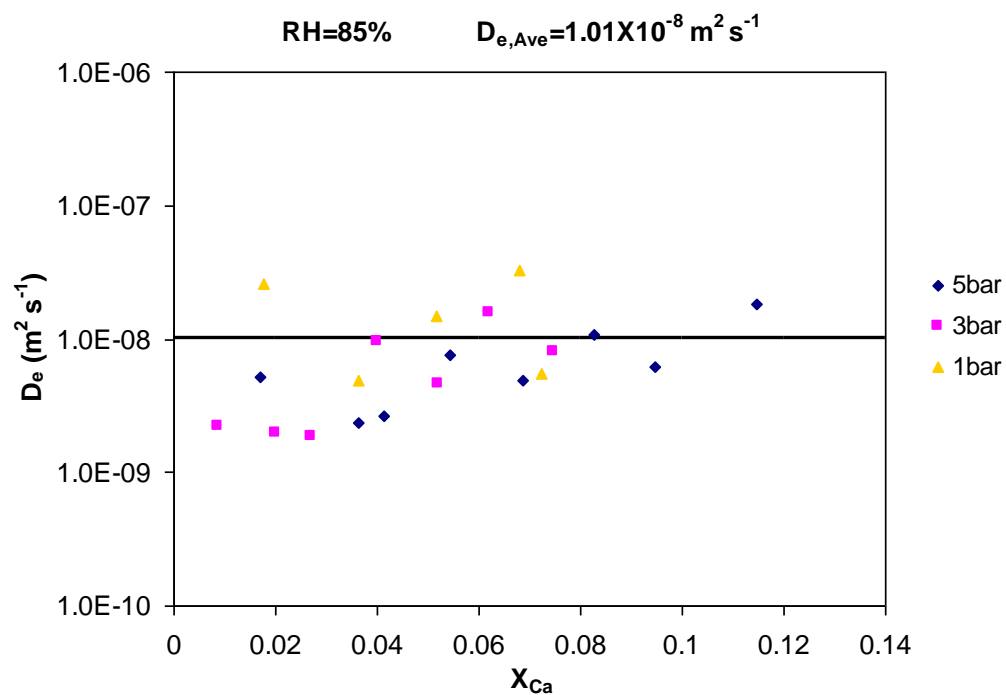


Figure 5-11 Analysis of diffusion-controlled model for 85% RH 3:1 BFS/OPC specimens

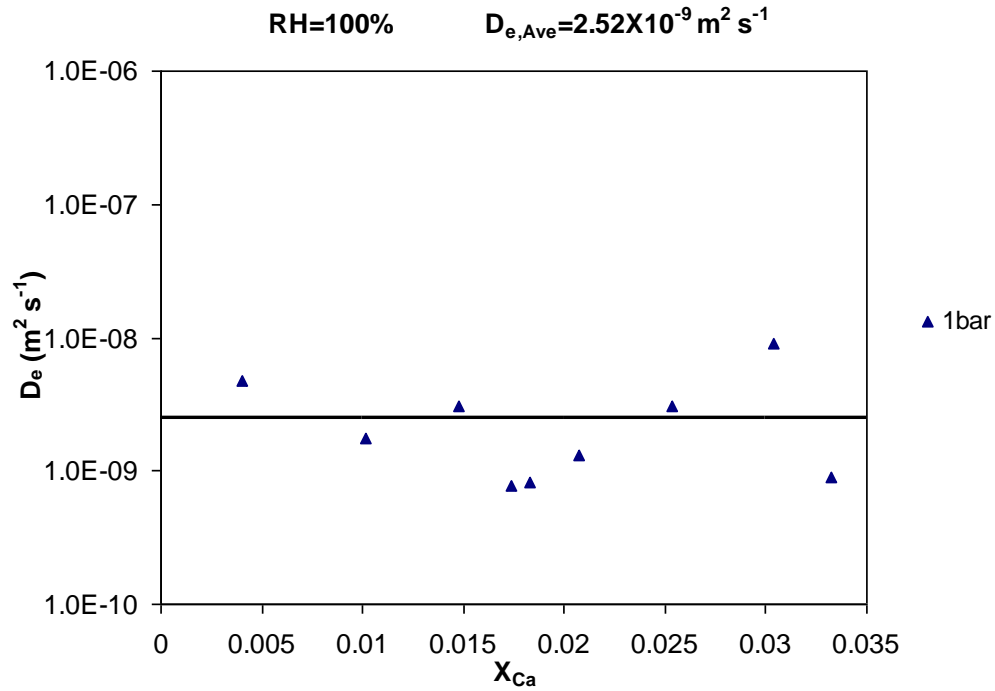


Figure 5-12 Analysis of diffusion-controlled model for 100% RH 3:1 BFS/OPC specimen

RH	$D_{e,Ave} \text{ (m}^2 \text{ s}^{-1}\text{)}$	Estimated Error (m ² s ⁻¹)
75%	1.48×10^{-8}	$\pm 0.74 \times 10^{-9}$
85%	1.01×10^{-8}	$\pm 0.81 \times 10^{-9}$
100%	2.52×10^{-9}	$\pm 2.49 \times 10^{-9}$

Table 5-2 Average effective diffusion coefficients of CO₂ in 3:1 PFA/OPC

specimens conditioned at 75%RH, 85% RH and 100% RH respectively (Errors were determined by average deviation)

Table 5-2 lists the average effective diffusion coefficients of CO₂ in 3:1 BFS/OPC specimens conditioned at 75%RH, 85% RH and 100% RH, respectively. The higher the relative humidity, the lower the $D_{e,Ave}$. The relatively large estimated errors

were due to the experimental errors caused by the extremely slow reaction.

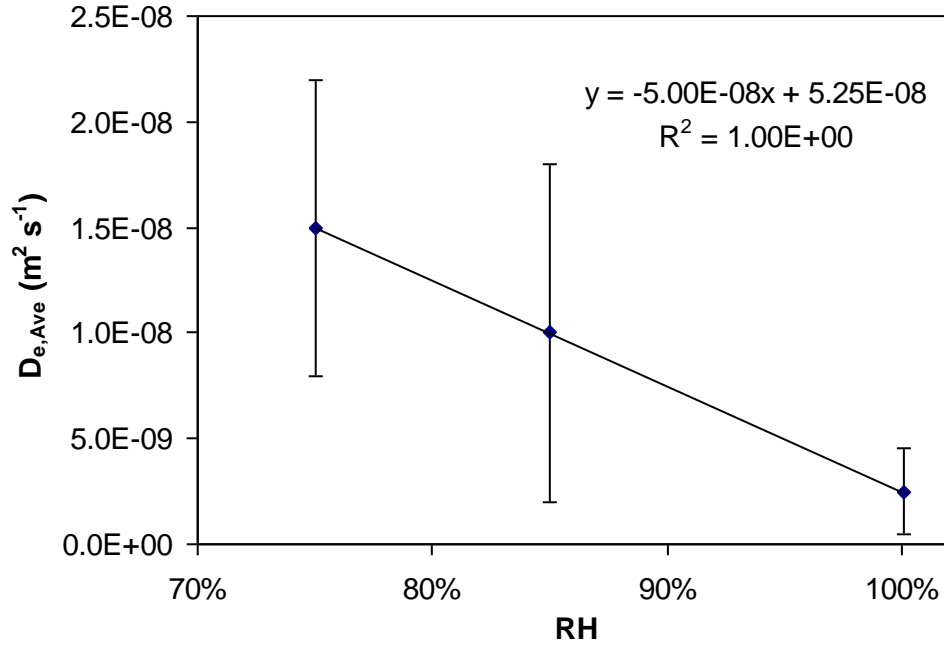


Figure 5-13 Relationship between $D_{e,Ave}$ and relative humidity for 3:1 BFS/OPC

The relationship between $D_{e,Ave}$ and relative humidity is plotted in Figure 5-13 and Equation (5.16) is the empirical equation of the fitted trend curve.

$$D_e = -5 \times 10^{-8} RH + 5.25 \times 10^{-8} \quad (5.16)$$

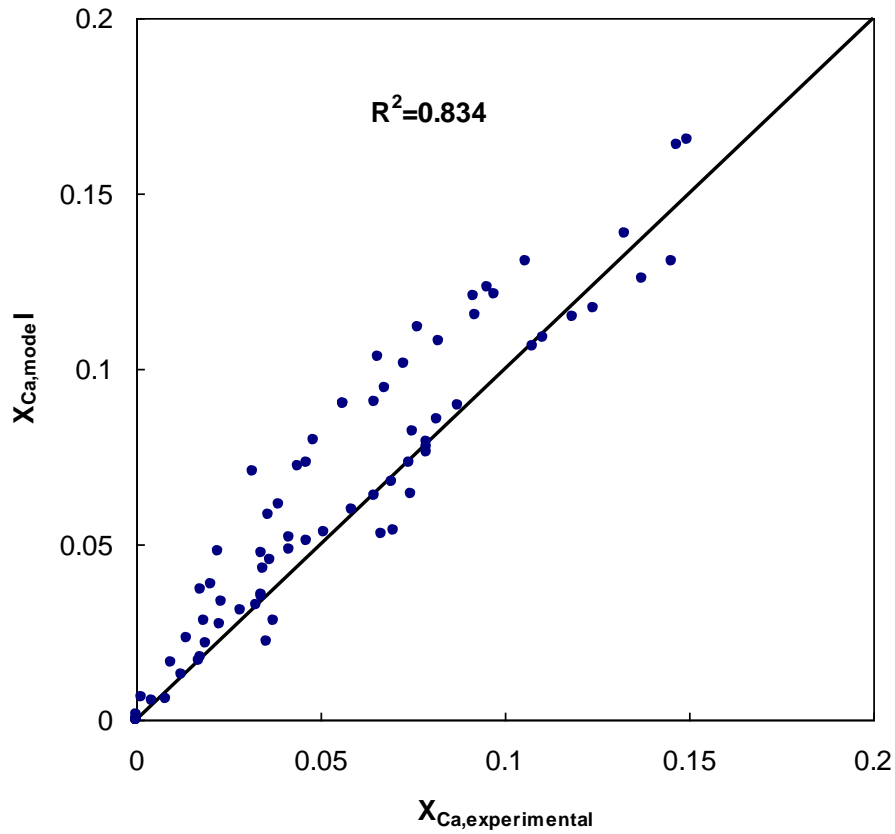


Figure 5-14 Relationship between X_{Ca} calculated from experimental data and X_{Ca} determined by the kinetic model (3:1 BFS/OPC grout)

In Figure 5-14, X_{Ca} calculated from experimental data were compared with X_{Ca} determined by the kinetic model and the Coefficient of Determination R^2 was 0.834, which means the model can simulate the carbonation process of 3:1 BFS/OPC quite well.

The depth of carbonation of 3:1 BFS/OPC grout can also described by Equation (5.14). The reaction constant k for 3:1 BFS/OPC grout can be calculated by Equation (5.17):

$$k = \sqrt{\frac{2D_e C_{CO2}}{\rho_{Ca}}} = \sqrt{\frac{2C_{CO2}(-5 \times 10^{-8} RH + 5.25 \times 10^{-8})}{15016}} \quad (5.17)$$

The reaction conditions that Equation (5.16) is valid for are: T=20 °C, RH range from 75% to 100%, 100% CO₂ with pressure range from 1bar to 5bar.

5.4 Discussion

In this chapter, a CO₂-Diffusion-Controlled Model was developed based on Fick's first law of diffusion. For the carbonation of 3:1 PFA/OPC and 3:1 BFS/OPC, the model is capable of predicting the measured carbonation conversion (X_{Ca}) over a range of pressure and relatively humidity.

However, the model is less adequate to describe the carbonation kinetics of NRVB. The purposely-designed high porosity makes NRVB different from conventional cementitious material. Due to the high gas-filled porosity of unsaturated NRVB, the diffusion rate of CO₂ is faster than the rate of decalcification of C-S-H, which means the reaction is not solely diffusion controlled. The high porosity of NRVB also means when NRVB is saturated with water, more than half of the total volume is occupied by water. The reaction mechanism under such a high quantity of water needs further investigation.

6 CONCLUSIONS AND FUTURE WORK

6.1 Conclusions

The significance of this work is that it provides a fundamental understanding of the carbonation reaction of NRVB, 3:1 PFA/OPC and 3:1 BFS/OPC at relatively high pressure and high relative humidity.

Specimens conditioned at relative humidities of 75% - 100% were carbonated in batch reactors, in which the initial CO₂ pressures ranged from 1 to 5bar. The impact of the carbonation reaction on the chemical and physical properties of each material was studied. In order to predict the long term performance of each material, a CO₂-Diffusion-Controlled Model, based on Fick's first law of diffusion, was proposed and adapted to the kinetic data collected from the carbonation tests.

The rate of carbon dioxide uptake has been shown to be dependent on the nature of the material, the degree of water saturation, as well as the pressure of CO₂. The impacts of these parameters are:

- Material with higher porosity has a faster carbonation rate;
- Increasing the degree of water saturation (controlled by conditioning) in the solid matrix decelerates the carbonation progress;

- A higher pressure of CO₂ enhances carbonation, but the effect of CO₂ pressure is less significant than the effect of degree of saturation.

The concentrations of the theoretical reactive calcium for NRVB, 3:1 PFA/OPC, 3:1 BFS/OPC are 7514 mol m⁻³, 4248 mol m⁻³ and 15016 mol m⁻³, respectively. The concentration of theoretical reactive calcium is equal to the maximum amount of CO₂ that can be absorbed per volume of material.

In **NRVB**, calcium hydroxide is the main alkaline phase that can react with CO₂, but C-S-H also contributes to the carbonation reaction. Two distinctly different carbonation regimes were observed for NRVB: an ‘unsaturated’ regime (NRVB conditioned at 75% and 85% RH) and a ‘saturated’ regime (NRVB conditioned at 100% RH).

- For the unsaturated regime, a sharp carbonation front exists, which is parallel to the exposure surface. The diffusion rate of CO₂ is slower than the reaction rate of calcium hydroxide, but faster than that of C-S-H. As a result, the reactive calcium consumed above the carbonation front, which is called effective calcium, is less than the content of theoretical reactive calcium in that range. According to the timescale of the experiments, the concentration of effective calcium of unsaturated NRVB is 5437 mol m⁻³. It is also the concentration of calcium that can effectively confine the CO₂ in the repository.

- For the saturated regime, a sharp carbonation front exists, but the shape is irregular (i.e. it is not parallel to the exposure surface). The reaction is diffusion controlled. The concentration of effective calcium in saturated NRVB is equal to the concentration of theoretical reactive calcium. The carbonation rate is very slow and decreases rapidly as carbonation proceeds.

In **3:1 PFA/OPC Grout**, C-S-H is the only calcium containing compound that can react with CO₂. Sharp carbonation fronts can be observed in both saturated and unsaturated specimens. When sprayed with phenolphthalein indicator, no colour change was observed above the carbonation front, which means all the reactive calcium in the carbonated zone is consumed by CO₂. However, in the unsaturated 3:1 PFA/OPC specimens, tiny cracks due to drying shrinkage exist and these cracks are amplified due to the carbonation. As it is easier for CO₂ to diffuse through the cracks, CO₂ tends to react along the cracks. Therefore, the carbonation front is not consistent, which makes the measurement of carbonation depth difficult.

Although **3:1 BFS/OPC Grout** has the highest content of reactive calcium, it has the lowest carbonation rate due to its low porosity. The main reactive compound in 3:1 BFS/OPC grout is C-S-H, along with small amounts of calcium hydroxide. Similar to 3:1 PFA/OPC, cracks due to drying and carbonation reaction exist in unsaturated specimens.

The diffusion-controlled model fits the experimental data well for unsaturated NRVB. The effective diffusion coefficient of NRVB conditioned at 75% and 85% relative humidity is $(2.07 \pm 0.87) \times 10^{-5} \text{ m}^2\text{s}^{-1}$ and $(1.04 \pm 0.87) \times 10^{-5} \text{ m}^2\text{s}^{-1}$, respectively. However, the carbonation process of saturated NRVB cannot be described by the proposed model, which may be due to the high amount of water in the solid matrix.

For both 3:1 PFA/OPC and 3:1 BFS/OPC, the diffusion-controlled model describes the reaction kinetics very well. The relations between effective diffusion coefficient and relative humidity are determined for both grouts. The carbonation depths (d) can be predicted by the following equations:

$$\begin{aligned} \text{3:1 PFA/OPC } d &= \sqrt{\frac{2C_{CO_2}(-9.6 \times 10^{-6} RH - 2.12 \times 10^{-5} RH + 1.17 \times 10^{-5})}{4248}} \sqrt{t} \\ \text{3:1 BFS/OPC } d &= \sqrt{\frac{2C_{CO_2}(-5 \times 10^{-8} RH + 5.25 \times 10^{-8})}{15016}} \sqrt{t} \end{aligned}$$

After the closure of a radioactive waste repository, the relative humidity within the repository can reach 100% due to the intrusion of underground water. This saturated condition can last for several hundred years, until the end of the service life of the repository. Therefore research on carbonation under saturated conditions is very important. According to the literature, most of the carbonation tests on cementitious materials were conducted between 50~70% relative humidity, for

optimum carbonation [Thiery, et al., 2007]. Almost all the kinetic models assume that carbonation cannot occur at 100% relative humidity as CO₂ will not diffuse into pores saturated with water [Muntean, et al. 2005]. This work has proved that carbonation reactions are able to proceed in fully saturated specimens. Both the kinetic data at 100% RH and the-diffusion controlled models, which predict the RH range from 75% to 100%, will help to evaluate more correctly the long-term performance of NRVB and waste-form grouts.

6.2 Future Work

6.2.1 Effect of Temperature

Due to the limitation of the reactor design, the effect of temperature on carbonation was not studied. In order to create a homogeneous environment up to 80 °C, better reactor design is necessary. To eliminate the temperature gradients inside the reactor, two potential designs are proposed below:

- install a heating jacket around the reactor wall,
- fit the reactor in an environmental chamber, in which the temperature is constantly controlled.

6.2.2 Formation and Effect of Cracks

Cracks in the surface of unsaturated waste-form grouts are unavoidable. These cracks become a main path for CO_2 penetration so that the carbonation is accelerated in cracked grouts [Sullivan-Green et al. 2007]. Meanwhile, carbonation also amplifies these cracks, which may cause the deterioration of the solid structure. Therefore, the carbonation behaviour, especially the equivalent diffusivity of CO_2 , in cracked grouts could be studied in future work. Changes in crack depth and width, before and after carbonation, could also be studied.

6.2.3 Competition of Carbonation Reactions

This work has shown that in NRVB, the carbonation rate of C-S-H was slower than that of calcium hydroxide. This reaction rate difference could cause a reduction of reactive calcium in the NRVB, which could effectively constrain CO_2 within the repository. Therefore, another area of future work could be to analysis the competition of calcium hydroxide and C-S-H for CO_2 . There is a lack of knowledge on the relative fractional conversion of the different phases as the process goes on. Techniques which are able to give results enabling access to this question are of importance for the progression of the understanding of the carbonation process. Currently, TGA, XRD and in situ neutron diffraction technology are used to identify the consumption of different phases during carbonation [Castellote et al.

2008]. Peter et al. [2005, 2008] also modelled the competition of carbonation reactions.

6.2.4 Kinetic Modelling

Carbonation of cementitious material is quite a complex process. The description of the system in terms of a diffusion-controlled model is a good and simple first approach. However, this approach is not suitable for the carbonation of NRVB. Most of the existing models assume the diffusion of CO₂ in water is negligible and carbonation can hardly proceed in a fully saturated system. This work has shown slow carbonation in saturated NRVB. Therefore, other possible future work would be to consider Complex Models which could consider gas phase diffusion as well as liquid phase diffusion of CO₂.

REFERENCE LIST

ACI Education Bulletin 2001. Cementitious materials for concrete. American Concrete Institute. E3-01, American Concrete Institute.

Ařcin, P. 2000. Cements of yesterday and today: Concrete of tomorrow. *Cement and Concrete Research*, 30: 1349-1359.

Al-Kadhimi, T. K. H., Banfill, P. F. G., Millard, S. G. and Bungey, J., H. 1996. An accelerated carbonation procedure for studies on concrete. *Advances in Cement Research*, 8 (30): 47-59.

American Society for Testing and Materials 1995. Standard specification for Portland cement. *PA: ASTM*, C 150-95.

Andrade, C., Mart ínez, I., Castellot, M. And Zuloaga, P. 2006. Some principles of service life calculation of reinforcements and in situ corrosion monitoring by sensors in the radioactive waste containers of El Cabril disposal (Spain). *Journal of Nuclear Materials*, 356: 82-95.

Anstice, D. J., Page, C. L. and Page, M. M. 2005. The pore solution phase of carbonated cement pastes. *Cement and Concrete Research*, 35: 377-383.

Atiř, C. D. 2003. Accelerated carbonation and testing of concrete made with fly ash. *Construction and Building Materials*, 17: 147-152.

Atkins, M. and Glasser, F. P. 1992. Application of Portland cement-based materials to radioactive waste immobilization. *Waste Management*, 12(2-3): 105-131.

Bacocchi, R., Poletti, A., Pomi, R., Prigobbe, V., Zedtwitz-Nikulshyna, V. and Steinfeld, A. 2006. Accelerated gas/solid carbonation of incinerator residues: kinetics and effects on metal mobility. First International Conference on Accelerated Carbonation for Environmental and Materials Engineering, London.

Bary, B. and Sellier, A. 2004. Coupled moisture-carbon dioxide-calcium transfer model for carbonation in concrete. *Cement and Concrete Research*, 34: 1859-1872.

Beaudoin, J. J., Feldman, R. F. and Tumidajski, P. J. 1994. Pore Structure of hardened Portland cement pastes and its influence on properties. *Advanced Cement Based Materials*, 1: 224-236.

Bensted, J. 1997. Cements: past, present and future. Dartford, Kent: Greenwich

University Press.

Blezard, R. G, 1998 Part 1: The history of Calcareous Cements. *Lea's chemistry of cement and concrete*. Fourth Edition, London: Arnold.

Borges, P. H. R., Costa, J. O., Milestone, N. B., Lyndsdales, C. J. and Streatfield, R. E. 2010. Carbonation of CH and C-S-H in composite cement pastes containing high amounts of BFS. *Cement and Concrete Research*, 40: 284-292.

Burkan Isgor, O. and Ghani Razaqpur, A. 2004. Finite element modelling of coupled heat transfer moisture transport and carbonation processes in concrete structure. *Cement & Concrete Composites*, 26: 57-53.

Carl Knopf, F., Roy, A., Samrow, H. A. and Dooley, K. M. 1999. High-pressure molding and carbonation of cementitious materials. *Industrial & Engineering Chemistry Research*, 38: 2641-2649.

Castellote, M. and Andrade, C. 2008. Modelling the carbonation of cementitious matrix by means of the unreacted-core model, UR-CORE. *Cement and Concrete Research*, 38: 1374-1384.

Castellote, M., Andrade, C., Turrillas, X., Campo, J. and Guello, G. 2008.

Accelerated Carbonation of cement pastes in situ monitored by neutron diffraction.

Cement and Concrete Research, 38: 1365-1373.

Chen, J. J., Thomas, J. J. and Jennings, H. M. 2006. Decalcification shrinkage of cement paste. *Cement and Concrete Research*, 36: 801-809.

Cizer, O., Van Balen, K., Van Gemert and D., Elsen, J. 2006. Carbonation reaction of lime hydrate and hydraulic binders at 20°C. First International Conference on Accelerated Carbonation for Environmental and Materials Engineering, London

Comite Euro-International du Beton 1982. Draft CEB guide to durable concrete structures. *CEB Bullitin d'Information*, No. 148: 2.48-2.53

Cultrone, G., Sebastian, E. and Ortega Huertas, M. 2005. Forced and natural carbonation of lime-based mortars with and without additives: Mineralogical and textural changes. *Cement and Concrete Research*, 35: 2278-2289.

De Ceukelaire, L. and Van Nieuwenburg, D. 1993. Accelerated carbonation of blast-furnace cement concrete. *Cement and Concrete Research*, 23: 442-452.

DEFRA 2008. Managng radioactive waste safely: A framework for implementing geological disposal. June.

El-Turki, A., Ball, R. J. and Allen, G. C. 2007. The influence of relative humidity on structural and chemical changes during carbonation of hydraulic lime. *Cement and concrete research*, 37: 1233-1240.

Fattuhi, N. I. 1988. Concrete carbonation as influenced by curing time. *Cement and Concrete Research*, 18: 426-430.

Fernández Bertos, M., Simons, S. J. R., Hills, C. D. and Carey, P. J. 2004. A review of accelerated carbonation technology in the treatment of cement-based materials and sequestration of CO₂. *Journal of Hazardous Materials*, B112: 193-205.

Fernández Bertos, M. 2005. Accelerated carbonation for the treatment of MSWIr: Optimisation and Reaction Modelling. PhD Thesis, University College London.

Francis, A. J., Cather, R. and Crossland, I. G. 1997. Development of the Nirex Reference Vault Backfill; report on current status in 1994. Nirex Report S/97/014,

Fuji, K. and Kondo, W. 1974. Kinetics of the hydration of tri- calcium silicate. *Journal of the American Ceramic Society*, 57: 492-502.

García-González, C. A., el Grouh, N., Hidalgo, A., Fraile, J., López-Periago, A. M.,

Andrade, C. and Domingo, C. 2008. New insights on the use of supercritical carbon dioxide for the accelerated carbonation of cement pastes. *Journal of supercritical Fluids*, 43: 500-509.

Glasser, F. P. 1992. Progress in the immobilization of radioactive wastes in cement. *Cement and Concrete Research*, 22(2-3): 201-216.

Goñi, S. and Guerrero, A. 2003. Accelerated carbonation of Friedel's salt in calcium aluminate cement paste. *Cement and Concrete Research*, 33: 21-26.

Gorcer, J. and Milestone, N. B. 2007. Probing the microstructure and water phases in composite cement blends. *Cement and Concrete Research*, 37(3): 310-318

Groves, G. W., Rodway, D. I. and Richardson, I. G., 1990. The carbonation of hardened cement pastes. *Advances in Cement Research*, 3: 117-125.

Harris, A. W. 1997. An assessment of the pH buffering provided by the nirex reference vault backfill within a radioactive waste repository. Nirex Report NSS/R323.

Harris, A. W., Boulton, K. A., Manning, M. C. and Tearle, W. M. 2002. Experimental study of carbon dioxide uptake by NRVB and 3:1 BFS/OPC grout, Nirex Report

SERCO/ERRA-0453.

Harris, A. W., Manning, M. C. and Tearle, W. M. 2003. Carbonation of Nirex Reference Vault Backfill. Nirex report SERCO/ERRA-0454.

Hills, C. D., Sweeney, R. E. H. and Buenfeld, N. R. 1999. Microstructural study of carbonated cement-solidified synthetic heavy metal waste. *Waste Management*. 19: 325-331.

Houst, Y. F. 1996. The role of moisture in the carbonation of cementitious materials. *International Zeitschrift Für Bauinstandsetzen*, 2 Jahrgang, Heft 1: 49-66.

Houst, Y. F. and Wittmann, F. H. 2002. Depth profiles of carbonates formed during natural carbonation. *Cement and Concrete Research*, 32: 1923-1930.

Huntzinger, D. N., Gierke, J. S., Komar Kawatra, S., Eisele, T. C. and Sutter, L. L. 2009. Carbon dioxide sequestration in cement kiln dust through mineral carbonation. *Environmental Science & Technology*, 43(6): 1986-1992.

Hyvert, N., Sellier, A., Duprat, F., Rougeau, P. And Francisco, P. 2010. Dependency of C-S-H carbonation rate on CO₂ pressure to explain transition from accelerated tests to natural carbonation. *Cement and Concrete Research*, 40: 1582-1589.

Ishida, T and Maekawa, K. 2000 Modeling of pH profile in pore water based on mass transport and chemical equilibrium theory. Proceedings of JSCE, No. 648/V-47.

Jackson, P. J. 1998. Part 2: Poland cement: classification and manufacture. Lea's chemistry of cement and concrete. Fourth Edition, London: Arnold.

Jiang, L., Lin, B. and Cai, Y. 2000. A model for predicting carbonation of high-volume fly ash concrete. *Cement and Concrete Research*, 30: 699-702.

Johannesson, B. and Utgenannt, P. 2001. Microstructural changes caused by carbonation of cement mortar. *Cement and Concrete research*, 31: 925-931.

Khunthongkeaw, J., Tangtermsirikul, S. and Leelawat, T. 2006. A study on carbon depth prediction for fly ash concrete. *Construction and Building Materials*, 20: 744-753.

Lange, L. C., Hills, C. D. and Poole, A. B. 1996. The effect of accelerated carbonation on the properties of cement-solidified waste forms. *Waste Management*, 16(8): 757-763.

Lange, L. C., Hills, C. D. and Poole, A. B. 1998. The influence of mix parameter and binder choice on the carbonation of cement solidified wastes. *Waste Management*, 16: 749-756.

Langley, W. S., Carette, G. G. and Malhotra, V. M. 1989. Structural concrete in incorporating high volumes of ASTM Class F fly ash. *AMI Material Journal*, 86: 507-514.

Lawrence, C. D. 1998. Part 4: The constitution and specification of Portland cements. *Lea's chemistry of cement and concrete*, Fourth Edition, London: Arnold.

Lawrence, C. D. 1998. Part 9: The production of low-energy cements. *Lea's chemistry of cement and concrete*, Fourth Edition, London: Arnold.

Liu, L., Ha, J., Hashida, T. and Teramura, S. 2001. Development of a CO₂ solidification method for recycling autoclaved lightweight concrete waste. *Journal of materials science letters*, 20: 1791-1794.

Loo, Y. H., Chin, M. S., Tam, C. T. and Ong, K. C. G. 1994. A carbonation model for accelerated carbonation testing of concrete. *Magazine of Concrete Research*, 46: 191-200.

Massazza, F. 1998. Part 10: Pozzolana and pozzolanic cements. *Lea's chemistry of cement and concrete*, Fourth Edition, London: Arnold.

Matschei, T., Lothenbach, B. and Glasser, F. P. 2007. The AFm phase in Portland cement. *Cement and Concrete Research*, 37: 118-130.

McCarter et al., Crossland, I. and Chrisp, T. M. 2004. Hydration and drying of Nirex reference vault backfill. *Building and Environment*, 39: 211-221.

McGinnes, D. F. 2007. Waste sources and classification. *Radioactivity in the Environment*, 9: (8-40).

Meier, S. A., Peter, M. A., Muntean, A. and Böhm, M. 2007. Dynamics of the internal reaction layer arising during carbonation of concrete. *Chemical Engineering Science*, 62: 1125-1137.

Mohite, V. 2004. Self controlled magnetic hyperthermia. MSc Thesis, The Florida State University.

Muntean, A., Meier, S. A., Peter, M. A. Böhm, M. and Kropp, J. 2005, A note on limitations of the use of accelerated concrete-carbonation tests for service-life predictions. Berichte aus der Technomathematik 05-04, ZeTeM, University of

Bremen.

Nirex, 2005. The viability of a phased geological repository concept for the long-term management of the UK's radioactive waste. Nirex report N/122.

NDA and DEFRA, 2008. The 2007 UK radioactive waste inventory: A review of the processes contributing to radioactive wastes in the UK. Defra/RAS/08/004. NDA/RWMD/006.

Odler, I. 1998. Part 6: Hydration, setting and hardening of Portland cement. *Lea's chemistry of cement and concrete*, Fourth Edition, London: Arnold.

Openshaw, S., Carver, S. and Fernie, J. 1989. Britain's nuclear waste: Siting and safety. London: Bellhaven Press.

Papadakis, V. G., Vayenas, C. G. and Fardis, M. N. 1989. A reaction engineering approach to the problem of concrete carbonation. *AIChE Journal*, 35: 1639-1650.

Papadakis, V. G., Fardis, M. N. and Vayenas, C. G., 1992. Hydration and carbonation of pozzolanic cements. *ACI Materials Journal*, 89: 119-130.

Papadakis, V. G. 1999. Experimental investigation and theoretical modelling of

silica fume activity in concrete. *Cement and Concrete research*, 29: 79-86.

Papadakis, V. G. 1999. Effect of fly ash on Portland cement systems Part I. low-calcium fly ash. *Cement and Concrete Research*, 29: 1727-1736.

Parrot, L. J., Patel, R. C., Killoh, D. C. and Jennings, H. M. 1984. *Journal of the American Ceramic Society*, 67: 233-237.

Parrot, L. J. 1987. A review of carbonation in reinforced concrete. Cement and Concrete Association, Report C/1-0987.

Peter, M. A., Muntean, A., Meier, S. A. and Böhm, M. 2005. Modelling and simulation of concrete carbonation: competition of several carbonation reactions. *Berichte aus der Technomathematik*, Report 05-03.

Peter, M. A., Muntean, A., Meier, S. A. and Böhm, M. 2008. Competition of several carbonation reaction in concrete: a parametric study. *Cement and Concrete Research*, 38(12): 1385-1393

Purnell, P., Short, N.R. and Page, C.L. 2001. Super-critical carbonation of glass-fiber reinforced cement. Part 1. Mechanical testing and chemical analysis, *Composites A* 32 : 1777–1787.

Rahman, A. A. and Glasser, F. P. 1989. Comparative studies of the carbonation of hydrated cements. *Advances in Cement Research*, 2: 49-54.

Reardon, E.J, James, B. R. and Abouchar, J. 1989. High pressure carbonation of cementitious grout. *Cement and Concrete Research*, 19: 385-300.

Richardson, M. G. 1988 Carbonation of reinforced concrete: Its causes and management. Dublin, London and New York: CITIS LTD.

Richardson, I. G. and Groves, G. W. 1993. Microstructure and Microanalysis of. Hardened Ordinary Portland Cement Pastes. *Journal of Materials Research*, 28: 265-277.

Rigo da Silva, C. A., Reis, R. J. P., Lameiras, F. S. and Vaconcelos, W. L. 2002. Carbonation-related microstructural changes in long-term durability concrete. *Materials Research*, 5: 287-293.

Saetta, A. V., Schrefler, B. A. and Vitaliani, R. V. 1993. The carbonation of concrete and the mechanism of moisture, heat and carbon dioxide flow through porous materials. *Cement and Concrete Research*, 23(4): 761-771.

Saetta, A. V., Schrefler, B. A. and Vitaliani, R. V. 1995. 2-D model for carbonation and moisture/heat flow in porous materials. *Cement and Concrete Research*, 25(8): 1703-1712.

Sauman, Z. 1971. Carbonization of porous concrete and its main binding components. *Cement and Concrete Research*, 1: 645-662.

Sisomphon, K. and Franke, L. 2007. Carbonation rates of concrete containing high volume of Pozzolanic materials. *Cement and Concrete Research*, 37: 1647-1653.

Smolczyk, H. G. 1976. Physical and chemical phenomena of carbonation,. RILEM International Symposium on Carbonation of Concrete, C&CA, Fulmer grange.

Song H., Kwon, S., Byun, K. and Park, C. 2006. Predicting carbonation in early-aged cracked concrete. *Cement and Concrete Research*, 36: 979-989.

Steffen, A., Dinkler, D. and Ahrens, H. 2002. Modeling carbonation for corrosion risk prediction of concrete structures. *Cement and Concrete Research*, 32: 935-941.

Steinour, H. H. 1959. Some effects of carbon dioxide on mortars and concrete-discussion. *Journal of the American Concrete Institute*, 30: 905-907.

Sulapha, P., Wong, S. F., Wee, T. H. and Swaddiwudhipongm S. 2003. Carbonation of concrete containing mineral admixtures. *Journal of Materials in Civil engineering*, 15: 134-142.

Sullivan-Green, L., Hime, W. and Dowding, C. 2007. Accelerated protocol for measurement of carbonation through a crack surface. *Cement and Concrete Research*, 37:916-923.

Tam, V. W. Y., Gao, X. F. and Tam, C. M. 2005. Carbonation around near aggregate region of old hardened concrete cement paste. *Cement and Concrete Research*, 35: 1180-1186.

Thiery, M., Villain, G., Dangla, P. and Platret, G. 2007. Investigation of carbonation front shape on cementitious materials: Effects of the chemical kinetics. *Cement and Concrete Research*, 37: 1047-1058.

UK Environment Agency, 2007. Blast furnace slag (BFS): A technical report on the manufacture of blast furnace slag and material status in the UK.
<http://www.handapp.co.uk/web/BF%20Slag%20a%20technical%20report%20on%20manufacturing%20of%20BF%20Slag%20&%20material%20status%20in%20UK.pdf>

Van Balen, K. and Van Gemert, D. 1994. Modelling lime mortar carbonation. *Material and Structures*, 27: 393-398.

Verbeck, G. 1958. Carbonation of hydrated Portland cement. Research Department Bulletin RX087, Portland Cement Association.

Villain, G. and Platret, G. 2006. Two experimental methods to determine carbonation profiles in concrete. *ACI Materials Journal*, 103: 265-271.

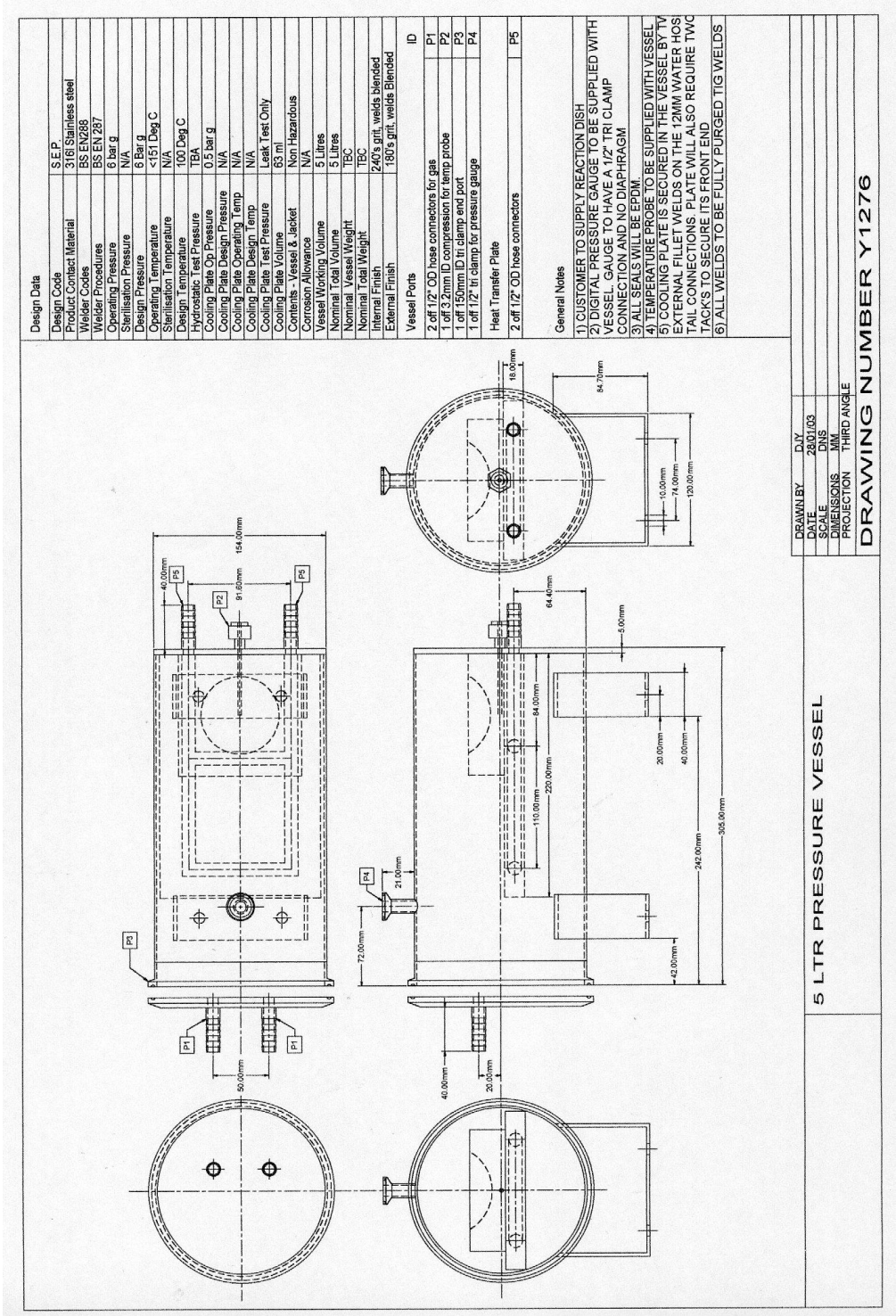
Wang, X. and Lee, H. 2009. A model for predicting the carbonation depth of concrete containing low-calcium fly ash. *Construction and Building Materials*, Volume 23: 725-733.

Young, J. F., Berger, R. L. and Breese, J. 1974. Accelerated curing of compacted calcium silicate mortars on exposure to CO₂. *Journal of the American concrete Society*, 57: 394-397.

Yousuf, M., Mollah, A., Hess, T. R., Tsai, Y.-N. and Cocke D.L. 1993. An FTIR and XPS investigations of the effects of carbonation on the solidification/stabilization of cement based systems-Portland type V with Zn. *Cement and Concrete Research*, 23: 773-784.

APPENDIX A

Technology Drawing – Reactor I



Technology Drawing – Reactor II

